

Physics of Active Emulsions

Christoph A. Weber^{1,2,3,*}, David Zwicker^{1,4,*}, Frank Jülicher^{1,2} and Chiu Fan Lee⁵

¹ Max Planck Institute for the Physics of Complex Systems, Nöthnitzer Str. 38, 01187 Dresden, Germany

² Center for Systems Biology Dresden, CSBD, Dresden, Germany

³ Paulson School of Engineering and Applied Sciences, Harvard University, Cambridge, MA 02138, USA

⁴ Max Planck Institute for Dynamics and Self-Organization, Am Faßberg 17, 37077 Göttingen, Germany

⁵ Department of Bioengineering, Imperial College London, South Kensington Campus, London SW7 2AZ, U.K.

* equal contribution

E-mail: weber@pks.mpg.de, david.zwicker@ds.mpg.de, julicher@pks.mpg.de, c.lee@imperial.ac.uk

Abstract. Phase separating systems that are maintained away from thermodynamic equilibrium via molecular processes represent a class of active systems, which we call *active emulsions*. These systems are driven by external energy input for example provided by an external fuel reservoir. The external energy input gives rise to novel phenomena that are not present in passive systems. For instance, concentration gradient can spatially organise emulsions and cause novel droplet size distributions. Another example are active droplets that are subject to chemical reactions, so their nucleation and size can be controlled and they can spontaneously divide. In this review we discuss the physics of phase separation and emulsions and show how the concepts that governs such phenomena can be extended to capture the physics of active emulsions. This physics is relevant to the spatial organisation of the biochemistry in living cells and for the development novel applications in chemical engineering.

PACS numbers: 47.55.D-, 05.70.Ln, 47.10.ab, 82.40.Qt, 82.60.Hc, 83.80.Tc, 87.10.Ca, 87.15.R-, 87.16.Uv

Keywords: active emulsions, active droplets, liquid phase separation, droplet ripening in concentration gradients, positioning of droplets, driven chemical reactions in emulsions, suppression of Ostwald-ripening, division of droplets, shape deformations and instabilities of droplets.

1. Introduction: From passive to active emulsions

The formation and dynamics of condensed phases such as droplets represent ubiquitous phenomena that we all experience in our daily life [1]. Examples are droplets condensing on the leaves of flowers and trees due to the supersaturated fog in the morning of some autumn day, or the “ouzo effect”, where the oil droplets in Ouzo grow in size and cloud the liquid. These transitions from a homogeneous mixture to a system with coexisting phases can be controlled by temperature or by changing the composition of the mixture. The physical conditions under which a mixture phase separates are well-understood. The interactions that favour the accumulation of components of the same type must exceed the entropic tendency of the system to remain mixed [2–4]. After drops have been nucleated, they undergo a ripening dynamics. Droplets either fuse, or larger droplets grow at the expense of smaller ones which then disappear. The latter phenomenon is referred to as Ostwald ripening [5]. During the ripening dynamics the droplet size distribution continuously broadens. In the case of Ostwald ripening the droplet size distribution exhibits an universal scaling in time t with the mean droplet size $\propto t^{1/3}$, which was derived by Lifschitz and Slyozov [6–8]. However, at large times-scales, droplet growth saturates and ripening stops as there is only one droplet left in the system. This condensed droplet stably coexists with a surrounding minority phase of lower solute concentration.

The behaviour of droplets can change in more complex environments. For instance, liquid condensed phases can interact with surfaces by wetting [9–11]. Droplets embedded in a gel matrix interact such that the droplet size can be tuned by changing the mechanical properties of the gel [12]. Droplets can also behave differently in transient systems, which have not yet reached equilibrium. For instance, surfactants exchanging with the surrounding solvent can induce Marangoni flows, which can propel droplets [13–17] and even lead to spontaneous division [18]. Generally, more complex behavior can be expected when multiple phases of different composition come in contact and exchange material [19–22].

Liquid condensed phases are also influenced by external “forces” such as gravitation, concentration or temperature gradients, magnetic or electric fields [23, 24]. In industrial manufacturing and processing, temperature gradients and sedimentation are explicitly taken advantage of, e.g., for extracting crude oil [25]. Moreover, concentration [26, 27] and temperature gradients [28, 29] are commonly used to assemble synthetic membranes for electro-optical devices. Recently, the equations governing the ripening dynamics of droplets

derived by Lifschitz and Slyozov have been extended to account for the presence of a concentration gradient [30, 31]. It has been theoretically shown that droplets can be positioned along the concentration gradient and that the universal scaling in time of droplet ripening breaks down.

Liquid condensed phases are also ideal compartments to organise chemical reactions since they can enrich specific chemical components. In particular, chemical agents mix rapidly in small droplets, and thus control the timing of chemical reactions [32]. The interface of droplets can serve to concentrate reactants, resulting in a speed up of the reaction [33]. Liquid droplets in the presence of chemical reactions can even propel across a solid substrate [15, 34–36] or flow past a chemically patterned substrate leading to unique morphological instabilities [37]. They also provide model systems to study interactions of pattern forming systems. For example, droplets containing agents undergoing oscillatory Belousov-Zhabotinsky reactions have been considered as coupled phase oscillators [38, 39]. In all these systems, the droplet material does not participate in the chemical reaction.

If the phase separated material undergoes a chemical reaction itself, new physical behaviours can emerge. In passive systems, where phase separation and chemical reactions are in thermal equilibrium, coexisting phases cannot be stable. These systems settle in a homogeneous state that corresponds to the free energy minimum [40]. Conversely, if the chemical reaction is driven away from equilibrium, phase separation can be maintained. Under some conditions an arrest of the ripening dynamics has been observed in numerical simulations [41–54] and in experiments where chemical reactions are induced by light [55–62] or proceed spontaneously [63–70]. Recently, it has been shown that the chemical reaction between the droplet material can indeed suppress Ostwald ripening leading to an emulsion composed of drops of identical size [71, 72]. Driven chemical reactions can even trigger the division of droplets [73]. Recent experiments on droplets in the presence of non-equilibrium turnover reactions showed the assembly of supramolecular structures with a tunable lifetime [74] and serve as a model for molecular selection of reaction products and their assemblies [75]. These examples highlight the rich phenomenology emerging from the interplay of phase separation with chemical reactions.

Phase separated systems in the presence of external forces and chemical reactions actively driven away from thermal equilibrium are a novel class of physical systems. Many physical properties known from passive emulsions are altered and novel phenomena occur. Since energy input is typically necessary to generate external forces, and to drive

chemical reactions away from equilibrium, we refer to these systems as *active emulsions*.

An intriguing example where the physics of these active emulsions is relevant are living cells. Biological function inside cells is attained by the spatial-temporal organisation of biomolecules and the control of their chemical reactions. For this purpose the interior of the cell is divided into compartments, referred to as organelles. Each organelle has a chemical identity due to a distinct composition of functional biomolecules. Some organelles, such as mitochondria, are surrounded by membranes that are permeated by active channels regulating chemical potential differences across the membrane [76]. However, there are also organelles that do not possess any membrane; they are called non-membrane bound compartments or biomolecular condensates [77–82]. To maintain their chemical identity in the absence of a membrane, it has been suggested that these compartments are liquid droplets formed by liquid-liquid phase separation [30, 83, 84]. Recently, many organelles have been found with properties reminiscent of liquid droplets [81]. Examples range from mRNA-protein-condensates [84, 85] over centrosomes [71, 86] to multiple subcompartments of the nucleoli [87, 88]. These findings suggest that the cytoplasm can be regarded as a multi-component emulsion hosting a large variety of coexisting phases, each of distinct composition [89, 90]. However, in contrast to passive emulsions, cellular droplets exist in the non-equilibrium environment of biological cells. The associated continuous dissipation of energy can be used to drive chemical reactions or generate concentration gradients of molecular species. Both processes can affect the dynamics and stability of these active droplets and cause behaviours not observed for passive droplets [82, 91].

Here we review recent theoretical approaches used to describe droplets and emulsions under conditions that deviate from passive phase separating systems. Our review starts with an introduction to passive phase separation and dynamics of emulsion undergoing Ostwald ripening (section 2). In section 3, we discuss phase separation and dynamics of droplets in the presence of external forces and concentration gradients, while section 4 considers the dynamics and stability of droplets under the influence of chemical reactions that are driven away from thermal equilibrium.

2. Liquid-liquid phase separation of binary mixtures

Phase separation refers to the spontaneous partitioning of a system into subsystems with distinct macroscopic

properties. Examples include the cellular compartments mentioned in the introduction, but also many everyday phenomena that range from fog in the morning to oil droplet formation in salad dressings. In this section, we will discuss the physical principles and derive the equations describing the dynamics of phase separation and the ripening of droplets in liquid emulsions.

2.1. Statistical mechanics of a binary mixture

We start by considering a binary, incompressible mixture consisting of two types of molecules on a lattice with M sites. Each lattice site is occupied by either molecule A or B , with N_A and N_B representing their total numbers in the system, so $N_A + N_B = M$. The system is at thermal equilibrium with a heat bath at temperature T . The thermodynamic properties of the system are thus dictated by the partition function [92]

$$Z = \sum_{\Omega} \exp\left(-\frac{H(\sigma_1, \dots, \sigma_M)}{k_B T}\right), \quad (2.1)$$

where the Hamiltonian $H(\sigma_1, \dots, \sigma_M)$ denotes the energy of a particular arrangement $\sigma_1, \dots, \sigma_M$ of the molecules on the lattice and k_B is the Boltzmann constant. Here, we encode the arrangements using a binary variable σ_n , where $\sigma_n = 1$ if the lattice site n is occupied by molecule A and $\sigma_n = 0$ if it is occupied by B . Ω refers to the set of all possible arrangements considering that the molecules A are indistinguishable from each other; the same applies to molecules B [93]. For simplicity, we only consider nearest neighbour interactions, which are described by the following Hamiltonian [94]

$$H(\{\sigma\}) = \frac{1}{2} \sum_{(m,n)} \left(e_{AA} \sigma_m \sigma_n + e_{BB} (1 - \sigma_m)(1 - \sigma_n) + e_{AB} [\sigma_m(1 - \sigma_n) + \sigma_n(1 - \sigma_m)] \right), \quad (2.2)$$

where the summation is over all nearest neighbour pairs (m, n) on the lattice and the factor $\frac{1}{2}$ avoids the double counting of interaction pairs. Here, the interaction parameters e_{ij} determine what particle types tend to be next to each other. For instance, if $e_{AA} < 0$, two A molecules on neighbouring sites lower the total energy, making this configuration more probable. In general, these interaction parameters can arise from various physical interactions that may include dipolar and van der Waals interactions, screened electrostatic interactions between charged molecular groups or entropy-driven hydrophobic interactions [94–96].

2.1.1. Thermodynamics of a homogeneous mixture.

Within the canonical ensemble a homogeneous binary

mixture of volume V can be characterised by the Helmholtz free energy $F = E - TS$, which combines the internal energy E and the entropy S of a system. This free energy can be expressed by the partition function (2.1) [92, 97, 98]

$$F(T, V, N_A, N_B) = -k_B T \ln Z(T, V, N_A, N_B). \quad (2.3)$$

Derivatives of the free energy F are related to thermodynamic quantities that are relevant in our discussion of phase separation. In particular, the entropy is given as $S = -\partial F/\partial T|_{V, N_A, N_B}$, the pressure is $p = -\partial F/\partial V|_{T, N_A, N_B}$ and the chemical potentials read $\mu_A = \partial F/\partial N_A|_{T, V, N_B}$ and $\mu_B = \partial F/\partial N_B|_{T, V, N_A}$.

For simplicity, we focus on an incompressible binary system of constant volume $V = \nu M$ and constant molecular volume ν of the two components. In this case, adding an A molecule to the system corresponds to removing a B molecule. Consequently, the relevant thermodynamic quantities are the *exchange chemical potential* $\bar{\mu}$ and the *osmotic pressure* Π [94, 99]:

$$\bar{\mu} = \frac{\partial F}{\partial N_A}\bigg|_{T, V} = -\frac{\partial F}{\partial N_B}\bigg|_{T, V} = \nu \frac{\partial f}{\partial \phi}\bigg|_T, \quad (2.4a)$$

$$\Pi = -\frac{\partial F}{\partial V}\bigg|_{T, N_A} = -f + \phi \frac{\partial f}{\partial \phi}\bigg|_T, \quad (2.4b)$$

where the number of lattice sites M is slaved to the total volume by $M = V/\nu$. Here, we used the homogeneity of the system, $F = Vf(\phi)$, where $f(\phi)$ is the free energy density as a function of the volume fraction $\phi = N_A\nu/V$ of A molecules.

The homogeneous state for a given volume is a stable thermodynamic state if it corresponds to a minimum of the free energy F . This requires that the curvature of the free energy density as a function of volume fraction is convex, i.e., $f''(\phi) \geq 0$. The link between stability and curvature of the free energy density can be understood qualitatively: conservation of molecule numbers implies that raising the volume fraction in one spatial region requires lowering it in another. If the free energy density is convex, any such perturbation increases the overall free energy. This can be shown rigorously by considering spatially inhomogeneous perturbations that conserve molecule numbers. We will discuss this approach after introducing the free energy functional in section 2.1.5.

The stability of the homogenous state can also be shown using an ensemble where the particle number N_A is fixed and the volume V can change. This ensemble is governed by the thermodynamic potential $G(N_A, \Pi) = F(N_A, V) + V\Pi$, where Π is the osmotic pressure given by equation (2.4b) and the volume $V = \partial G/\partial \Pi$. A homogeneous state with the osmotic pressure Π is stable if the free energy G as a function of Π is concave, $\partial^2 G/\partial \Pi^2 < 0$. The concavity of G with

respect to variations of the osmotic pressure can be seen by writing $\partial^2 G/\partial \Pi^2 = \partial V/\partial \Pi = -V\kappa$, where κ is the osmotic compressibility $\kappa = -V^{-1}\partial V/\partial \Pi$. For the homogeneous state to be stable, the osmotic pressure should increase as the volume decreases, i.e., $\kappa > 0$, to push the system back to its thermodynamic state after a perturbation in volume. This condition is satisfied if the free energy density is convex, $f''(\phi) > 0$, since $\kappa = (\phi^2 f''(\phi))^{-1}$. In the thermodynamic limit, ensembles become equivalent and thus the convexity of the free energy density determines the thermodynamic stability of the homogeneous state, not only in the ensemble (N_A, Π) where the osmotic pressure is imposed but also in the ensemble (N_A, V) where the volume is fixed.

2.1.2. Mean field free energy density of an incompressible mixture. To determine the relevant thermodynamic quantities for phase separation, we need to evaluate the free energy and the partition function given in equation (2.3). Since this is generally difficult, we discuss a *mean-field approximation* for the homogeneous case of the incompressible binary mixture on a lattice characterised by the Hamiltonian given in equation (2.2). This approximation neglects the spatial correlations between the molecules. Within the mean field approximation, the probability that lattice site n is occupied by A , is given by $\langle \sigma_n \rangle = N_A/M$, where $\langle \dots \rangle$ denotes the average in the canonical ensemble and $\phi = N_A/M$ is the volume fraction of A molecules in the system. Due to incompressibility the probability of the site being occupied by B is $N_B/M = 1 - \phi$. The partition function hence is

$$Z \simeq |\Omega| \exp\left(-\frac{E(\phi)}{k_B T}\right) \quad (2.5)$$

with the internal energy given as

$$E(\phi) = \frac{zM}{2} [e_{AA}\phi^2 + 2e_{AB}\phi(1 - \phi) + e_{BB}(1 - \phi)^2], \quad (2.6)$$

where z is the number of neighbours per lattice site (e.g., $z = 6$ for a cubic lattice), and $zM/2$ is the total number of distinct nearest neighbours. The number $|\Omega|$ of all possible arrangements on the lattice appearing in equation (2.5),

$$|\Omega| = \binom{M}{N_A} = \binom{M}{N_B} = \frac{M!}{N_A! N_B!}, \quad (2.7)$$

determines the entropy $S = k_B \ln |\Omega|$ for the incompressible binary mixture on a lattice, which is also referred to as mixing entropy. Using equations (2.3), we obtain the free energy density

$$f(\phi) \simeq \frac{z}{2\nu} [e_{AA}\phi^2 + 2e_{AB}\phi(1 - \phi) + e_{BB}(1 - \phi)^2] + \frac{k_B T}{\nu} [\phi \ln \phi + (1 - \phi) \ln(1 - \phi)], \quad (2.8)$$

where we have used Stirling's approximation, $\ln N! \simeq N \ln N - N$, to evaluate the factorials. The free energy density can also be written as $f(\phi) = \phi f(1) + (1 - \phi)f(0) + f_{\text{mix}}(\phi)$, which separates the contribution of the pure systems from the *free energy of mixing* [94, 96],

$$f_{\text{mix}}(\phi) = \frac{k_B T}{\nu} [\phi \ln \phi + (1 - \phi) \ln(1 - \phi) + \chi \phi(1 - \phi)] \quad (2.9)$$

where

$$\chi = \frac{z}{2k_B T} (2e_{AB} - e_{AA} - e_{BB}) \quad (2.10)$$

is the Flory-Huggins interaction parameter [3, 4]. f_{mix} captures the competition between the mixing entropy $S = -k_B(V/\nu)[\phi \ln \phi + (1 - \phi) \ln(1 - \phi)]$ and the molecular interactions characterised by the single parameter χ . In the next section, we will see that both the free energy density (equation (2.8)) and the free energy density of mixing (equation (2.9)) lead to the same phase separation equilibrium. However, the difference will become apparent when we discuss chemical reactions in section 4.

The free energy density f_{mix} is a symmetric function with respect to $\phi = \frac{1}{2}$. This symmetry stems from considering equal molecular volumes of components A and B and the subtraction of the free energy before mixing. Conversely, if the molecules A and B have different molecular volumes $n_A \nu$ and $n_B \nu$, the free energy of mixing is not symmetric [3, 4]:

$$\tilde{f}_{\text{mix}}(\phi) = \frac{k_B T}{\nu} \left[\frac{\phi}{n_A} \ln \phi + \frac{(1 - \phi)}{n_B} \ln(1 - \phi) + \chi \phi(1 - \phi) \right], \quad (2.11)$$

where n_A and n_B denote the non-dimensional molecular size in multiples of the volume ν of a single lattice site.

Homogeneous states governed by the free energy density $f(\phi)$ are only stable when the free energy density is convex, $f''(\phi) > 0$; see section 2.1.1. For the expression given in equation (2.8) this is the case for all ϕ in the absence of interactions ($e_{ij} = 0$ for $i, j = A, B$) and when entropic effects dominate. In the presence of interactions however, the free energy density of the homogeneous system can become concave ($f''(\phi) < 0$) within a range of volume fractions ϕ , see figure 2.1(a). Within this range, the homogeneous state is not stable, implying that the thermodynamic equilibrium state is inhomogeneous.

2.1.3. Phase coexistence. The simplest inhomogeneous state corresponds to two subsystems of different volume fractions, also referred to as phases. The

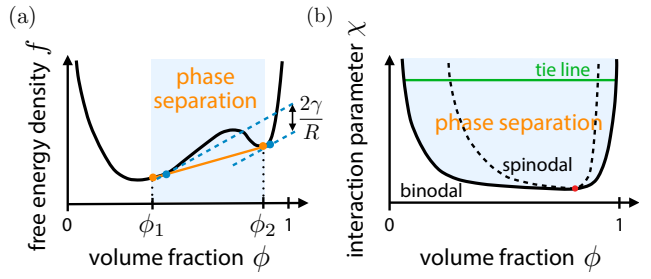


Figure 2.1. (a) Sketch of an asymmetric free energy density $f(\phi)$ for an incompressible binary mixture as a function of volume fraction ϕ , e.g., equation (2.11) for the case $n_B > n_A$ and $\chi > 2$. In the presence of interactions, there can be a range of volume fractions where the free energy density is concave with $f''(\phi) < 0$. The Maxwell tangent construction modifies the free energy within the volume fraction range $[\phi_1, \phi_2]$ (orange line). As a result the free energy density becomes convex for all volume fractions. The equilibrium volume fraction of each phase are ϕ_1 and ϕ_2 . The impact of surface tension slightly increases the equilibrium volume fractions (blue dots, see section 2.5.1). (b) Phase diagram as a function of the Flory-Huggins interaction parameter χ and volume fraction ϕ . For large enough interaction parameters, phase separation can occur. The corresponding region in the phase diagram is bordered by the binodal line. The tie lines (green) connect the equilibrium volume fractions of two coexisting phases on the binodal line. The dashed line refers to the spinodal. Within the spinodal lines, the mixture can undergo a spontaneous partitioning into two phases, while between the spinodal and the binodal, only large enough phase separated domains can grow. This regime is referred to as nucleation & growth.

associated free energy can be written as

$$F \simeq V_1 f(\phi_1) + V_2 f(\phi_2), \quad (2.12)$$

where ϕ_α and V_α denote the volume fraction and volume of phase α , with $\alpha = 1, 2$. The incompressibility assumption combined with conservation of particles implies $V_1 + V_2 = V$ and $V_1 \phi_1 + V_2 \phi_2 = V\phi$. Consequently, there are only two independent variables in the free energy above, e.g., ϕ_1 and V_1 . In equation (2.12) we neglected the energetic contribution of the interface region that separates the two phases. This is valid in the thermodynamic limit where the system and the volumes of the phases are infinitely large, so the energetic contribution of the interface is negligible relative to the contribution of the phases. We will have to refine equation (2.12) when discussing finite systems in section 2.2.

The inhomogeneous state is stable if it corresponds to a minimum of the free energy (2.12) consistent with the imposed constraint of particle conservation and in the absence of vacancies. To find this minimum, we differentiate F with respect to ϕ_1 and V_1 , respectively, use the relationship $\phi_2 = (\phi V - \phi_1 V_1)/(V - V_1)$ and

set each expression to zero:

$$0 = f'(\phi_1) - f'(\phi_2), \quad (2.13a)$$

$$0 = f(\phi_1) - f(\phi_2) + (\phi_2 - \phi_1) f'(\phi_2). \quad (2.13b)$$

The first equation is a balance of the exchange chemical potentials between phases, $\bar{\mu}_1 = \bar{\mu}_2$, with $\bar{\mu}_\alpha = \bar{\mu}|_{\phi=\phi_\alpha}$ with $\alpha = 1, 2$; see equation (2.4a)). The second equation corresponds to the balance of the osmotic pressures between the two phases, $\Pi_1 = \Pi_2$, with $\Pi_\alpha = \Pi|_{\phi=\phi_\alpha}$; see equation (2.4b).

Obviously, equations (2.13) are satisfied for homogeneous systems with $\phi_1 = \phi_2$. To see that there also exist solutions with $\phi_1 \neq \phi_2$, the two conditions can be represented by a graphical tangent construction using the free energy density $f(\phi)$, see figure 2.1(a). Here, condition (2.13a) implies that the slopes at the volume fractions ϕ_1 and ϕ_2 are the same and condition (2.13b) states that they are also equal to the slope of the line connecting the points $(\phi_1, f(\phi_1))$ and $(\phi_2, f(\phi_2))$. Taken together, these conditions can only be satisfied by a common tangent to the two points. This procedure of finding the equilibrium volume fractions is known as *Maxwell's tangent construction or construction of the convex hull*. The orange line in figure 2.1(a) shows the result of such a construction. In fact, inserting condition (2.13b) into equation (2.12) (and using conservation of A particles) shows that this line corresponds to the volume weighted average of the free energy density of the two subsystems. Consequently, the corresponding demixed system is the thermodynamic equilibrium since it has a lower free energy than the mixed system described by the black line in figure 2.1(a). Accordingly, ϕ_1 and ϕ_2 are referred to as equilibrium volume fractions of the coexisting phases. Clearly, a separation into two phases with volume fractions ϕ_1 and ϕ_2 is only possible when the average volume fraction ϕ obeys $\phi_1 < \phi < \phi_2$. Outside this region, the homogeneous state is stable, since $f''(\phi) > 0$.

The parameter region where phase separation is possible can be determined from the solutions ϕ_1 and ϕ_2 as a function of the interaction parameter χ , see figure 2.1(b). The corresponding line is called the *binodal line*. In the simple case of the symmetric free energy of mixing (equation (2.9)), $f_{\text{mix}}(\phi_1) = f_{\text{mix}}(\phi_2)$ and $f'_{\text{mix}}(\phi_1) = f'_{\text{mix}}(\phi_2) = 0$. The binodal line is then given by $\chi_b(\phi) = \ln(\phi/(1-\phi))/(2\phi-1)$ and phase separation occurs only for $\chi > \chi_b$. In particular, the minimal interaction parameter is $\chi_b^{\min} = 2$, which is obtained at the critical point $\phi = \frac{1}{2}$. Near the critical point, the equilibrium volume fractions inside each phase obey $\phi_1 \simeq \frac{1}{2} - [\frac{3}{8}(\chi-2)]^{1/2}$ and $\phi_2 \simeq \frac{1}{2} + [\frac{3}{8}(\chi-2)]^{1/2}$. Note that the same results are obtained when equation (2.8) is used instead of f_{mix} , since terms linear in ϕ do not alter the conditions given in equations (2.13).

2.1.4. Free energy of inhomogeneous systems. The discussion of the previous section neglected the contribution of the interfacial region on the equilibrium free energy. This interfacial region is always present since the volume fraction is continuous in space and must thus interpolate between the values ϕ_1 and ϕ_2 in the two phases. The additional free energy contribution associated with this spatial variations can be estimated within our lattice model. For simplicity, we first consider a one-dimensional system with discrete lattice positions x_n for which the Hamiltonian given in equation (2.2) can be written as

$$H(\{\sigma\}) = \sum_n [e_{AB}(\sigma_n(1-\sigma_{n+1}) + \sigma_{n+1}(1-\sigma_n)) + e_{AA}\sigma_n\sigma_{n+1} + e_{BB}(1-\sigma_n)(1-\sigma_{n+1})]. \quad (2.14)$$

We proceed analogously to section 2.1 and perform a mean-field approximation after rewriting the coupling terms using $2\sigma_n(1-\sigma_{n+1}) = (\sigma_n - \sigma_{n+1})^2 - \sigma_n^2 - \sigma_{n+1}^2 + 2\sigma_n$. Additionally, generalising to three dimensions and taking the continuum limit, we replace $\sum_n \mapsto \nu^{-1} \int d^3r$, $\langle \sigma_n \rangle \mapsto \phi(\mathbf{r})$, and $\langle \sigma_{n+1} - \sigma_n \rangle \mapsto \nu^{\frac{2}{3}} \nabla \phi(\mathbf{r})$. Hence,

$$E \simeq \frac{k_B T \chi}{\nu} \int d^3r \left[\phi(\mathbf{r})(1-\phi(\mathbf{r})) + \frac{\nu^{\frac{2}{3}}}{2} |\nabla \phi(\mathbf{r})|^2 \right] + \frac{z}{2\nu} \int d^3r \left[e_{AA} \phi(\mathbf{r}) + e_{BB}(1-\phi(\mathbf{r})) \right], \quad (2.15)$$

where χ is the Flory-Huggins parameter given in equation (2.10). The associated free energy F can be expressed as a functional of $\phi(\mathbf{r})$,

$$F = \frac{1}{\nu} \int d^3r \left[\frac{\kappa}{2\nu} |\nabla \phi|^2 + \frac{z}{2} (e_{AA} \phi + e_{BB} (1-\phi)) + k_B T [\phi \ln(\phi) + (1-\phi) \ln(1-\phi) + \chi \phi(1-\phi)] \right], \quad (2.16)$$

where

$$\kappa = k_B T \chi \nu^{\frac{5}{3}} \quad (2.17)$$

characterises the change of free energy density due to concentration inhomogeneities. Since the interaction parameter $\chi > 2$ in the phase separating regime, we have $\kappa > 0$ and the gradient term thus penalises spatial inhomogeneities. We identify the integrand of the free energy given in equation (2.16) as the total free energy density f_{tot} . Expressing it in terms of concentrations $c = \phi/\nu$, we obtain

$$f_{\text{tot}}(c, \nabla c) = f_{\text{mix}}(c) + f_0(c) + \frac{\kappa}{2} |\nabla c|^2, \quad (2.18)$$

where f_{mix} follows from equation (2.9) and $f_0(c) = (z/2) (e_{AA} c + e_{BB} (\nu^{-1} - c))$ is the free energy of the pure system before mixing.

2.1.5. Ginzburg-Landau free energy. In the previous sections we have derived the free energy density of an incompressible binary mixture using statistical mechanics. We have seen that phase separation occurs when the free energy density exhibits a concave region enclosed by convex branches. The simplest free energy for an incompressible mixture that has such a shape is known as the *Ginzburg-Landau free energy* [8]:

$$F_{\text{GL}}[c] = \int d^3r \left(f_{\text{GL}}(c) + \frac{\kappa}{2} |\nabla c|^2 \right), \quad (2.19)$$

with the corresponding free energy density given as

$$\begin{aligned} f_{\text{GL}}(c) &= \tilde{b}(c - c_c) - \frac{b}{2}(c - c_c)^2 \\ &+ \frac{\tilde{a}}{3}(c - c_c)^3 + \frac{a}{4}(c - c_c)^4. \end{aligned} \quad (2.20)$$

This free energy density is parameterised by the phenomenological coefficients a , \tilde{a} , b , \tilde{b} , and c_c . As discussed in section 2.1.3, phase separation equilibrium is not affected by the linear term, thus we choose $\tilde{b} = 0$, and for reason of simplicity, we also consider the special case $\tilde{a} = 0$, leading to the bi-quadratic form of the Ginzburg-Landau free energy density:

$$f_{\text{GL}}(c) = -\frac{b}{2}(c - c_c)^2 + \frac{a}{4}(c - c_c)^4, \quad (2.21)$$

which is symmetric around the concentration c_c . This free energy density has a concave region if $b > 0$ and the parameter $a > 0$ characterises the convex branches of the energy density. Using equation (2.13a) the equilibrium concentrations within each phase separated domain are

$$c_1 = c_c - \sqrt{b/a}, \quad (2.22a)$$

$$c_2 = c_c + \sqrt{b/a}. \quad (2.22b)$$

The Ginzburg-Landau free energy density $f_{\text{GL}}(c)$ given in equation (2.21) can either be understood as a phenomenological free energy density that exhibits the qualitative feature necessary for phase separation, i.e., a concave domain enclosed by two convex domains, or as an expansion of the free energy of mixing around a constant concentration c_c , typically the critical concentration [8, 100–102]. In particular, expanding the symmetric free energy of mixing $f_{\text{mix}}(c)$ (equation (2.9)) around $c_c = 1/(2\nu)$ up to the fourth order, we find

$$a = \frac{4}{3}k_B T \nu^3, \quad b = (\chi - 2)k_B T \nu, \quad (2.23)$$

which links the phenomenological parameters a and b with the molecular parameters of the lattice model.

2.2. Equilibrium states of a binary mixture

In this section, we determine the equilibrium concentration profiles that minimise the free energy F_{GL} . Specifically, we calculate the extremal solutions of F_{GL} and discuss their stability in different regions of the phase diagram, see figure 2.1(b). An explicit expression of the interfacial profile will allow us to relate the free energy contribution characterised by κ to the surface tension between phases.

2.2.1. Stationary states. We start by determining the stationary states $c_*(\mathbf{r})$ of the bi-quadratic Ginzburg-Landau free energy F_{GL} given in equation (2.19). Such states have an extremal free energy subjected to the constraint that the number of A and B molecules are conserved, i.e.,

$$\bar{c} = \frac{1}{V} \int_V d^3r c(\mathbf{r}), \quad (2.24)$$

where $\bar{c} = N_A/V$ denotes the mean concentration of A molecules in the mixture the finite volume V . To enforce this constraint, we introduce a Lagrange multiplier λ and vary the functional $F_{\text{GL}} - \lambda \int_V d^3r c(\mathbf{r})$. Here, the functional derivative of the free energy is the generalization of the exchange chemical potential generalized to inhomogeneous systems,

$$\bar{\mu} = \frac{\delta F}{\delta c}, \quad (2.25)$$

which reads $\bar{\mu} = a(c(\mathbf{r}) - c_c)^3 - b(c(\mathbf{r}) - c_c) - \kappa \nabla^2 c(\mathbf{r})$ for F_{GL} . Consequently, the Euler-Lagrange equation for the stationary state is

$$\bar{\mu} = \lambda, \quad (2.26)$$

where we dropped a boundary term proportional to $\kappa \nabla c$, assuming no-flux boundary conditions at the system boundary. The stationary states thus correspond to a spatially uniform exchange chemical potential $\bar{\mu}$, which may be realised for both homogeneous and inhomogeneous concentration profiles $c_*(\mathbf{r})$.

We start by considering the spatially homogeneous equilibrium states $c_*(\mathbf{r}) = c_0$. Particle conservation implies $c_0 = \bar{c}$ (equation (2.24)) and the Euler-Langrange equations read $\lambda = a(\bar{c} - c_c)^3 - b(\bar{c} - c_c)$. The homogeneous state $c(\mathbf{r}) = \bar{c}$ is thus an extremal state of the free energy F_{GL} and we will check whether it corresponds to a minimum in the next section.

We showed above that states with coexisting phases can be stable in some regions of the phase diagram shown in figure 2.1(b). Here, we determine the concentration profile that connects the two phases from extremising the free energy F_{GL} . In the following, we restrict ourselves to a flat interface oriented perpendicular to the x -axis at the position $x = 0$ with

a concentration $c(x = 0) = c_c$. For simplicity, we extend the system to infinity while keeping the position and concentration value of the interface fixed. For the symmetric free energy density (equation (2.21)), this implies $\bar{\mu} = 0$, thus $\lambda = 0$, at the interface, and in the case of an extremal inhomogeneous state, $\bar{\mu} = 0$ at all positions. Far away from the interface, the concentration inside the phases should be governed by the equilibrium concentrations (equation (2.22)),

$$\lim_{x \rightarrow -\infty} c(x) = c_1, \quad \lim_{x \rightarrow \infty} c(x) = c_2. \quad (2.27)$$

With the boundary conditions above the unique solution is [40]:

$$c_I(x) = c_c + \sqrt{\frac{b}{a}} \tanh\left(\sqrt{\frac{b}{2\kappa}} x\right). \quad (2.28)$$

Since this interfacial profile varies substantially only within the region $|x| \lesssim \sqrt{2\kappa/b}$, we introduce the *interfacial width*

$$w = \sqrt{\frac{2\kappa}{b}} \simeq \nu^{\frac{1}{3}} \sqrt{\frac{\chi}{\chi - 2}}. \quad (2.29)$$

The right hand side relates w to the lattice model using equations (2.17) and (2.23). In the limit of strong phase separation (large χ) the interfacial width approaches the linear dimension $\nu^{1/3}$ of the molecules.

2.2.2. Stability of stationary states. The homogeneous and inhomogeneous stationary states of the Ginzburg-Landau free energy, $c_*(x) = \bar{c}$ and $c_*(x) = c_I(x)$, respectively, can be either stable or unstable. They are stable if they correspond to a free energy minimum, i.e., if all small concentration perturbations increase the free energy. To test this, we consider concentration profiles $c = c_* + \epsilon$, where $\epsilon(\mathbf{r})$ is a small, position dependent concentration perturbation. To quadratic order, the change in the free energy due to this perturbation is

$$\begin{aligned} \Delta F[c_*, \epsilon] &= F_{\text{GL}}(c_* + \epsilon) - F_{\text{GL}}(c_*) \\ &\simeq \int d^3r \left[\frac{\epsilon^2}{2} (3a(c_* - c_c)^2 - b) + \frac{\kappa}{2} (\nabla \epsilon)^2 \right]. \end{aligned} \quad (2.30)$$

The state $c_*(\mathbf{r})$ is stable if all perturbations increase the free energy, i.e., if $\Delta F[c_*, \epsilon] > 0$ for all $\epsilon(\mathbf{r})$. In the case of the homogeneous state $c_*(\mathbf{r}) = \bar{c}$ both terms in the integrand are positive if $|\bar{c} - c_c| > \sqrt{b/(3a)}$, which implies $\Delta F[c_*, \epsilon] > 0$. Conversely, $\Delta F[c_*, \epsilon]$ can be negative for $|\bar{c} - c_c| < \sqrt{b/(3a)}$ in sufficiently large systems, e.g., for the perturbation $\epsilon(x) \propto \tanh(x/w)$, which implies that the homogeneous state is unstable for these parameters. Consequently, the stationary homogeneous state can be either stable or

unstable to infinitesimal perturbations. In contrast, the inhomogeneous state $c_*(x) = c_I(x)$ given by equation (2.28) is always stable if it is a stationary state, i.e., when $|\bar{c} - c_c| < \sqrt{b/a}$, see Appendix A.

Taken together, we can distinguish three different parameter regimes with different stable stationary states. For mean concentrations \bar{c} far away from the symmetry point c_c , i.e., when $|\bar{c} - c_c| > \sqrt{b/a}$, the homogeneous state is the only stable one. Conversely, when $|\bar{c} - c_c| < \sqrt{b/(3a)}$, only the inhomogeneous state is stable and phase separation will thus happen spontaneously. This region is known as the *spinodal decomposition* region [103–109] which is enclosed by the spinodal line (dashed line in figure 2.1(b)). Between the spinodal region and the homogeneous region, for $\sqrt{b/(3a)} < |\bar{c} - c_c| < \sqrt{b/a}$, both states are stable to infinitesimal perturbations. In this case, phases can only originate from the homogeneous state by large fluctuations, known as nucleation events. Consequently, the respective region in the phase diagram is known as the *nucleation and growth* regime. All three phases are shown in the phase diagram in figure 2.1(b).

2.3. Surface tension of interfaces.

The surface tension of the interface can be determined from the profile $c_I(x)$. To this end, we separate the energetic contributions of the bulk phases to the free energy from a contribution that is related to the interface. For large volumes of the coexisting phases V_1 and V_2 , the total free energy F can be written as

$$F = V_1 f(c_1) + V_2 f(c_2) + \gamma A, \quad (2.31)$$

where c_1 and c_2 are the corresponding equilibrium concentrations. Here, A is the area of the interface and γ denotes the surface energy, which is also known as the *surface tension* [110]. Its value is obtained from the condition that the total free energy given in equation (2.31) equals the free energy of the interfacial profile, $F = F[c_I]$:

$$\gamma A = \int_V d^3r \left[f(c_I) + \frac{\kappa}{2} (\nabla c_I)^2 \right] - V_1 f(c_1) - V_2 f(c_2). \quad (2.32)$$

In the simple case where a flat interface is oriented perpendicular to the x -axis and the system is extended to infinity while keeping the position of the interface fixed at $x = 0$, the surface tension reads

$$\gamma = \int_{-\infty}^{\infty} dx \left[f(c_I) - \frac{1}{2} [f(c_1) + f(c_2)] + \frac{\kappa}{2} (\nabla c_I)^2 \right]. \quad (2.33)$$

Considering the Ginzburg-Landau free energy and the corresponding interfacial profile $c_I(x)$ (equation (2.28)),

we find $f_{\text{GL}}(c_1) = f_{\text{GL}}(c_2) = -b^2/(4a)$ and thus

$$\begin{aligned} \gamma &= \int_{-\infty}^{\infty} dx \left[f_{\text{GL}}(c_1) + \frac{\kappa}{2} (\partial_x c_1)^2 + \frac{b^2}{4a} \right] \\ &= \frac{2\sqrt{2\kappa b^3}}{3a} \simeq \frac{k_B T \chi^{\frac{1}{2}} (\chi - 2)^{\frac{3}{2}}}{2\nu^{\frac{2}{3}}}. \end{aligned} \quad (2.34)$$

In the last approximation, we have used the expressions for the lattice model (equations (2.17) and (2.23)), which shows that γ scales like χ^2 in the limit of strong phase separation (large χ).

2.4. Dynamical equations of phase separation

We next derive the dynamical equations describing how the binary mixture reaches its equilibrium state. Considering an incompressible mixture, the volume fractions obey $\phi_A + \phi_B = 1$, and thus $\partial_t \phi_A = -\partial_t \phi_B$. Using $\phi_i = c_i \nu_i$ ($i = A, B$) and considering for simplicity the case where molecular volumes of the two components are equal to $\nu_i = \nu$, the incompressibility condition leads to $\partial_t c_A = -\partial_t c_B$. The particle conservation of A and B molecules can be expressed by the continuity equations

$$\partial_t c_A = -\nabla \cdot \mathbf{j}_A, \quad (2.35a)$$

$$\partial_t c_B = -\nabla \cdot \mathbf{j}_B, \quad (2.35b)$$

where incompressibility and equal molecular volumes imply that the particle fluxes of component A and B read $\mathbf{j}_A = \mathbf{v} c_A + \mathbf{j}$ and $\mathbf{j}_B = \mathbf{v} c_B - \mathbf{j}$, and that the volume flow velocity \mathbf{v} obeys $\nabla \cdot \mathbf{v} = 0$. In the following sections, we restrict ourselves to a reference frame where $\mathbf{v} = \mathbf{0}$. In this case the exchange current reads $\mathbf{j} = (\mathbf{j}_A - \mathbf{j}_B)/2$, which drives the time evolution of the concentration of components A ,

$$\partial_t c = -\nabla \cdot \mathbf{j}, \quad (2.36)$$

where we abbreviated $c = c_A$ for simplicity. In linear response, the exchange current is proportional to the thermodynamic force of the gradient of the exchange chemical potential $-\nabla \bar{\mu}$, implying $\mathbf{j} = -\Lambda(c) \nabla \bar{\mu}$; see Appendix B. Here, $\Lambda(c)$ denotes a mobility coefficient, which is positive to ensure that the second law of thermodynamics is fulfilled, i.e., that the corresponding entropy production, $-\int d^3r \mathbf{j} \cdot \nabla \bar{\mu}$, is positive [98, 111]. The resulting dynamical equation is

$$\partial_t c = \nabla \cdot (\Lambda(c) \nabla \bar{\mu}(c)). \quad (2.37)$$

This equation is also known as the deterministic version of the so-called model B [102, 112]. Note, that by considering $\mathbf{v} = \mathbf{0}$, we do not discuss the transport of momentum and the associated couplings to fluid flow. The interested reader is referred to Refs. [8, 100, 101, 113].

In the simple case of the Ginzburg-Landau free energy functional F_{GL} given in equation (2.19), the dynamical equation (2.37) reads

$$\partial_t c = \nabla \cdot [\Lambda(c) \nabla (a(c - c_c)^3 - b(c - c_c) - \kappa \nabla^2 c)], \quad (2.38)$$

which is known as the *Cahn-Hilliard equation* [103]. We can use this equation to scrutinize the stability of the homogeneous state, $c(\mathbf{r}) = \bar{c}$, by performing a linear stability analysis. We denote the perturbed state as $c(\mathbf{r}, t) = \bar{c} + \epsilon \exp(i\omega t + i\mathbf{q} \cdot \mathbf{r})$, where ω denotes the perturbation growth rate, \mathbf{q} the perturbation wave vector, and ϵ the associated small amplitude, $|\epsilon| \ll \bar{c}$. To linear order, the growth rate is

$$\omega(\mathbf{q}) = -\mathbf{q}^2 \Lambda(\bar{c}) [3a(\bar{c} - c_c)^2 - b + \kappa \mathbf{q}^2]. \quad (2.39)$$

The homogeneous state is stable if all perturbations decay, i.e., if $\omega(\mathbf{q}) < 0$ for all \mathbf{q} . However, $\omega(\mathbf{q})$ can become positive for small $|\mathbf{q}|$ if $|\bar{c} - c_c| < \sqrt{b/3a}$. This parameter region corresponds to the spinodal decomposition that we found above (figure 2.1). The stability associated with the dynamical equations is therefore consistent with the one derived from the free energy discussed in section 2.2.2.

Beyond the linear regime, equation (2.38) is difficult to solve as it is non-linear and involves fourth order spatial derivatives. However, inside the two coexisting phases and far away from the interface, concentration variations are small, so we can ignore the fourth order derivative and linearize equation (2.37) around the equilibrium concentrations c_1 and c_2 (equation (2.22)). Hence, we arrive at two diffusion equations which are valid inside phase 1 and 2, respectively,

$$\partial_t c \simeq D_\alpha \nabla^2 c, \quad (2.40)$$

where the collective diffusion coefficient inside phase $\alpha = 1, 2$ reads

$$D_\alpha = \Lambda(c_\alpha) f''(c_\alpha). \quad (2.41)$$

Note that D_α is positive when phase separation occurs ($f''(c_\alpha) > 0$) and that an equivalent argument leads to positive diffusivity when phase separation is absent ($f''(\bar{c}) > 0$). In the simple case of the symmetric Ginzburg-Landau free energy given in equation (2.21) and for a constant mobility Λ , the diffusion coefficients are identical in both phases and equal to $D = 2b\Lambda$. Using the expressions corresponding to the lattice model (equation (2.23)), we obtain $D \simeq 2(\chi - 2)\nu \Lambda k_B T$ close to the critical point, which is positive as phase separation occurs only when $\chi > 2$.

2.5. Dynamics of droplets

In this section, we focus on droplets, which are small condensed phases coexisting with a large dilute phase.

2.5.1. Impact of surface tension on the local equilibrium concentrations. One important difference between droplets and the condensed phases that we discussed so far is the curvature of the droplet interface, which is inevitable due to the finite size. The surface tension γ of this curved interface affects the equilibrium concentrations inside and outside the droplet, which we denote by $c_{\text{in}}^{\text{eq}}$ and $c_{\text{out}}^{\text{eq}}$, respectively. In the following, we consider the case where the surface tension γ is constant and independent of the interface curvature, which is valid for droplets large compared to the *Tolman length* [114, 115]. To derive how the equilibrium concentrations depend on the droplet curvature, we write equation (2.31) for a spherical droplet of radius R ,

$$F = V_{\text{d}} f(c_{\text{in}}^{\text{eq}}) + (V - V_{\text{d}}) f(c_{\text{out}}^{\text{eq}}) + 4\pi R^2 \gamma, \quad (2.42)$$

where $V_{\text{d}} = \frac{4\pi}{3} R^3$ denotes the droplet volume and V is the volume of the system. Minimizing the free energy above analogously to section 2.1.3, we obtain the equilibrium conditions

$$0 = f'(c_{\text{in}}^{\text{eq}}) - f'(c_{\text{out}}^{\text{eq}}), \quad (2.43a)$$

$$0 = f(c_{\text{in}}^{\text{eq}}) - f(c_{\text{out}}^{\text{eq}}) + (c_{\text{out}}^{\text{eq}} - c_{\text{in}}^{\text{eq}}) f'(c_{\text{out}}^{\text{eq}}) + \frac{2\gamma}{R}. \quad (2.43b)$$

Comparing these expressions to equations (2.13) in the thermodynamic limit, we find that the pressure balance (2.43b) contains an additional term $2\gamma/R$, which is known as the *Laplace pressure*. Graphically, the Laplace pressure corresponds to the free energy difference of the tangents in the Maxwell construction, see Fig. 2.1(a). The Laplace pressure is proportional to the interface curvature R^{-1} and thus disappears in the thermodynamic limit ($R \rightarrow \infty$).

The conditions (2.43) determine the equilibrium concentrations $c_{\text{in}}^{\text{eq}}$ and $c_{\text{out}}^{\text{eq}}$ inside and outside the droplet, respectively. We derive approximate expressions by expanding $c_{\text{in}/\text{out}}^{\text{eq}} = c_{\text{in}/\text{out}}^{(0)} + \delta c_{\text{in}/\text{out}}$ in equations (2.43) to linear order in $\delta c_{\text{in}/\text{out}}$. Here, $c_{\text{in}}^{(0)}$ and $c_{\text{out}}^{(0)}$ denote the equilibrium concentration in the thermodynamic limit in the condensed and dilute phase, respectively, so $\delta c_{\text{in}/\text{out}}$ captures the effects of Laplace pressure. We find

$$\delta c_{\text{out}} \simeq \frac{2\gamma}{(c_{\text{in}}^{(0)} - c_{\text{out}}^{(0)}) f''(c_{\text{out}}^{(0)}) R}, \quad (2.44a)$$

$$\delta c_{\text{in}} \simeq \frac{f''(c_{\text{out}}^{(0)})}{f''(c_{\text{in}}^{(0)})} \delta c_{\text{out}}, \quad (2.44b)$$

which are known as the *Gibbs-Thomson relations*. Since both expressions are positive, the Laplace pressure elevates the concentrations both inside and

outside the droplet. This effect is stronger for smaller droplets, which becomes explicit when writing the equilibrium concentrations as

$$c_{\text{out}}^{\text{eq}} = c_{\text{out}}^{(0)} \left(1 + \frac{\ell_{\gamma,\text{out}}}{R} \right), \quad (2.45a)$$

$$c_{\text{in}}^{\text{eq}} = c_{\text{in}}^{(0)} \left(1 + \frac{\ell_{\gamma,\text{in}}}{R} \right), \quad (2.45b)$$

where we defined for both phases the *capillary lengths*

$$\ell_{\gamma,\text{out}} = \frac{2\gamma}{(c_{\text{in}}^{(0)} - c_{\text{out}}^{(0)}) f''(c_{\text{out}}^{(0)}) c_{\text{out}}^{(0)}}, \quad (2.45c)$$

$$\ell_{\gamma,\text{in}} = \frac{f''(c_{\text{out}}^{(0)}) c_{\text{out}}^{(0)}}{f''(c_{\text{in}}^{(0)}) c_{\text{in}}^{(0)}} \ell_{\gamma,\text{out}}. \quad (2.45d)$$

In the following, we are interested in the limit of strong phase separation with $c_{\text{in}}^{(0)} \gg c_{\text{out}}^{(0)}$ and thus $\ell_{\gamma,\text{in}} \ll \ell_{\gamma,\text{out}}$. In this case, the impact of the Laplace pressure on the equilibrium concentration inside the droplet can be neglected, i.e., $c_{\text{in}}^{\text{eq}} \simeq c_{\text{in}}^{(0)}$. Since this leaves us with a single capillary length, which we define $\ell_{\gamma} = \ell_{\gamma,\text{out}}$. When the phase outside is dilute, i.e., the chemical potential can be written as $\bar{\mu}(c) \simeq k_{\text{B}} T \ln(\nu c)$ [116], we find

$$\ell_{\gamma} \simeq \frac{2\gamma}{c_{\text{in}}^{(0)} k_{\text{B}} T}. \quad (2.46)$$

If we additionally assume that the condensed phase is highly packed such that $c_{\text{in}}^{(0)} \simeq \nu^{-1}$, equation (2.46) provides a useful estimate of the capillary length when the surface tension γ is known [116]. Using equation (2.34) from our lattice model, the capillary length can also be expressed as $\ell_{\gamma} \simeq \chi^{1/2} (\chi - 2)^{3/2} \nu^{1/3}$. This expression demonstrate that for interaction parameters not too far away from the critical value, $\chi_{\text{b}}^{\text{min}} = 2$, it is typically on the order of the molecular length scale $\nu^{1/3}$. Consequently, we have $\ell_{\gamma} \ll R$ and the increase of the equilibrium concentrations predicted by the Gibbs Thomson relations (2.45) is actually small, supporting the validity of the linear approximation.

2.5.2. Growth of a single droplet in a supersaturated environment. The dynamics of the droplet size and its shape are linked to the movement of its interface, which we assume to be thin compared to the droplet size in the following. To describe the dynamics of the interface, we consider a spherical coordinate system (r, φ, θ) centered on the droplet. Assuming the interface does not deviate strongly from a spherical shape, we parameterize its shape $\mathbf{R}(\varphi, \theta; t) = \mathcal{R}(\varphi, \theta; t) \mathbf{e}_r$ by the radial distance $\mathcal{R}(\varphi, \theta; t)$ as a function of the polar angle φ and the azimuthal angle θ . The movement of the interface is most naturally

described in the local coordinate system spanned by the two tangential directions $\mathbf{e}_1 = \partial \mathbf{R} / \partial \varphi$ and $\mathbf{e}_2 = \partial \mathbf{R} / \partial \theta$ and the outward normal vector $\mathbf{n} = \frac{\mathbf{e}_1 \times \mathbf{e}_2}{|\mathbf{e}_1 \times \mathbf{e}_2|}$. Note that the droplet shape is only affected by the normal component v_n of the interfacial velocity, while the tangential components transport material along the interface. Material conservation implies that this normal component is proportional to the net material flux toward the interface,

$$v_n = \frac{\mathbf{j}_{\text{in}} - \mathbf{j}_{\text{out}}}{c_{\text{in}}^{\text{eq}} - c_{\text{out}}^{\text{eq}}} \cdot \mathbf{n}, \quad (2.47)$$

where $\mathbf{j}_{\text{in}} = \lim_{\epsilon \rightarrow 0} \mathbf{j}(\mathbf{R} - \epsilon \mathbf{n})$ and $\mathbf{j}_{\text{out}} = \lim_{\epsilon \rightarrow 0} \mathbf{j}(\mathbf{R} + \epsilon \mathbf{n})$ are the local material fluxes right inside and outside of the interface, respectively. Expressing the time evolution of the interface in the spherical coordinate system gives $\partial_t \mathbf{R} = \partial_t \mathcal{R} \mathbf{e}_r$, while in the local coordinate system of the interface,

$$\partial_t \mathbf{R} = v_n \mathbf{n} + v_{t,1} \mathbf{e}_2 + v_{t,2} \mathbf{e}_2. \quad (2.48)$$

We can use the connection between the local and the global coordinate system to identify conditions $\partial_t \mathbf{R} \cdot \mathbf{e}_\theta = 0$ and $\partial_t \mathbf{R} \cdot \mathbf{e}_\varphi = 0$, which can be used to obtain the in plane velocity components $v_{t,1}$ and $v_{t,2}$. The radial interface velocity then reads

$$\partial_t \mathcal{R} = v_n \left[1 + \left(\frac{\partial_\theta \mathbf{R}}{R} \right)^2 + \left(\frac{\partial_\varphi \mathbf{R}}{R \sin(\theta)} \right)^2 \right]^{\frac{1}{2}}. \quad (2.49)$$

In the case where the dynamics within the phases are described by the diffusion equation (2.40), the material flux is given by $\mathbf{j} = -D \nabla c$ and equation (2.49) directly determines the time evolution of the interface.

Before we consider shape perturbations in the subsequent chapters, we here focus on a spherical droplet, $\mathcal{R}(\varphi, \theta; t) = R(t)$, in a spherically symmetric system. To derive its growth dynamics, we employ the *quasi-static approximation*, which assumes that the droplet radius varies slowly such that transients in the diffusion equation (2.40) can be neglected. Within this approximation, the diffusion equation (2.40) reduces to a Laplace equation inside and outside the droplet,

$$0 \simeq \nabla^2 c(r) = \frac{1}{r^2} \frac{\partial}{\partial r} \left(r^2 \frac{\partial c}{\partial r} \right), \quad (2.50)$$

where we have written the Laplace operator in spherical coordinates considering that there is no polar and azimuthal dependence of the concentration field. The associated boundary conditions are given by the Gibbs-Thomson relations (2.45) at the droplet interface and no flux conditions at the droplet centre. Moreover, we consider the case where the droplet is embedded in a large system and the concentration far

away is fixed to c_∞ :

$$\partial_r c(r) = 0 \quad \text{at} \quad r = 0, \quad (2.51a)$$

$$\lim_{r \rightarrow \infty} c(r) = c_\infty. \quad (2.51b)$$

Using these boundary conditions the solutions inside and outside the droplet read

$$c(r) = c_\infty + (c_{\text{out}}^{\text{eq}} - c_\infty) \frac{R}{r}, \quad r > R, \quad (2.52a)$$

$$c(r) = c_{\text{in}}^{\text{eq}}, \quad r < R, \quad (2.52b)$$

which are illustrated in figure 2.2(a). These solutions imply that the fluxes $\mathbf{j}_{\text{in}} = \mathbf{0}$ and $\mathbf{j}_{\text{out}} = DR^{-1}(c_{\text{out}}^{\text{eq}} - c_\infty)\mathbf{e}_r$ inside and outside of the interface, respectively. The growth rate of the droplet then follows from equation (2.47),

$$\frac{dR}{dt} = \frac{D c_{\text{out}}^{(0)}}{R c_{\text{in}}^{(0)}} \left(\varepsilon - \frac{\ell_\gamma}{R} \right), \quad (2.53)$$

where we consider the case of strong phase separation ($c_{\text{in}}^{(0)} \gg c_{\text{out}}^{(0)}$). We have defined the *supersaturation*

$$\varepsilon = \frac{c_\infty}{c_{\text{out}}^{(0)}} - 1, \quad (2.54)$$

which measures the excess concentration relative to the equilibrium concentration $c_{\text{out}}^{(0)}$ in the dilute phase. Equation (2.53) shows that the droplet only grows in sufficiently supersaturated environments where $\varepsilon > \ell_\gamma R^{-1}$. The droplet dynamics are thus directly linked to the concentration of droplet material in its environment. In particular, we can define the *critical radius* $R_c = \ell_\gamma \varepsilon^{-1}$, below which the droplet shrinks, see figure 2.2(b). Although this deterministic description cannot account for the spontaneous emergence of droplets, the critical radius is key to estimate the frequency of such nucleation events [117, 118]. In essence, nucleation relies on large fluctuations that spontaneously enrich droplet material in a region of radius R_c . In this case, the resulting droplet starts growing spontaneously according to equation (2.53).

2.5.3. Droplet coarsening by Ostwald ripening. So far, we focused on a single droplet, but most phase separated systems contain many droplets. In such emulsions, large droplets typically grow at the expense of smaller droplets, which vanish eventually. This phenomena is referred to as *Ostwald ripening* [5].

In the following we consider the interactions of many droplets that are far apart from each other in a dilute system with small supersaturation. In this case, nucleation events are rare and the surrounding of droplets can be considered to be spherically symmetric

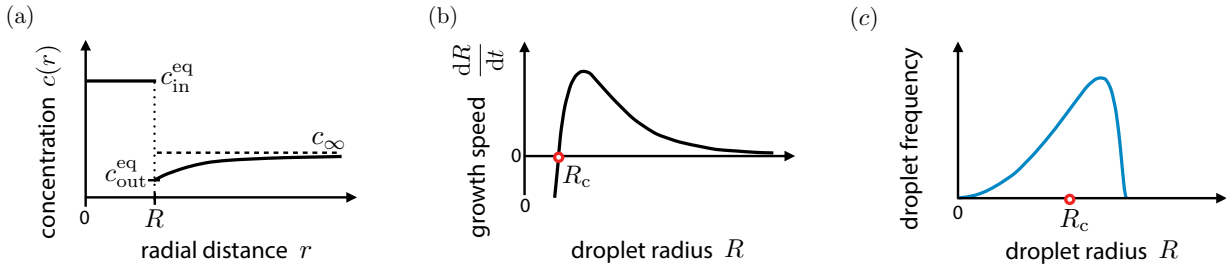


Figure 2.2. (a) Illustration of the concentration field inside and outside of the droplet; see equations (2.52). These concentration fields can be obtained from solving the diffusion equations (2.40) using quasi-static approximation and considering the case of an infinitely thin interface. (b) The droplet growth speed dR/dt is shown as a function of droplet radius R . There is a critical radius $R_c(t) = \ell_\gamma/\varepsilon(t)$ above/below which a droplet grows/shrinks. As the supersaturation $\varepsilon(t)$ decreases with time, the critical radius increases. (c) Frequency of droplets as a function of droplet radius R . As the critical radius increases with time, the distribution broadens. Rescaling the radius by $R_c(t) \propto t^{1/3}$, leads to a collapse of all droplet radius distributions.

with a common concentration c_∞ far away from each droplet. This implies a common supersaturation ε , which depends on time and mediates the interactions between the droplets. As the supersaturation ε can be determined from the total amount of material, the state of the system is fully specified by the radii R_i of the N droplets in the system. Their dynamics follows from equation (2.53) and reads [6]:

$$\frac{dR_i(t)}{dt} = \frac{D c_{\text{out}}^{(0)}}{R_i(t) c_{\text{in}}^{(0)}} \left(\frac{c_\infty(t)}{c_{\text{out}}^{(0)}} - 1 - \frac{\ell_\gamma}{R_i(t)} \right), \quad (2.55a)$$

$$\begin{aligned} \bar{c}V &= c_{\text{in}}^{(0)} \sum_{i=1}^N \frac{4\pi}{3} R_i(t)^3 \\ &+ c_\infty(t) \left[V - \sum_{i=1}^N \frac{4\pi}{3} R_i(t)^3 \right]. \end{aligned} \quad (2.55b)$$

Equation (2.55b) states that the material is shared between the droplets of radius R_i and the dilute phase of concentration $c_\infty(t)$. In order to neglect the spatial correlations between the droplets [119, 120], we assumed that the system volume V is large compared to all droplets, $V \gg \sum_i V_i$ with $V_i = \frac{4\pi}{3} R_i^3$. In this limit, equation (2.55b) can also be approximated as $\bar{c}V \simeq c_{\text{in}}^{(0)} \sum_{i=1}^N V_i(t) + c_\infty(t)V$.

In the limit of many droplets, the system can be described by a continuous droplet size distribution. If additionally the supersaturation is small, Lifshitz and Slyozov [6] demonstrated that this size distribution converges to a universal form

$$\begin{aligned} P(\tilde{R}) &= \frac{4}{9} \tilde{R}^2 \left(1 + \tilde{R}/3 \right)^{-7/3} \\ &\times \left(1 - 2\tilde{R}/3 \right)^{-11/3} \exp \left(-\frac{1}{1 - 2\tilde{R}/3} \right), \end{aligned} \quad (2.56)$$

when normalized by the critical radius R_c , i.e., $\tilde{R} = R/R_c$, irrespective of the initial size distribution, see figure 2.2(c). Since the initial condition is irrelevant,

the critical radius $R_c(t)$ can only depend on the ratio $D\ell_\gamma c_{\text{out}}^{(0)}/c_{\text{in}}^{(0)}$, which is the only kinetic parameter in equations (2.55). As the dimension of $D\ell_\gamma c_{\text{out}}^{(0)}/c_{\text{in}}^{(0)}$ is volume per time, by dimensional analysis, both the critical radius $R_c(t)$ and the mean radius scale as

$$\langle R(t) \rangle \propto \left(\frac{D\ell_\gamma c_{\text{out}}^{(0)}}{c_{\text{in}}^{(0)}} t \right)^{\frac{1}{3}}, \quad (2.57)$$

which is the *Lifshitz-Slyozov scaling law*. In summary, the increasing mean droplet radius and critical radius reflect coarsening dynamics where large droplets grow at the expense of smaller ones.

2.5.4. Droplet coarsening by coalescence. Another coarsening mechanism in emulsions, besides Ostwald ripening, is the coalescence of droplets driven by their Brownian motion [113, 121]. Brownian coalescence is not included in the theory presented here, since we neglected momentum transport and thermal fluctuations. However, the evolution of the mean droplet size due to droplet coalescence can be determined by estimating the change in radius $\Delta\langle R \rangle$ for a typical fusion event and the frequency Δt^{-1} of inter-droplet encounters assuming that most encounters lead to coalescence. Since the droplet volume is conserved during fusion, two equally sized droplet of size $\langle R \rangle$ lead to a change of the mean radius of $\Delta\langle R \rangle \simeq 2^{\frac{1}{3}}\langle R \rangle$. The frequency of inter-droplet encounters can be estimated by the diffusion time leading to $\Delta t^{-1} \simeq D_R/\ell_p^2$, where $D_R = k_B T / (6\pi\eta_R \langle R \rangle)$ is the Stokes-Einstein diffusion constant of a spherical droplet with η_R denoting the viscosity of the surrounding fluid experienced by the droplet of average size $\langle R \rangle$. Moreover, $\ell_p = V / (\pi N \langle R \rangle^2)$ is the mean free path between the droplets, where the droplet number can be estimated as $N \simeq V_{\text{tot}} / (\frac{4\pi}{3} \langle R \rangle^3)$ and the volume occupied by droplets V_{tot} is determined by particle

conservation, i.e., $V_{\text{tot}}/V = (\bar{c} - c_{\text{out}}^{\text{eq}})/(c_{\text{in}}^{\text{eq}} - c_{\text{out}}^{\text{eq}})$. By writing $\langle R \rangle^{-1} d\langle R \rangle/dt \simeq \langle R \rangle^{-1} \Delta \langle R \rangle/\Delta t \simeq k_B T V^2 / (V_{\text{tot}}^2 \eta_R \langle R \rangle^3)$, we obtain a differential equation for the mean radius $\langle R \rangle$, where integration gives the scaling for the mean radius arising from fusion of droplets:

$$\langle R(t) \rangle \propto \left(\left(\frac{c_{\text{in}}^{\text{eq}} - c_{\text{out}}^{\text{eq}}}{\bar{c} - c_{\text{out}}^{\text{eq}}} \right)^2 \frac{k_B T}{\eta_R} t \right)^{\frac{1}{3}}. \quad (2.58)$$

Remarkably, the coarsening due to droplet coalescence has the same scaling with time as the growth of droplets by Ostwald ripening described by equation (2.57).

2.5.5. Comparison between coarsening via Ostwald ripening and coalescence. We can use our lattice model to determine the relative contributions of the two coarsening mechanisms to the growth of droplets. In the case of Ostwald ripening, we have to estimate the molecular diffusion constant D , the capillary length ℓ_γ and the relative dilution of the minority phase, $c_{\text{out}}^{(0)}/c_{\text{in}}^{(0)}$. We use the Stokes-Einstein relationship to express the diffusivity as $D \simeq k_B T / (6\pi\eta_m\nu^{1/3})$, where η_m denotes the fluid viscosity felt by the molecules of volume ν . Moreover, from equations (2.34) and (2.46), the capillary length $\ell_\gamma \simeq \frac{1}{2}\nu^{1/3}\chi^{1/2}(\chi - 2)^{3/2}$. Finally, the binodal line corresponding to our lattice model with equal-size molecules A and B (see end of section 2.1.3) can be used to estimate the relative dilution of the minority phase. It turns out that the fraction between the equilibrium concentrations $c_{\text{out}}^{(0)}/c_{\text{in}}^{(0)} \propto \exp(-\chi)$, i.e., it decreases exponentially to zero as the interaction strength χ becomes large (limit of strong phase separation), while $c_{\text{out}}^{(0)}/c_{\text{in}}^{(0)} \simeq 1 - \sqrt{6(\chi - 2)}$ changes only weakly close to the critical point (weak phase separation). By comparing equation (2.57) to (2.58), we find that Ostwald ripening dominates coarsening if

$$\chi^{\frac{1}{2}}(\chi - 2)^{\frac{3}{2}} \frac{c_{\text{out}}^{(0)}}{c_{\text{in}}^{(0)}} \left(\frac{\bar{c} - c_{\text{out}}^{\text{eq}}}{c_{\text{in}}^{\text{eq}} - c_{\text{out}}^{\text{eq}}} \right)^2 \frac{\eta_R}{\eta_m} \gg 1, \quad (2.59)$$

where we dropped all numerical prefactors. In the simple case of a constant size-independent viscosity, $\eta_m = \eta_R$, our estimates from the simple binary lattice model indicate that coalescence typically dominates Ostwald ripening for most interaction parameters χ . In particular, the left hand side of equation (2.59) goes to zero close to the critical point ($\chi = 2$) and in the limit of strong phase separation ($\chi \rightarrow \infty$). However, for intermediate χ -values, the dominant coarsening mechanism could still be Ostwald ripening because the ratio of the viscosities often satisfies $\eta_R/\eta_m \gg 1$. Such different viscosities are particularly

relevant for condensed phases in polymer or protein solutions, or droplet-like compartments in living cells. These complex, phase separated liquids can even show visco-elastic effects leading to a dramatic slow down of the movements of large droplet-like phases [122–124]. In particular, inside cells, diffusion of very large compartments is strongly suppressed by the cytoskeleton [125], while the diffusion of small molecules may experience less hinderance. We therefore expect that Ostwald ripening is the dominant mechanism of droplet coarsening inside cells since it relies on evaporation and condensation of small diffusing molecules.

3. Positioning of condensed phases

In this chapter, we discuss the positioning of condensed phases (e.g., droplets) by external fields and non-equilibrium concentration gradients. We focus on the case where two components phase separate while a third component, referred to as regulator, influence the phase separation. There are two general scenarios of how the position of a condensed phases can be affected: (i) The position of a condensed phase can be influenced by an external field such as gravitation, electric or magnetic fields [126]. These fields position the phase of higher mass density, larger charge or larger magnetic moment toward regions of lower potential energy. The resulting stationary states correspond to a minimum of the total free energy of the system and are inhomogeneous thermodynamic states. (ii) Positioning of a condensed phase can also be affected by a regulator gradient that is driven and maintained by boundary conditions. The presence of a regulator flux may let the system settle in (stationary) non-equilibrium states. Such a concentration gradient could be generated for example by concentration boundary conditions, or sources and sinks [85], or via position-dependent reaction kinetics with broken detailed balance [127, 128].

In section 3.1, we discuss a simple system of two phase separating components and illustrate how an external field can affect the average position of the phase separated concentration profiles. The corresponding stationary states are inhomogeneous thermodynamic states and can thus be accessed through a minimisation of the free energy. Section 3.2 is then devoted to discuss how a concentration gradient of a regulator can affect the dynamics of droplet position.

3.1. Positioning of condensed phases by external fields

External fields can influence the position of components in a mixture and thereby also the position of condensed phases. In this section, we investigate how

external fields affect a mixture which undergoes phase separation. To this end, we briefly review the thermodynamics with external fields.

3.1.1. Thermodynamics of binary mixtures in external fields. Here we discuss the thermodynamics of binary mixtures in the presence of external fields such as gravitation with a gravitational acceleration g , and electric or magnetic, position-dependent potentials denoted as $U(x)$. The presence of such an inhomogeneous external potential can influence the shape and the mean position of the concentration profiles $c_A(x)$ and $c_B(x)$, which can be defined as

$$x_i = \frac{1}{L} \int_0^L dx x \frac{c_i(x)}{\bar{c}_i}, \quad (3.1)$$

where $\bar{c}_i = L^{-1} \int_0^L dx c_i(x)$ denotes the mean concentration and L is the size of the system.

For a compressible system the binary mixture is described by two concentration fields c_A and c_B . Considering the case where the external fields vary along the x -coordinate, the total free energy density reads

$$f_{\text{tot}} = f(c_A, c_B, \nabla c_A, \nabla c_B) + \rho g x + U_A(x)c_A + U_B(x)c_B. \quad (3.2)$$

The interactions between the components are governed by the free energy density f , $\rho = m_A c_A + m_B c_B$ is the mass density, and m_A and m_B denote the molecular mass of each component. The contributions of the external potentials can be combined to $\tilde{U}_A(x)c_A + \tilde{U}_B(x)c_B$, where $\tilde{U}_i(x) = U_i(x) + m_i g x$, $i = A, B$.

Thermodynamic equilibrium for systems with external fields can be defined at each position. The position-dependent equilibrium profile $c_i(x)$ is then determined by a spatially constant generalised chemical potential, $\mu_{\text{tot},i} = \mu_i + \tilde{U}_i(x)$, where $\mu_i = \delta F / \delta c_i$ with $F = \int d^3x f$. As an example for such a position-dependent equilibrium profile we consider an incompressible system ($\nu_A c_A + \nu_B c_B = 1$) with gravitation as the only external potential and where the A -molecules are dilute, $\nu_A c_A \ll 1$ [126]. The generalised exchange chemical potential then reads $\bar{\mu}_{\text{tot}} \simeq k_B T \ln(\nu c_A) + \nu_A \Delta \rho g x$ with the density difference $\Delta \rho = m_A / \nu_A - m_B / \nu_B$. At thermodynamic equilibrium, this gives the barometric height formula, $c_A(x) \propto \exp(-\Delta \rho \nu_A g x / (k_B T))$. Thus gravitation always positions the molecules of highest mass density toward the lower gravitational potential. A similar result occurs if the binary mixture phase separates. In this case the condensed phase of larger mass density is positioned toward the region of lower gravitational potential. However, for fixed difference in mass density and gravitational potential, there is no way

to switch the concentration profiles or the position of the condensed phases with respect to gravitation. In order to create a possibility to switch the position of condensed phases, we ask what happens if an additional component that affects phase separation is added to the system and subject to an external potential? Specifically, we wonder what are the stationary concentration profiles and which physical parameters control their positions?

3.1.2. Positioning of condensed phases by a regulator potential. To explore the propensity to switch the position of condensed phases using such an additional component we propose a simple ternary model. This model accounts for the demixing of two components, A and B , and a regulator component R that interacts with the other components and thereby affects phase separation between A and B . The regulator component R is influenced by an external potential $U(x)$. Interactions between the components i and j are captured by the mean-field interaction parameters χ_{ij} . The scenario of regulation of phase separation can be described by the following free energy density

$$f_{\text{tot}} = k_B T \left[\sum_{i=A,B,R} c_i \ln(\nu c_i) + \chi_{AB} \nu c_A c_B + c_R (\chi_{BR} c_B + \chi_{AR} c_A) \nu \right] + U(x) c_R + \frac{\kappa_R}{2} |\nabla c_R|^2 + \frac{\kappa_A}{2} |\nabla c_A|^2, \quad (3.3)$$

which is a Flory-Huggins free energy density [3, 4] for three components. Analogously to the case of the binary system discussed in section 2.1, the ternary free energy given above can be derived from a partition sum using a mean-field approximation [129, 130]. In equation (3.3) we consider an incompressible system where the molecular volumes are constant and equal to ν for all components, and the concentrations thus obey $c_B = \nu^{-1} - c_R - c_A$. The logarithmic terms in equation (3.3) correspond to entropic contributions related to the number of possible configurations. The remaining contributions characterise the interactions between the three components with the (dimensionless) mean field interaction parameter χ_{ij} , also referred to as Flory-Huggins interaction parameter. The interaction parameter between A and B , χ_{AB} , determines the tendency of A and B to phase separate. The two terms in equation (3.3) proportional to the regulator concentration c_R describe the interactions between the regulator R and the demixing components A and B . To ensure that R acts as a regulator we choose these interaction parameters such that the regulator R does not demix from A or B . The terms in equation (3.3)

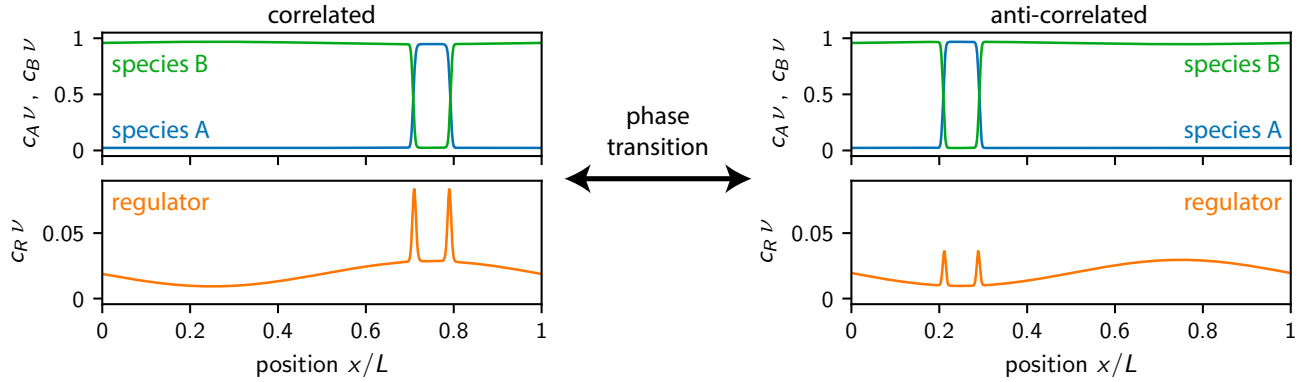


Figure 3.1. Spatial regulation of phase separation in an external potential by a discontinuous phase transition. The regulator forms a spatially inhomogeneous profile due to an external potential. As the interactions with the regulator are changed, the spatial distribution of component A switches from a spatially correlated (left) to an anti-correlated (right) distribution with respect to the regulator. The switch corresponds to a discontinuous phase transition.

with spatial derivatives represent contributions to the free energy associated with spatial inhomogeneities \ddagger .

In the following we consider a periodic system with a periodic potential $U(x)$ that varies solely along the x -coordinate. We choose a potential that affects the distribution of the regulator component of the form

$$U(x) = -k_B T \ln(1 - Q \sin(2\pi x/L)), \quad (3.4)$$

where $Q > 0$ characterises the strength of the potential and L denotes the size of the system along the x -direction.

In the case where the components A and R are dilute, $\nu \bar{c}_A \ll 1$ and $\nu \bar{c}_R \ll 1$, and for very strong external potentials (large Q), the profile of the regulator component is solely given by the external potential $U(x)$ with $c_R(x) \propto \sin(2\pi x/L)$. Thus the regulator profile has one minimum and one maximum in the periodic domain. The interaction of such a regulator profile with the components A and B causes a positional dependence of their concentration profiles. We would like to understand how these interactions affect the system if A and B phase separate.

For simplicity, we also consider a one dimensional system of size L in the absence of boundaries. In this one dimensional system the periodic boundary conditions are $c_i(0) = c_i(L)$ and $c'_i(0) = c'_i(L)$, where the primes denote spatial derivatives. For the considered case of an external potential $U(x)$ varying only along the x -coordinate, the restriction to a one dimensional, phase separating system represents a valid approximation for large system sizes, where the interface between the condensed phases becomes flat.

3.1.3. Minimisation of free energy. To find the equilibrium states in a phase separating system in the

\ddagger We neglected a mixed term proportional to $\nabla c_A \cdot \nabla c_B$ since it has only little quantitative impact on the spatial profiles of the phase separated profiles [131].

presence of a regulator gradient induced by the external potential $U(x)$, we determine the concentration profiles $c_i(x)$ of all components $i = A, B, R$ by minimising the total free energy (equation (3.3); see Ref. [131]). Due to particle number conservation, there are two constraints for the minimisation imposing $\bar{c}_i = L^{-1} \int_0^L dx c_i(x)$ for $i = A, R$, where \bar{c}_i are the average concentrations and $\bar{c}_B = \nu^{-1} - \bar{c}_A - \bar{c}_R$. Variation of the total free energy with the constraints of particle number conservation implies ($i = A, R$):

$$0 = \int_0^L dx \left(\frac{\partial f_{\text{tot}}}{\partial c_i} - \frac{d}{dx} \frac{\partial f_{\text{tot}}}{\partial c'_i} + \lambda_i \right) \delta c_i + \kappa_i \delta c_i c'_i \Big|_0^L, \quad (3.5)$$

where λ_R and λ_A are Lagrange multipliers and the δc_i is the variation of the concentration corresponding to component i . The boundary term in equation (3.5) is zero in case of periodic boundary conditions. Using the explicit form of the free energy density (equation (3.3)), a set of Euler-Lagrange equations can be derived from equation (3.5) [131]. These equations can be solved numerically using a finite difference solver. As control parameters we consider the three interaction parameters χ_{AR} , χ_{AB} and χ_{BR} , the strength of the external potential Q and the mean concentration of A -material, \bar{c}_A . The mean concentration of the regulator material is fixed to a small volume fraction $\nu \bar{c}_R = 0.02$ in all presented studies to avoid phase separation of the regulator. Moreover, we focus on the limit of strong phase segregation, where the interfacial width determined by κ_A are small compared to the system size. We verified that our results depend only weakly on the specific values of κ_A and κ_R .

3.1.4. Discontinuous switching of average position of phase separated concentration profiles in external fields. Solving the Euler-Lagrange equations, we find two extremal profiles of the phase separating component

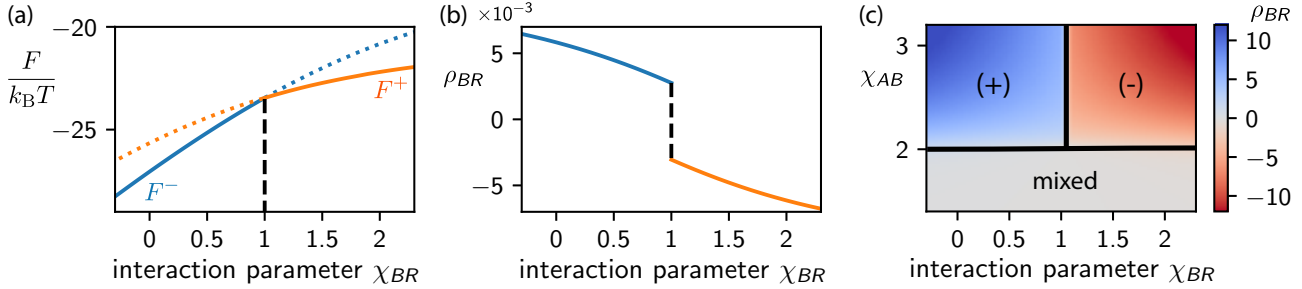


Figure 3.2. Discontinuous phase transition of a ternary phase separating systems in a periodic potential and with periodic boundary conditions. (a) Free energy F as a function of the B - R interaction parameter χ_{BR} . F^- and F^+ are the free energies of the correlated and anti-correlated stationary solution with respect to the regulator gradient, respectively. Lines are dashed when solutions are metastable. At χ_{BR}^* , F^- and F^+ intersect and the solution of minimal free energy exhibits a kink. This shows that the transition between correlation and anti-correlation is a discontinuous phase transition. (b) The order parameter ρ_{BR} corresponding to the solution of minimal free energy jumps at χ_{BR}^* . (c) Phase diagrams of our ternary model for spatial regulation in a periodic potential and periodic boundary conditions ($\nu\bar{c}_A = 0.1$). The color code depicts the order parameter ρ_{BR} . Component B is spatially correlated (+) with the regulator profile if $\rho_{BR} > 0$, and anti-correlated (-) otherwise. When the system is mixed, $\rho_{BR} \approx 0$, and spatial profiles of all components are only weakly inhomogeneous (no phase separation). The black lines corresponds to the transition where the free energy has a kink. Parameters for (a-c): $\chi_{AR} = 1$, $\nu\bar{c}_A = 0.5$, $\nu\bar{c}_R = 0.02$, $\kappa_R/(k_B T \nu L^2) = 7.63 \cdot 10^{-5}$, $\kappa_A/(k_B T \nu L^2) = 6.10 \cdot 10^{-5}$, $Q = 0.5$. For (a) and (b), $\chi_{AB} = 4$. For plotting, $\nu = L/256$ was chosen.

A , $c_A^-(x)$ and $c_A^+(x)$, and two corresponding profiles of the regulator component R , denoted as $c_R^-(x)$ and $c_R^+(x)$ (the profile of B follows from number conservation). The phase separating material A can be accumulated at larger regulator concentration and correlates (+) with the concentration of the regulator material (figure 3.1(a)). The corresponding solutions are $c_A^+(x)$ and $c_R^+(x)$. Alternatively, the A -material accumulates at smaller regulator concentrations ($c_A^-(x)$ and $c_R^-(x)$) corresponding to an anti-correlation (-) with respect to the regulator profile (figure 3.1(b)). The free energies of the correlated and the anti-correlated states, $F^+ = F[c_A^+, c_R^+]$ and $F^- = F[c_A^-, c_R^-]$, are different for most interaction parameters. The free energies only intersect at one point $\chi_{BR} = \chi_{BR}^*$ (figure 3.2(a)). At this point the minimal free energy exhibits a kink. This means that the system undergoes a *discontinuous phase transition* when switching between a spatially anti-correlated (-) and a spatially correlated (+) solution with respect to the regulator.

To study this phase transition the appropriate set of order parameters can be defined from the changes of the free energy upon varying the interaction parameters (see figure 3.2):

$$\rho_{ij} = (k_B T \mathcal{N}_{ij} \nu L)^{-1} \frac{d}{d\chi_{ij}} \Delta F(c_i(x), c_j(x)), \quad (3.6)$$

where $\Delta F(c_i(x), c_j(x)) = F(c_i(x), c_j(x)) - F(\bar{c}_i, \bar{c}_j)$. The normalisation \mathcal{N}_{ij} is chosen such that $-1 < \rho_{ij} < 1$. When inserting equations (3.3), the order parameter ρ_{ij} becomes the covariance,

$$\rho_{ij} = (\mathcal{N}_{ij} L)^{-1} \int_0^L dx (c_i(x) c_j(x) - \bar{c}_i \bar{c}_j), \quad (3.7)$$

which characterises the spatial correlation between the concentration profiles $c_i(x)$ and $c_j(x)$. If the fields are spatially correlated (+), $\rho_{ij} > 0$, and if they are anti-correlated (-), $\rho_{ij} < 0$, and $\rho_{ij} = \pm 1$ if the concentration profiles of component i and j follow spatially correlated or anti-correlated step functions. If the regulator is homogeneous, $c_R(x) = \bar{c}_R$, the order parameter is zero, $\rho_{iR} = 0$ for $i = A, B$.

Varying the interaction parameter χ_{BR} (figure 3.2(b)), the order parameters ρ_{BR} and ρ_{AR} jump at the threshold value χ_{BR}^* . The jump of both order parameters in the presence of a regulator gradient indicates that the spatial correlation of A and B with respect to R changes abruptly, which is expected in case of a first order phase transition.

By means of the order parameter ρ_{BR} (equation (3.7)) we can now discuss the phase diagrams as a function of the interaction parameters. In the case of a spatial correlation (+), we have $\rho_{ij} > 0$, while for an anti-correlation (-), $\rho_{ij} < 0$. We thus find three regions (figure 3.2(c)): A mixed region, where concentration profiles are only weakly inhomogeneous and no phase separation occurs, and two additional regions, where components A and B phase separate and A is spatially correlated or anti-correlated with the regulator R , respectively. There exists a triple point where all three states have the same free energy.

In summary, the presence of a concentration gradient in phase separating systems leads to equilibrium states of different spatial correlation with the regulator profile. The regulator gradient creates a bias in the position of the phase separated concentration profiles for almost all parameters in the phase diagram. If the external potential acting on the regulator has exactly one minimum and one maximum, there are two station-

ary states with different mean positions of the phase separating material. One of these stationary states corresponds to a global minimum of the free energy while the other state is only locally stable. The parameters characterising the interactions between the regulator and the phase separating material determine whether a state is stable or not. There is a *discontinuous phase transition* between both states upon changing these interaction parameters.

For simplicity we discussed a phase separating system which is inhomogeneous in one dimension. Preliminary Monte-Carlo studies in three dimensions with phase separated droplets in a regulator gradient suggest that the position of droplets can be switched in a discontinuous manner [132].

3.2. Dynamics and coarsening of droplets in concentration gradients

In this section we discuss the dynamics of multiple droplets in a one-dimensional gradient of a regulator component that affects the phase separation of droplets. For simplicity, we consider the case where the regulator profile is not affected by the phase separation components. Given a regulator gradient $c_R(x)$ we introduce a set of physical quantities such as the position dependent supersaturation, which determine the inhomogeneous ripening dynamics. These quantities depend on position and will be used to develop a generic theory of droplet ripening in concentration gradients. This theory extends the classical laws of droplet growth derived by Lifschitz & Slyozov [6] and can explain the positioning of droplets in concentration gradients by droplet drift and spatially dependent growth.

3.2.1. Spatially varying supersaturation. Here we discuss the ripening dynamics of droplets in a regulator gradient that varies only along the x -coordinate. To this end, we modify the concept of a common far field concentration introduced in section 2.5.3 to a concentration field $c_\infty(x)$ that changes on the length scale of the system size L .

In the absence of a regulator gradient, the concentration outside approaches the “far field” of the droplet, c_∞ , as the distance to the droplet interface increases. The far field is created by the surrounding droplets and is well reached if the length scale corresponding to the mean distance ℓ between droplets exceeds the droplet radius R , i.e., $\ell \gg R$.

In the presence of a regulator gradient varying along the x -coordinate, the far field seen by the droplet $c_\infty(x)$ is now also position dependent and can be

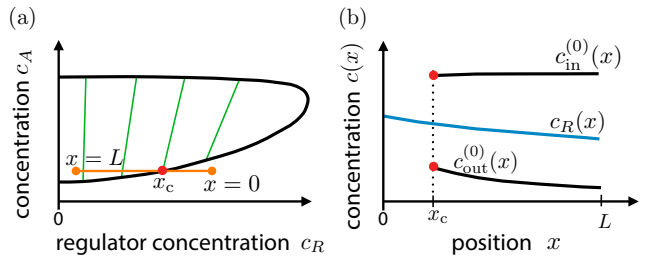


Figure 3.3. (a) Sketch of a ternary phase diagram as a function of the homogenous regulator concentration c_R and the droplet material concentration c_A . The tie lines (green) connect the equilibrium concentration values of the coexisting phases. Each position x of a system subject to a different regulator gradient (e.g. blue line in (b)) may correspond to a point in the phase diagram along the orange line. If the position is inside the phase separation region, droplets can form, while outside phase separation is absent. The position x_c marks the location below which there is no phase separation and vice versa. (b) Sketch of a representative regulator gradient $c_R(x)$ (blue) and the equilibrium concentration $c_{in}^{(0)}(x)$ and $c_{out}^{(0)}(x)$ obtained from the phase diagram (a).

approximately written as:

$$c_\infty(x) \simeq \frac{1}{L_y L_z} \int_0^{L_y} dy \int_0^{L_z} dz c_{out}(x, y, z), \quad (3.8)$$

where $c_{out}(x, y, z)$ is the concentration field outside the droplets and L_y and L_z denote the system size in the y and z -direction, respectively. The expression above is an approximation as we have neglected weak concentration perturbations close to droplet interfaces described by the Gibbs Thomson relationship (2.45). However, for the typical case of droplet radii exceeding the capillary length ($R \gg \ell_\gamma$) and the mean interdroplet distance being larger than the droplet size ($\ell \gg R$), these concentration perturbations are very small (see section 2.5.1).

Finally, to make sure that the spatial variations of the position dependent far field are large on the system size but comparably small on the droplet scale, we consider the case where all these length scales separate, $\ell_\gamma \ll R \ll \ell \ll L$. This separation of length scales will allow us to investigate weak perturbations of the droplet shape parallel to the concentration gradient and also to construct the equilibrium concentration at each position x along the gradient.

The separation of length scales suggests to divide the system into independent slices of a size corresponding to the intermediate length scale ℓ . The phase separation dynamics can then be discussed locally for each position x corresponding to a slice element of linear length ℓ . For this discussion, we consider a simplified model with a free energy density given by equation (3.3) and calculate the corresponding phase diagram (figure 3.3(a)). Each position x maps

on a single point in the phase diagram because the regulator profile is fixed and the droplet material is roughly constant. The corresponding curve in the phase diagram due to the spatial dependence of the regulator defines local values of the equilibrium concentrations inside and outside of the droplet (figure 3.3(b)). In other words, droplets in the slice corresponding to the position x feels the local equilibrium concentrations, $c_{\text{in}}^{(0)}(x)$ and $c_{\text{out}}^{(0)}(x)$. For simplicity, we restrict ourselves to a special case where the equilibrium concentration inside is position independent, $c_{\text{in}}^{(0)}(x) \simeq c_{\text{in}}^{(0)}$, thus droplet growth is solely determined by the conditions outside of the droplet. Moreover, as concentration inhomogeneities are in general weak, we do not consider weak transients of $c_{\text{out}}^{(0)}(x)$ due to the space and time varying $c_{\infty}(x)$. The actual concentration of droplet material outside, $c_{\infty}(x)$, together with the equilibrium concentration outside, $c_{\text{out}}^{(0)}(x)$, determine a spatially dependent supersaturation

$$\varepsilon(x) = \frac{c_{\infty}(x)}{c_{\text{out}}^{(0)}(x)} - 1. \quad (3.9)$$

There is a dissolution boundary with position $x = x_c$ at which the supersaturation is zero, $\varepsilon(x_c) = 0$. In the illustration in figure 3.3(a), the fluid is mixed for $x < x_c$, while droplets can form ($\varepsilon > 0$) for $x > x_c$. In the absence of droplets, the concentration field $c_{\infty}(x)$ evolves in time satisfying a diffusion equation, which we will derive in the next section. When droplets are nucleated, their local dynamics of growth or shrinkage is guided by the local supersaturation $\varepsilon(x)$ as well as $c_{\text{out}}^{(0)}(x)$ (see section 2.5.3). This local droplet dynamics then in turn also influences the concentration field $c_{\infty}(x)$. As time proceeds, diffusion of droplet material occurs on length scales larger than the intermediate length scale ℓ . For this regime, we will derive a dynamical theory and extend the Lifschitz & Slyozov theory to concentration gradients.

3.2.2. Dynamics of a single droplet in a concentration gradient. A regulator concentration gradient generates a position-dependent equilibrium concentration $c_{\text{out}}^{(0)}(x)$ and a position-dependent supersaturation $\varepsilon(x)$ (equation (3.9)). This supersaturation will drive the droplet dynamics and lead to a position-dependent growth, drift of droplets and even deformations of their shape. In the following we discuss the dynamics of growth of a single droplet where the equilibrium concentration, $c_{\text{out}}^{(0)}(x)$, and the concentration of droplet material, $c_{\infty}(x)$, are position dependent. The case of multiple droplets is studied in the next section.

The concentration inside the droplet can be approximated by the equilibrium concentration $c_{\text{in}}^{\text{eq}} \simeq$

$c_{\text{in}}^{(0)}$ in the limit of strong phase separation ($c_{\text{in}}^{(0)} \gg c_{\text{out}}^{(0)}$; see section 2.5.1). This allows us to restrict the analysis to the concentration field $c(r, \theta, \varphi)$ outside of a droplet. Here, we use spherical coordinates centred at the droplet position x_0 , with r denoting the radial distance from the centre, and θ and φ are the azimuthal and polar angles relative to the x -axis. Within the quasi-stationary approximation (see section 2.5.2) the concentration outside but near the droplet obeys the steady state of a diffusion equation (2.50). For large r the concentration field approaches the “far field” which in the presence of a linear gradient reads (figure 3.4):

$$c_{\infty} \simeq \lim_{r \rightarrow \infty} c(r, \theta, \varphi) = \alpha + \beta r \cos \theta. \quad (3.10)$$

This inhomogeneous far field concentration is locally (with respect to inter-droplet distance ℓ) characterised by the concentration $\alpha = c_{\infty}(x_0)$ and the gradient $\beta = \partial_x c_{\infty}(x)|_{x_0}$ at the position of the droplet x_0 . At the surface of the spherical droplet, $r = R$, the boundary condition is

$$c(R, \theta, \varphi) = c_{\text{out}}^{\text{eq}}(\theta) \simeq \left(c_{\text{out}}^{(0)} + R \cos(\theta) \partial_x c_{\text{out}}^{(0)}(x)|_{x_0} \right) (1 + \ell_{\gamma}/R). \quad (3.11)$$

Here, ℓ_{γ} is the capillary length as introduced in section 2.5.1. Equation (3.11) corresponds to the Gibbs-Thomson relation (see section 2.5.2), which describes the increase of the local concentration at the droplet interface relative to the equilibrium concentration due to the surface tension of the droplet interface. The presence of spatial inhomogeneities on the scale of the droplet R lead to an additional term in the Gibbs-Thomson relation. To linear order, this contribution to $c_{\text{out}}^{\text{eq}}$ reads $R \cos(\theta) \partial_x c_{\text{out}}^{(0)}(x)|_{x_0}$. The values of β and α characterising the far field, $c_{\infty}(x_0)$, together with the local equilibrium concentration at the droplet surface, $c_{\text{out}}^{\text{eq}}(\theta)$, determine the local rates of growth or shrinkage of the drop at $x = x_0$ in a spatially inhomogeneous regulator gradient.

The solution to the stationary diffusion equation (2.50) is of the form $c(r, \theta) = \sum_{i=0}^{\infty} (A_i r^i + B_i r^{-i-1}) P_i(\cos \theta)$, where $P_i(\cos \theta)$ are the Legendre polynomials. Using the boundary conditions (3.10) and (3.11), we find

$$c(r, \theta) = \alpha \left(1 - \frac{R}{r} \right) + \beta \cos \theta \left(r - \frac{R^3}{r^2} \right) + \left(c_{\text{out}}^{(0)} + R \cos(\theta) \partial_x c_{\text{out}}^{(0)}(x)|_{x_0} \right) \left(1 + \frac{\ell_{\gamma}}{R} \right) \frac{R}{r}. \quad (3.12)$$

The droplet could grow, drift or deform due to normal fluxes of droplet material at the interface leading to a movement of the interface. The speed normal to the interface reads $v_n = \mathbf{n} \cdot \mathbf{v}_n$, where \mathbf{n} denotes the normal vector to the interface. In case of a spherical droplet,

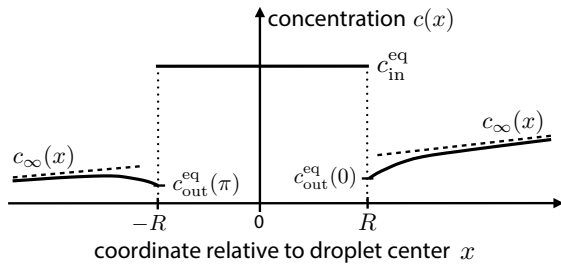


Figure 3.4. Sketch of the concentration field inside and outside of a droplet in a position-dependent supersaturation field. The droplet center is located at $x = 0$. The equilibrium concentration inside is $c_{\text{in}}^{\text{eq}}$. Right outside the droplet at $\pm R$ the concentration is given by the Gibbs-Thomson relation $c_{\text{out}}^{\text{eq}}$ (equation (3.10)). Far away from the droplet center, the concentration approaches $c_{\infty}(x)$ (equation (3.11)).

$\mathbf{n} = \mathbf{e}_r$, where \mathbf{e}_r is the radial unit vector in spherical coordinates. In the limit of strong phase separation, i.e., $c_{\text{in}}^{(0)} \gg c_{\text{out}}^{(0)}$, $c_{\text{in}}^{(0)} \simeq c_{\text{out}}^{\text{eq}}$, and the velocity normal to the interface, v_n (equation (2.47)), can be expressed by $v_n \simeq \mathbf{n} \cdot (\mathbf{j}_{\text{in}} - \mathbf{j}_{\text{out}})/c_{\text{in}}^{(0)}$. For weak spatial variations inside and outside of the droplet, the local flux is defined as $\mathbf{j} = -D\nabla c$. The concentration inside the droplet is approximately constant and for simplicity we consider it to be independent of the droplet position. Thus the flux inside the droplet vanishes, $\mathbf{j}_{\text{in}} = 0$, while the flux outside reads $\mathbf{j}_{\text{out}} = -D\nabla c|_R$.

Now we discuss how the normal speed v_n can be used to calculate the droplet growth speed v_0 , the droplet drift velocity v_1 , and the rate of deformations from the spherical shape, v_2 . To this end, we parametrise the surface of the droplet in terms of Legendre polynomials \S , which gives $\mathcal{R}(\theta, t) = \sum_i d_i(t) P_i(\cos \theta)$, where $d_i(t)$ are the expansion coefficients characterising the shape of the interface. The corresponding interface velocity of an approximately spherical droplet is $v_n \simeq \partial_t \mathcal{R}(\theta, t) = \sum_i v_i(t) P_i(\cos \theta)$, where the speeds for droplet growth, drift and deformations along the regulator gradient read $v_i(t) = \partial_t d_i(t)$. We can now identify the radius R as $d_0 = \langle \mathcal{R}, P_0 \rangle / \langle P_0, P_0 \rangle$, the position of the droplet center x_0 as $d_1 = \langle \mathcal{R}, P_1 \rangle / \langle P_1, P_1 \rangle$, and the deformations are characterised by $d_2 = \langle \mathcal{R}, P_2 \rangle / \langle P_2, P_2 \rangle$. Here, the brackets indicate the scalar product $\langle h, g \rangle = \int_0^\pi d\theta \sin \theta h g$ between the functions g and h . Most importantly, we can identify $v_0 = dR/dt$ as the rate of change of the radius and $v_1 = dx_0/dt$ as the drift velocity of the droplet center.

Using equation (3.12), we find for the droplet

\S Since $c(r, \theta)$ (equation (3.12)) does not depend on the polar angle φ , it is sufficient to expand in terms of the Legendre polynomials $P_n(\cos \theta)$; otherwise, one could use spherical harmonics.

growth speed

$$\frac{dR}{dt} = \frac{D}{c_{\text{in}}^{(0)} R} \left[\alpha - c_{\text{out}}^{(0)}(x_0) \left(1 + \frac{\ell_\gamma}{R} \right) \right]. \quad (3.13)$$

In the presence of concentration gradients there also exists a net droplet drift speed \parallel ,

$$\frac{dx_0}{dt} = \frac{D}{c_{\text{in}}^{(0)}} \left[3\beta - \partial_x c_{\text{out}}^{(0)}(x)|_{x_0} \left(1 + \frac{\ell_\gamma}{R} \right) \right]. \quad (3.14)$$

Note that both the growth rate and the drift speed are proportional to the molecular diffusion constant D of droplet material.

If the far field $c_{\infty}(x)$ is well parametrised by a linear gradient (equation (3.10)), there are no deformations from the spherical shape, $v_2 = 0$. Deformations of the spherical shape can only occur if higher order polynomials $P_n(\cos \theta)$ with $n \geq 2$ are necessary to describe the far field. If we include the quadratic order in the parametrisation of the far field (equation (3.10)), $(r \cos \theta)^2 \partial_x^2 c_{\infty}(x)|_{x_0}$, the deformation speed reads $v_2 = (10/3)(RD/c_{\text{in}}^{(0)}) \partial_x^2 c_{\infty}(x)|_{x_0}$. This quadratic contribution does not affect the droplet drift v_1 but the growth law v_0 is changed. The quadratic term gives an extra contribution inside the brackets of equation (3.13) of the form $(5/3)R^2 \partial_x^2 c_{\infty}(x)|_{x_0}$. Thus, shape deformations and their impact on the growth law in the case of a non-linear far field gradient are negligible if

$$\frac{5\partial_x^2 c_{\infty}(x)|_{x_0}}{3c_{\infty}(x)|_{x_0}} R^2 \ll 1. \quad (3.15)$$

For the system under consideration where length scales separate, i.e., $R \ll \ell \ll L$, deformations from the spherical shape can be neglected. In recent numerical studies considering a continuous phase separating Flory-Huggins model in a regulator gradient maintained by sink and source terms, droplet deformations are indeed visible when droplets approach the size of the system [85].

3.2.3. Dynamics of multiple droplets in a concentration gradient. We can now describe the dynamics of many droplets, $i = 1, \dots, N$, with positions x_i and radii R_i . If droplets are far apart from each other, the rate of growth of droplet i reads

$$\frac{dR_i}{dt} = \frac{D}{R_i} \frac{c_{\text{out}}^{(0)}(x_i)}{c_{\text{in}}^{(0)}} \left[\varepsilon(x_i) - \frac{\ell_\gamma}{R_i} \right]. \quad (3.16a)$$

\parallel In contrast to Ref. [31], we found an additional factor of 3 in front of the coefficient β .

The drift velocity of droplet i , $v_1(x_i) = dx_i/dt$, is

$$\frac{dx_i}{dt} = \frac{D}{c_{\text{in}}^{(0)}} \left[3\partial_x c_{\infty}(x)|_{x_i} - \partial_x c_{\text{out}}^{(0)}(x)|_{x_i} \left(1 + \frac{\ell_{\gamma}}{R_i} \right) \right]. \quad (3.16b)$$

If the distance between droplets is large relative to their size, droplets only interact via the far field concentration field $c_{\infty}(x, t)$. It is governed by a diffusion equation including gain and loss terms associated with growth or shrinkage of drops:

$$\begin{aligned} \partial_t c_{\infty}(x, t) &= D \frac{\partial^2}{\partial x^2} c_{\infty}(x, t) & (3.16c) \\ &- H(t) \sum_{i=1}^N \delta(x_i - x) \frac{4\pi}{3} \frac{d}{dt} R_i(t)^3, \end{aligned}$$

where the time-dependent function

$$H(t) = \frac{c_{\text{in}}^{(0)} - c_{\infty}(t)}{V - \sum_{i=1}^N \delta(x_i - x) \frac{4\pi}{3} R_i(t)^3} \quad (3.17)$$

is approximately constant, $H \simeq c_{\text{in}}^{(0)}/V$ in the limit of strong phase separation $c_{\text{in}}^{(0)} \gg c_{\infty}(t)$ and for very large inter-droplet distances corresponding to $V \gg \sum_{i=1}^N \delta(x_i - x) \frac{4\pi}{3} R_i(t)^3$ with V .

Equation (3.16c) describes the effects of large scale spatial inhomogeneities on the ripening dynamics for the case of a regulator gradient varying along the x -axis. Since large scale variations of $c_{\infty}(x, t)$ only build up along the x -directions, derivatives of c_{∞} along the y and z directions do not contribute as c_{∞} and $c_{\text{out}}^{(0)}$ are constant along these directions.

In the absence of a regulator gradient, $c_{\text{out}}^{(0)}$ and c_{∞} are constant in space implying a position-independent and common supersaturation level ε for all droplets (equation (3.9)). In this case equation (3.16a) gives the classical law of droplet ripening derived by Lifschitz-Slyozov [6, 7] (also referred to as Ostwald ripening), and the net drift vanishes (equation (3.16b)). In the case of Ostwald ripening, droplets larger than the critical radius $R_c = \ell_{\gamma}/\varepsilon$ grow at the expense of smaller shrinking drops which then disappear. This causes an increase of the average droplet size and a broadening of the droplet size distribution with time. Ostwald ripening is characterised by a supersaturation that decreases with time, leading to an increase of the critical droplet radius $R_c = \ell_{\gamma}/\varepsilon(t) \propto t^{1/3}$. The droplet size distribution $P(R)$ exhibits an universal shape and is nonzero only in the interval $[0, 3R_c/2]$ (figure 3.5(b), blue graph). In other words, there are no droplets larger than $3R_c/2$ and thus also no droplets exist beyond the maximum of dR/dt at $R = 2R_c$ where larger droplet could grow slower. Therefore, in homogeneous systems the broadening of $P(R)$ follows from larger droplets growing at a larger rate dR/dt

than smaller droplets. And because all droplets feel the same supersaturation level droplet positions remain homogeneously distributed in the system.

In the presence of a regulator gradient the droplet dynamics exhibits a different behaviour. First of all, there are two novel possibilities of how droplet material is transported: There is exchange of material between droplets at different positions along the concentration gradient due to a *position dependent droplet growth*, and *droplets can drift* along the concentration gradient.

Droplets grow or shrink with rates that vary along the gradient because the local equilibrium concentration $c_{\text{out}}^{(0)}(x)$ and the far field concentration $c_{\infty}(x)$ are position dependent (equation (3.16a)). For a supersaturation $\varepsilon(x) = c_{\infty}(x)/c_{\text{out}}^{(0)}(x) - 1 > \ell_{\gamma}/R$, a droplet located at position x grows, and shrinks in the opposite case. In other words, the critical droplet radius depends on position, and droplets with radii below or above $R_c(x) = \ell_{\gamma}/\varepsilon(x)$ shrink or grow.

The drift of a droplet (equation (3.16b)) results from an asymmetry of material flux at the interface parallel to the regulator gradient. For the case where $3|\partial_x c_{\infty}(x)| < |\partial_x c_{\text{out}}^{(0)}|$, the droplet drift velocity v_1 points toward regions of smaller $c_{\text{out}}^{(0)}(x)$. This situation corresponds to a typical scenario since the gradient of droplet material $\partial_x c_{\infty}(x)$ tends to flatten with time due to the diffusion of droplet material in the dilute phase.

3.2.4. Narrowing of the droplet size distribution. Numerically solving equations (3.16) for a large number of droplets we find that the droplet size distribution narrows during the positioning of droplets toward one boundary of the system. For details on the numerics, please refer to reference [31]. This narrowing of the droplet size distribution in a concentration gradient is fundamentally different from the broadening of the droplet size distributions during classical Ostwald ripening [6, 7]; see figure 3.5 for an illustration of the mechanism underlying the narrowing. Imagine we spatially quench the system by imposing a spatially varying equilibrium concentration $c_{\text{out}}^{(0)}(x) = c_{\text{out}}^{(0)}(0)(1 - mx)$, where $c_{\text{out}}^{(0)}(0)$ denotes the equilibrium concentration before the quench and m is the slope of the “spatial quench”. Such a spatial quench reduces the critical radius at the right boundary at $x = L$ from $R_c(0)$ (critical radius before the quench) to $R_c(x = L) = \ell_{\gamma}/\varepsilon(x = L)$ (equation (3.9)). This quench also shifts the maximum of dR/dt for droplets at $x = L$ to smaller radii since the radius corresponding to the maximum occurs at $R = 2R_c$. After the spatial quench there are many droplets with radii $R > 2R_c(x = L)$. According to dR/dt (figure 3.5(a)) these droplets grow more slowly than those around $R = 2R_c$ which leads to a *narrowing of the droplet size*

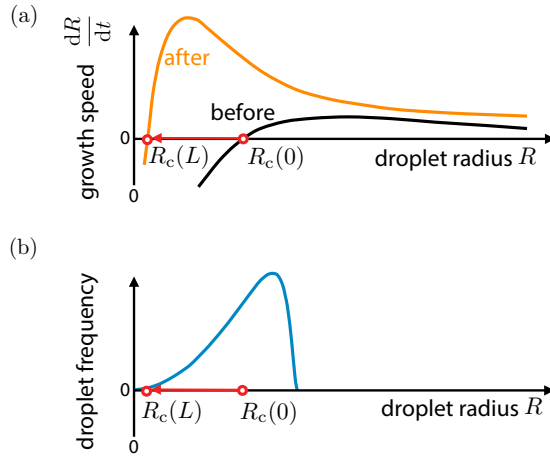


Figure 3.5. Sketch depicting the mechanism of the narrowing of the droplet size distribution due to the presence of concentration gradients. (a) The black curve depicts the droplet growth speed dR/dt before the spatial quench, where the system undergoes Ostwald ripening with a homogenous far field c_∞ and a homogenous equilibrium concentration $c_{\text{out}}^{(0)}(0)$. The corresponding droplet size distribution is shown in (b). The spatial quench $c_{\text{out}}^{(0)}(x) = c_{\text{out}}^{(0)}(0)(1 - mx)$ reduces the equilibrium concentration at $x = L$. Therefore, the local supersaturation increases which amounts to a decrease of the critical radius at $x = 0$ from $R_c(0)$ to $R_c(L)$ (indicated by red arrow). This change in supersaturation changes the droplet growth velocity dR/dt (orange). Subsequent to such a spatial quench mostly all droplets at $x = L$ grow. However, larger droplets typically grow less than smaller drops. Consequently, the size distribution will narrow. The narrowing is most pronounced close to the rightmost boundary at $x = L$ since the moving dissolution boundary dissolves all droplets at $x < L$. In addition, the dissolution of these droplets will keep the far field concentration $c_\infty(x)$ at $x = L$ at increased level which maintains a small value of critical radius until the dissolution boundary has reached the boundary at $x = L$.

distribution $P(R)$ at $x = L$. The critical radius $R_c(x = L)$ remains small because dissolution of droplets at $x < L$ leads to a diffusive flux toward $x = L$ and thus keeps the concentration $c_\infty(L)$ at increased levels. These conditions hold for a longer time if the spatial quench has a steeper slope. As a result the distribution narrows more for steeper quenches. For weak enough slopes of the quench, the narrowing of the droplet size distribution vanishes, however, droplet positioning still occurs as long as this slope is not zero.

When the dissolution boundary reaches the rightmost boundary close to $x = L$ the critical radius catches up with the mean droplet size. Concomitantly, narrowing of the droplet size distribution stops. Because all droplets are approximately of equal size the exchange of material between droplets via Ostwald ripening is slowed down dramatically. This slowing down of inter-droplet diffusion via Ostwald ripening leads to a long phase where droplet number and size is almost constant. Close to the end of this arrest phase,

the droplet distribution begins to broaden slowly and the dynamics approaches classical Ostwald ripening.

In summary, a concentration gradient of a regulator component that affects phase separation can significantly change the dynamics of droplet coarsening. The regulator gradient causes an inhomogeneity of the equilibrium concentration and the concentration field far away from the droplet. Both induce a position-dependent ripening process where droplets can drift along the gradient and dissolve everywhere besides to a region close to one boundary of the system. During this positioning process of droplets to one boundary the droplet size distribution can dramatically narrow for steep enough quenches which causes a transient arrest of droplet growth. After this arrest phase the positioned droplets are subject to a locally homogenous concentration environment and the system recovers the dynamics of classical Ostwald ripening.

4. Droplets driven by chemical turnover

Droplets can also be controlled by chemical reactions that directly affect the concentrations of the segregating species. While simple conversion reactions typically suppress phase separation, chemical reactions that are driven by an external energy input allow to control the droplet size as well as the count and can even lead to spontaneous droplet division. To describe such phenomena, we start by deriving the dynamical equations from a thermodynamic consistent description of phase separation in the presence of chemical reactions.

4.1. Thermodynamics of chemical reactions

Before we consider the coupling of phase separation and chemical reactions, we review the thermodynamics of chemical reactions in homogeneous systems. To highlight the core concepts, we here focus on very simple chemical reactions.

4.1.1. Chemical reactions in homogeneous systems
We start by considering an isolated system with two chemical species A and B that are converted into each other by the reaction

$$A \rightleftharpoons B. \quad (R1)$$

At constant temperature T and volume V , the system is described by a free energy $F(N_A, N_B)$, where N_i are the particle numbers of type $i = A, B$. The thermodynamic equilibrium of the system corresponds to the minimum of F . The necessary condition for this minimum reads $\mu_A dN_A + \mu_B dN_B = 0$, where the chemical potentials are $\mu_A = \partial F / \partial N_A|_{N_B}$ and $\mu_B = \partial F / \partial N_B|_{N_A}$. Note that in contrast to phase

separation without reactions, species can now be converted into each other and only the total number of particles, $M = N_A + N_B$, is conserved. This implies $dN_A = -dN_B$, such that the equilibrium condition requires $\mu_A = \mu_B$. Consequently, the chemical reaction equalises the chemical potentials of the two species.

The equilibrium condition of the chemical reaction also restricts the relaxation rate toward the equilibrium. This rate is quantified by the total reaction flux $s = -dc_A/dt = dc_B/dt$, where $c_i = N_i/V$ denotes the concentrations in the homogeneous system for $i = A, B$. Since the reaction can proceed in both directions, the total reaction flux $s = s_{\rightarrow} - s_{\leftarrow}$ is given by the difference of the forward reaction flux s_{\rightarrow} associated with the conversion of A to B and the reverse flux s_{\leftarrow} . As a consequence of detailed balance, the ratio of the two reaction fluxes obey (see Appendix C)

$$\frac{s_{\rightarrow}}{s_{\leftarrow}} = \exp\left(-\frac{\mu_B - \mu_A}{k_B T}\right), \quad (4.1)$$

which we call *detailed balance of the rates* [133]. The relation shows that the net direction in which the reaction proceeds depends on the sign of the chemical potential difference $\mu_B - \mu_A$. Moreover, the net reaction flux s vanishes in chemical equilibrium ($\mu_A = \mu_B$) since $s_{\rightarrow} = s_{\leftarrow}$. Close to chemical equilibrium, equation (4.1) can be linearized and the reaction flux $s = s_{\rightarrow} - s_{\leftarrow}$ can be expressed as

$$s = -\Lambda_r(c_A, c_B)(\mu_B - \mu_A), \quad (4.2)$$

where $\Lambda_r = (k_B T)^{-1} s_{\rightarrow}|_{\mu_A=\mu_B} = (k_B T)^{-1} s_{\leftarrow}|_{\mu_A=\mu_B}$ determines the reaction rate. Λ_r is an Onsager coefficient, which must be positive to ensure a positive entropy production rate [98, 111]; see Appendix B.

4.1.2. Chemical reactions in inhomogeneous systems and stability of homogeneous states To describe chemical reactions in inhomogeneous systems, we assume local thermodynamic equilibrium, i.e., there exist local volume elements where thermodynamic quantities such as concentrations and temperature can be defined. This is possible when the local volumes equilibrate quickly compared to the rates of the processes that we want to describe. In particular, the exchange with neighbouring volumes, associated with diffusive transport, and the conversion of particles into different species, associated with chemical reactions, should take place on timescales longer than the equilibration timescale of the volumes. If this is the case, a system of reacting and diffusing particles can be described by concentration fields $c_i(\mathbf{r})$ for all species i .

To study the interplay of the chemical reaction (R1) with phase separation, we first consider a binary, incompressible system described by the concentration

of the droplet component, $c_B(\mathbf{r}) = c(\mathbf{r})$, while $c_A(\mathbf{r}) = \nu^{-1} - c(\mathbf{r})$ with ν denoting the molecular volume of A and B . The behavior of the system is governed by the free energy $F[c]$, which is now a functional of the concentration field $c(\mathbf{r})$. For simplicity, we here consider the form

$$F[c] = \int d^3r \left(f(c) + \frac{\kappa}{2} |\nabla c|^2 \right), \quad (4.3)$$

which combines a local contribution of the free energy density $f(c)$ with a term that accounts for the free energy costs of spatial inhomogeneities proportional to κ , analogous to section 2.1.5. The exchange chemical potential $\bar{\mu} = \mu_B - \mu_A$ is thus given by $\bar{\mu} = \delta F[c]/\delta c$. The resulting equilibrium condition of the chemical reaction is $\bar{\mu}(\mathbf{r}) = 0$, which includes the equilibrium condition for phase separation, $\bar{\mu}(\mathbf{r}) = \text{const.}$, see section 2.2.1.

The dynamical equation of the system follows from the conservation law

$$\partial_t c + \nabla \cdot \mathbf{j} = s, \quad (4.4)$$

where \mathbf{j} is the diffusive flux and s is the net flux of the production of species B by the reaction (R1). These two thermodynamic fluxes are driven by their respective conjugated forces $\nabla \bar{\mu}$ and $\bar{\mu}$; see Appendix B. Using linear response theory, $\mathbf{j} = -\Lambda \nabla \bar{\mu}$ and $s = -\Lambda_r \bar{\mu}$, we arrive at the dynamical equation

$$\partial_t c = \nabla \cdot [\Lambda(c) \nabla \bar{\mu}(c)] - \Lambda_r(c) \bar{\mu}(c), \quad (4.5)$$

which describes a binary system that exhibits phase separation and chemical reactions. Note that we recover the Cahn-Hilliard equation if chemical reactions are absent ($\Lambda_r = 0$). Conversely, in the limit where Λ_r is constant and diffusive fluxes vanish ($\Lambda = 0$), we obtain the Allen-Cahn model [134], which is the deterministic version of model A [112].

We study the effects of chemical reactions by first analyzing homogeneous equilibrium states $c(\mathbf{r}) = c_0$, which are governed by the equilibrium condition $\bar{\mu}(\mathbf{r}) = 0$. This condition implies vanishing chemical reactions, see equation (4.2), and $f'(c_0) = 0$, so that c_0 is a (local) extremum of the free energy density $f(c)$. To assess the stability of these states, we consider harmonic perturbations with wave vector \mathbf{q} , as described in section 2.4. In the linear regime, these perturbations grow with a rate

$$\omega(\mathbf{q}) = -[\Lambda(c_0)\mathbf{q}^2 + \Lambda_r(c_0)][f''(c_0) + \kappa\mathbf{q}^2]. \quad (4.6)$$

The system is stable if all perturbations decay, i.e., if $\omega(\mathbf{q}) < 0$ for all wave vectors \mathbf{q} . Since $\Lambda, \Lambda_r \geq 0$, the stability is governed by the sign of the second bracket in equation (4.6) and the homogeneous state becomes unstable when $f''(c_0) < 0$ [135]. This

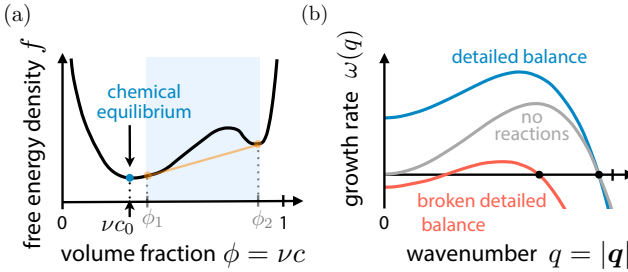


Figure 4.1. Schematic representation of the impact of chemical reactions on phase separation. (a) In chemical equilibrium, a system that is able to phase separate settles in the minimum of the free energy density corresponding to the homogeneous concentration c_0 . Phase separated states with concentrations $c_1 = \phi_1/\nu$ and $c_2 = \phi_2/\nu$ are no more stable. (b) Growth rate as a function of the wavenumber $q = |\mathbf{q}|$ (\mathbf{q} : wave vector) for phase separation in the presence of a chemical reaction tending toward chemical equilibrium satisfying detailed balance of the rates (blue), phase separation combined with non-equilibrium chemical reactions which break detailed balance of the rates (red) and phase separation in the absence of chemical reactions (grey).

condition is identical to the condition for the spinodal instability in the case without chemical reactions ($\Lambda_r = 0$). However, in the presence of chemical reactions only the homogeneous states with $f'(c_0) = 0$ are stationary states, while without chemical reactions all homogeneous states are stationary because the mass of the individual species is conserved. This also implies $\omega(0) = 0$ without chemical reactions, while the $q = 0$ mode is unstable when chemical reactions are present, see figure 4.1(b).

Taken together, we showed that if the system settles in a homogeneous state it will attain minimal free energy [135, 136], see figure 4.1(a). The major difference to the case without chemical reactions is that the species are not conserved individually and the system can thus relax by altering the composition locally. In the next section, we will show that this local conversion destabilises all inhomogeneous states including the ones corresponding to coexisting phases.

4.1.3. Dissolution of droplets by chemical reactions
 We now investigate the stability of inhomogeneous states to see how chemical reactions affect droplets. As an example, we first discuss the Ginzburg-Landau free energy presented in equation (2.19). When chemical reactions are present, this free energy permits two stable homogeneous solutions, corresponding to the two minima of the free energy density. Without chemical reactions, we have shown in section 2 that there is also a stable inhomogeneous stationary state, which consists of two bulk phases separated by an interfacial region. In the simple case of a one-dimensional system, the interfacial profile $c_1(x)$ is given by equation (2.28). This interfacial profile is also a

stationary state in the case with chemical reactions, since the symmetric free energy implies vanishing chemical potentials in the two bulk phases and thus satisfies the equilibrium condition $\mu(\mathbf{r}) = 0$.

To scrutinise the stability of the interfacial profile in the presence of chemical reactions, we determine whether a small change δc in the concentration profile could possibly decrease the free energy. Mathematically, this corresponds to calculating the second variation $\Delta F[c_1, \delta c]$ of the free energy, which is given by equation (2.30). The stationary state is stable if $\Delta F[c_1, \delta c]$ is positive for every nonzero variation δc . We show in Appendix A that indeed almost all perturbations δc increase the free energy. The only exception is $\delta c = \partial_x c_1$, for which $\Delta F = 0$, implying that this perturbation does not decay in time and the state is marginally stable. This perturbation corresponds to an infinitesimal translation, indicating that interfaces can move without changing the total free energy when chemical reactions are present. Note that this perturbation does not conserve the mass of the individual species and is thus forbidden in the case without chemical reactions discussed in section 2.2.2. Taken together, we showed that the sigmoidal interface profile given by equation (2.28) is neither stable nor unstable in the special case of the Ginzburg-Landau free energy, where both minima have the same energy.

In the general case where the minima of the free energy density are at different energies, the global free energy decreases when the interface moves such that the phase with the smaller free energy density expands [136]. Similarly, curved interfaces are unstable, since the associated Laplace pressure implies elevated concentrations on both sides of the interface, see equations (2.45). This asymmetry results in a net motion of the interface towards its concave side to reduce the interfacial curvature, the associated Laplace pressure, and thus the total free energy [136]. Taken together, these arguments show that inhomogeneous states are generally unstable when chemical reactions are present and the system attains the global free energy minimum everywhere, see figure 4.1(a).

A hint of these dynamics is visible in the simulation results shown in the middle column in figure 4.2, where the chemical potential difference $\bar{\mu}$ is very close to zero in the bulk phases but finite at the interfaces. In fact, the chemical potential deviates from zero more strongly at interfacial regions of larger curvature. One consequence of this observations is that the local entropy production $\Lambda_r \bar{\mu}^2$ by the chemical reactions is also largest at the interfaces.

The chemical reactions at the interface also affect the coarsening dynamics over long times. In particular, it has been shown that the domain size R scales as $R \propto t^{1/2}$ in the Allen-Cahn model [134, 137], where chemical

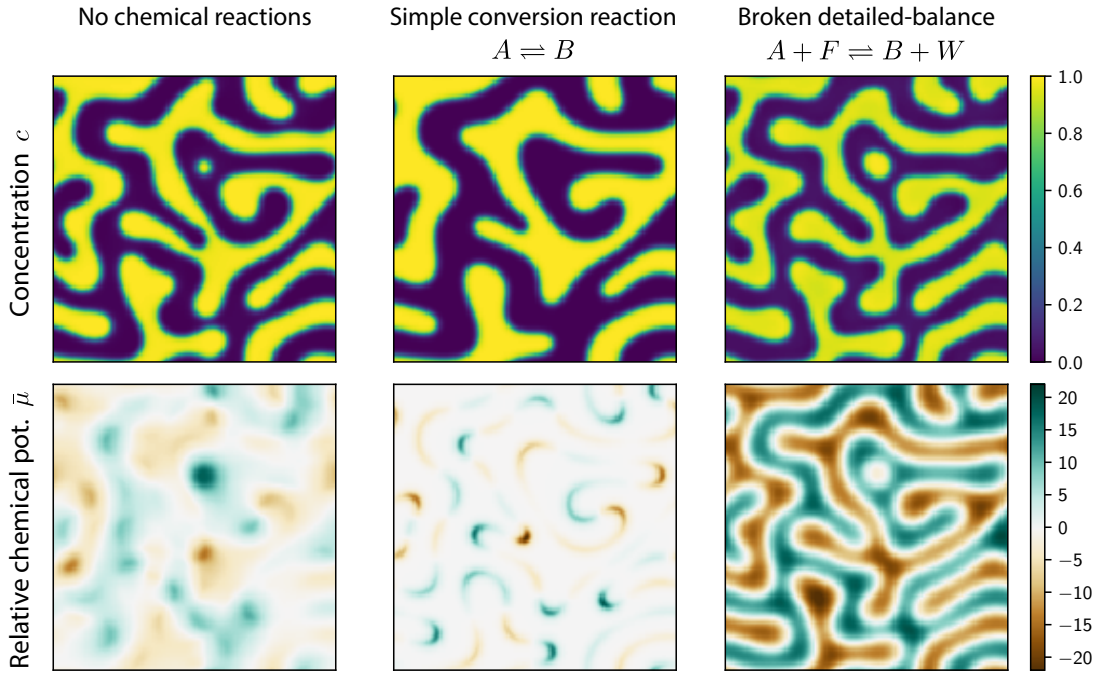


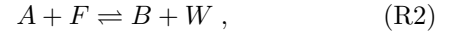
Figure 4.2. Influence of chemical reactions on phase separation. Shown are concentration profiles (upper row) and associated chemical potentials (lower row) of a binary system with equal amounts of A and B in different situations: Without chemical reactions the system undergoes coarsening by diffusive transport (left column). With an additional conversion reaction between the two species, the bulk phases relax quickly and the interface moves due to localised reactions (middle column). If detailed balance is broken, the system is driven away from equilibrium everywhere and more complex dynamics can occur (right column).

reactions dominate. Conversely, equation (2.57) shows that $R \propto t^{1/3}$ in a Cahn-Hilliard setting without chemical reactions. These qualitative differences are already visible in the perturbation growth rates ω of the homogeneous states given in equation (4.6), which reveal that chemical reactions ($\Lambda_r > 0$) lead to faster growing perturbations in the unstable regime.

Taken together, we showed that droplets are destabilised by the simple conversion reaction (R1) obeying detailed balance of the rates. In particular, the system always settles in a homogeneous state, even if droplets appear initially due to a spinodal instability or nucleation. This is the case because the chemical reaction allows to change the local composition of the system and the free energy density can thus be minimised locally. In order to use chemical reactions to control the behaviour of stable droplets, we will next discuss a system where additional chemical reactions in the bulk phases compensate the destabilising effects of reaction (R1). In particular, we will show that systems where droplet material is produced in one phase while it is destroyed in the other can lead to interesting phenomena. Such a situation can be found in active systems, where detailed balance of the rates is broken.

4.2. Phase separation with broken detailed balance of the rates

The detailed balance of the conversion reaction between A and B can be broken effectively by coupling the system to an external energy supply. This can for instance be achieved by adding a second reaction that converts A into B using additional energy supplied by fuel and waste components, which we respectively denote by F and W . The associated chemical reactions,



will allow us to drive the system out of equilibrium by controlling the concentrations of F and W externally. To study the interplay of these reactions with phase separation, we describe the system using a free energy density $f_4(c_A, c_B, c_F, c_W)$. For simplicity, we consider the case where the additional components F and W are dilute and thus do not affect the phase separation of A and B . Without chemical reactions, this system thus exhibits phase separation in thermodynamic equilibrium, similar to the binary system discussed in section 2. In this case, the chemical potentials $\mu_i = \partial f_i / \partial c_i$ for $i = A, B, F, W$ are homogeneous throughout the system and the chemical potential difference $\bar{\mu} = \mu_B - \mu_A$ between A and B is

generally non-zero.

When chemical reactions are present, they are driven by the chemical potential differences of their products and reactants. If the system is isolated, it will typically evolve toward a homogeneous thermodynamic equilibrium, as described in section 4.1.3. In contrast, this thermodynamic equilibrium may not be reached in open systems, for instance when the concentrations of the fuel and waste components are controlled at the boundary by coupling the system to a reservoir. In particular, the chemical potential difference $\bar{\mu}_2 = \mu_F - \mu_W$ between fuel and waste can be directly controlled at the boundary. To show that imposing $\bar{\mu}_2 \neq 0$ breaks detailed balance of the conversion rates between A and B , we next investigate the forward and backward fluxes of the two reaction pathways (R1) and (R2). These fluxes must obey conditions analogous to equation (4.1) since detailed balance holds microscopically. In particular, this implies the two conditions

$$\frac{s_{\rightarrow}^{(1)}}{s_{\leftarrow}^{(1)}} = \frac{s_{\rightarrow}^{(2)}}{s_{\leftarrow}^{(2)}} \exp\left(-\frac{\bar{\mu}_2}{k_B T}\right) = \exp\left(-\frac{\bar{\mu}}{k_B T}\right). \quad (4.7)$$

The left equation shows that equilibrium is reached ($s_{\rightarrow}^{(i)} = s_{\leftarrow}^{(i)}$ for $i = 1, 2$) only if the fuel and waste do not provide chemical energy ($\bar{\mu}_2 = 0$). Conversely, equilibrium cannot be reached if a chemical potential difference between fuel and waste is maintained. In particular, the total forward flux $s_{\rightarrow} = s_{\rightarrow}^{(1)} + s_{\rightarrow}^{(2)}$ and total reverse flux $s_{\leftarrow} = s_{\leftarrow}^{(1)} + s_{\leftarrow}^{(2)}$ of the conversion between A and B obey

$$\frac{s_{\rightarrow}}{s_{\leftarrow}} = e^{-\frac{\bar{\mu}}{k_B T}} \left[1 + \frac{1}{1 + \frac{s_{\leftarrow}^{(1)}}{s_{\leftarrow}^{(2)}}} \left(e^{\frac{\bar{\mu}_2}{k_B T}} - 1 \right) \right], \quad (4.8)$$

which implies $s_{\rightarrow} \neq s_{\leftarrow}$ for $\bar{\mu}_2 \neq 0$, so that detailed balance of the rates is broken in this case.

Detailed balance, expressed by equations (4.7) and (4.8), only constrains the ratios of the forward and backward fluxes of the two chemical reactions (R1) and (R2). Analogous to equation (4.2), the total reaction fluxes can be expressed in the linearised regime as

$$s^{(1)} = -\Lambda_r^{(1)}(\mathbf{c}) \bar{\mu} \quad (4.9a)$$

$$s^{(2)} = -\Lambda_r^{(2)}(\mathbf{c}) (\bar{\mu} - \bar{\mu}_2), \quad (4.9b)$$

where $\Lambda_r^{(1)}$ and $\Lambda_r^{(2)}$ are Onsager coefficients that set the reaction rates. These coefficients can depend on the concentrations $\mathbf{c} = \{c_A, c_B, c_F, c_W\}$ but must be positive to ensure that the entropy productions $\Lambda_r^{(1)} \bar{\mu}^2$ and $\Lambda_r^{(2)}(\bar{\mu} - \bar{\mu}_2)^2$ are positive; see Appendix B. For simplicity, we here consider the case where the fuel F and the waste W are dilute and diffuse fast, so the local composition can be described by a single concentration

$c = c_B \simeq \nu^{-1} - c_A$, where we consider equal molecular volume ν for A and B . In particular, $\Lambda_r^{(1)}$ and $\Lambda_r^{(2)}$ mainly depend on c in this case and we do not need to describe the dynamics of the additional components F and W explicitly. However, their chemical energy $\bar{\mu}_2$ affects the conversion between A and B . In particular, detailed balance of the conversion between A and B is broken in the reduced system where only these two components are described.

The dynamical equation of the system with broken detailed balance of the rates is given by the conservative diffusion fluxes driven by $\nabla \bar{\mu}$ together with the non-conservative reaction flux $s_{\text{tot}} = s^{(1)} + s^{(2)}$ given in equations (4.9). Using a conservation law analogous to equation (4.4), we obtain

$$\partial_t c = \nabla \cdot (\Lambda(c) \nabla \bar{\mu}(c)) + \kappa \Lambda_r^{(\text{tot})}(c) \nabla^2 c + s(c), \quad (4.10)$$

where $\Lambda_r^{(\text{tot})} = \Lambda_r^{(1)} + \Lambda_r^{(2)}$ and we split the total reaction flux s_{tot} into a contribution akin to a diffusion term related to surface tension and a local contribution $s(c) = \Lambda_r^{(2)}(c) \bar{\mu}_2 - \Lambda_r^{(\text{tot})}(c) f'(c)$. We will show below that the term $s(c)$ can affect the dynamics significantly, while the additional diffusion term has only a minor influence since it only increases the effective diffusion constant. Note that if detailed balance is obeyed ($\bar{\mu}_2 = 0$), equation (4.10) reduces to equation (4.5) when $\Lambda_r^{(\text{tot})}$ is replaced by Λ_r . In this case, the system approaches the homogeneous equilibrium states that we discussed in section 4.1. Conversely, more complex behavior can be expected when detailed balanced of the rates is broken by maintaining a non-zero chemical potential difference $\bar{\mu}_2$.

Equation (4.10) without the additional diffusion term has been proposed before as a simple combination of phase separation with chemical reactions [42, 47], albeit without an explicit breaking of detailed balance [138]. Instead, simple reaction rate laws $s(c)$ have been analyzed [42, 47, 48, 56]. For instance, it has been shown that first-order rate laws are equivalent to systems with long-ranged interactions of the Coulomb type [47, 139] and that such interactions affect pattern formation [49, 50, 139–142].

The effect of the chemical reactions with broken detailed balance of the rates can be highlighted by considering the stationary homogeneous states $c(\mathbf{r}) = c_0$. Equation (4.10) implies that c_0 must satisfy $s(c_0) = 0$, i.e., chemical reactions are balanced. When detailed balance is obeyed ($\bar{\mu}_2 = 0$), this condition is equivalent to the equilibrium condition $f'(c_0) = 0$ that we encountered before. Conversely, the homogeneous stationary states are altered when detailed balance of the rates is broken ($\bar{\mu}_2 \neq 0$).

We examine the stability of the homogeneous states using a linear stability analysis, as described in

section 2.4. We find that perturbations described by wave vectors \mathbf{q} grow in the linear regime with a rate

$$\omega(\mathbf{q}) = s'(c_0) - \mathbf{q}^2 \zeta(c_0) - \mathbf{q}^4 \Lambda(c_0) \kappa, \quad (4.11)$$

where $\zeta(c_0) = \Lambda(c_0)f''(c_0) + \kappa\Lambda_r^{(\text{tot})}(c_0)$ and primes denote derivatives with respect to c . The associated stationary state is stable only if $\omega(\mathbf{q})$ is negative for all \mathbf{q} , which is the case if the maximum

$$\max_{\mathbf{q}}(\omega(\mathbf{q})) = \begin{cases} s'(c_0) & \zeta(c_0) \geq 0 \\ s'(c_0) + \frac{\zeta^2(c_0)}{4\kappa\Lambda(c_0)} & \zeta(c_0) < 0 \end{cases} \quad (4.12)$$

is negative. Without reactions ($\Lambda_r^{(\text{tot})}(c) = 0$, implying $\zeta = \Lambda f''(c_0)$ and $s'(c_0) = 0$), we obtain the spinodal instability for $f''(c_0) < 0$, see section 2.4 and the grey line in figure 4.1(b). Chemical reactions can modify the stability conditions. If they obey detailed balance of the rates, we have $s(c) = -\Lambda_r f'(c)$ and the stability of homogeneous states is unchanged, see section 4.1.2 and the blue line in figure 4.1(b). Conversely, when detailed balance is broken, the reaction flux s is additionally affected by the chemical potential $\bar{\mu}_2$ that is controlled from the outside. In this case, a homogeneous state that was unstable without chemical reactions becomes stable if $s'(c_0) < -\zeta^2/(4\kappa\Lambda)$ [143, 144]. Since $s'(c)$ quantifies how the reaction flux changes when c is varied, this condition implies that a strong auto-inhibitory reaction can stabilise the homogeneous state. In contrast, if the reaction is auto-catalytic ($s'(c_0) > 0$), the system is always unstable. In between these two regimes, for weakly auto-inhibitory reactions ($-\zeta^2/(4\kappa\Lambda) < s'(c_0) < 0$), a range of finite wave vectors q becomes unstable and pattern formation is expected, see red line in figure 4.1(b). Generally, this suggests that droplets form and grow easily in auto-catalytic systems, while spontaneous formation might be suppressed by auto-inhibitory reactions. We show below that this difference leads to two fundamentally different classes of active droplets.

In this section, we discussed a model system where additional fuel and waste components break the detailed balance of the rates of the conversion of the main components A and B . We showed that this combination of phase separation with non-equilibrium chemical reactions can suppress the instability associated with spinodal decomposition and we will now analyse the impact on the dynamics of droplets.

4.2.1. Coarse-grained description of active droplets. We next discuss the dynamics of active droplets in the case of strong phase separation, where the interfacial width w is small compared to the droplet radius R .

In this case, the volume occupied by the interface and thus the chemical reactions inside the interfacial region are negligible. Conversely, we will show that the chemical reactions producing and destroying droplet material in the bulk phases influence the droplet dynamics significantly. We here consider a coarse-grained description, where a thin interface separates the inside of the droplet with a high concentration of droplet material B from the dilute phase outside, analogous to section 2.5.2. The dynamics in both phases is described by equation (4.10), but since the concentration variations are small within the phases, it can be approximated by a reaction-diffusion equation [72],

$$\partial_t c \simeq D \nabla^2 c + s(c), \quad (4.13)$$

where the diffusivity is $D = \Lambda(c_0)f''(c_0) + \kappa\Lambda_r^{(\text{tot})}(c_0)$. The first term in the expression for D stems from the conservative fluxes and is thus equivalent to equation (2.41) while the second term captures the apparent diffusion due to chemical conversion. The same approximation that led to equation (4.13) can also be used to linearize the reaction flux in the two phases,

$$s(c) \simeq \begin{cases} \Gamma_{\text{in}} - k_{\text{in}}(c - c_{\text{in}}^{(0)}) & \text{inside} \\ \Gamma_{\text{out}} - k_{\text{out}}(c - c_{\text{out}}^{(0)}) & \text{outside} \end{cases}, \quad (4.14)$$

where $\Gamma_{\text{in}} = s(c_{\text{in}}^{(0)})$ and $\Gamma_{\text{out}} = s(c_{\text{out}}^{(0)})$ are the reaction fluxes when the concentrations are at their equilibrium values $c_{\text{in}}^{(0)}$ and $c_{\text{out}}^{(0)}$ in the two phases, respectively. Deviations from these values are accounted for by $k_{\text{in}} = -s'(c_{\text{in}}^{(0)})$ and $k_{\text{out}} = -s'(c_{\text{out}}^{(0)})$, which can be interpreted as elasticity coefficients of the chemical reactions [145].

The basal fluxes Γ_{in} and Γ_{out} need to have opposite sign for droplets to exist. If they had the same sign, droplet material would either be destroyed ($\Gamma_{\text{in}}, \Gamma_{\text{out}} < 0$) or produced everywhere ($\Gamma_{\text{in}}, \Gamma_{\text{out}} > 0$), which both implies a homogeneous stationary state. To see under which conditions the basal fluxes have opposite sign, we express them as

$$\Gamma_{\text{in}} = -\Lambda_r^{(1)}(c_{\text{in}}^{(0)}) \bar{\mu} - \Lambda_r^{(2)}(c_{\text{in}}^{(0)}) (\bar{\mu} - \bar{\mu}_2) \quad (4.15a)$$

$$\Gamma_{\text{out}} = -\Lambda_r^{(1)}(c_{\text{out}}^{(0)}) \bar{\mu} - \Lambda_r^{(2)}(c_{\text{out}}^{(0)}) (\bar{\mu} - \bar{\mu}_2) \quad (4.15b)$$

using equations (4.9). To give a concrete example, we here consider a situation where the droplet material B is of higher energy than A ($\bar{\mu} > 0$). Equations (4.15) then imply that droplet material is produced outside the droplet ($\Gamma_{\text{out}} > 0$) and destroyed within ($\Gamma_{\text{in}} < 0$) if the fuel supplies sufficient energy ($\bar{\mu}_2 > \bar{\mu} > 0$) and the Onsager coefficients obey

$$\frac{\Lambda_r^{(1)}(c_{\text{in}}^{(0)})}{\Lambda_r^{(2)}(c_{\text{in}}^{(0)})} > \frac{\bar{\mu}_2}{\bar{\mu}} - 1 > \frac{\Lambda_r^{(1)}(c_{\text{out}}^{(0)})}{\Lambda_r^{(2)}(c_{\text{out}}^{(0)})}. \quad (4.16)$$

For instance, if $\bar{\mu}_2 = 2\bar{\mu}$, reaction (R1) must be faster than reaction (R2) inside the droplet, $\Lambda_r^{(1)}(c_{in}^{(0)}) > \Lambda_r^{(2)}(c_{in}^{(0)})$, while the opposite is true outside, $\Lambda_r^{(1)}(c_{out}^{(0)}) < \Lambda_r^{(2)}(c_{out}^{(0)})$. In this case, the conversion reaction (R1) proceeds from B to A spontaneously ($s^{(1)} < 0$), while reaction (R2) converts fuel to waste to produce the high-energy B from A ($s^{(2)} > 0$). If the coefficients $\Lambda_r^{(1)}$ and $\Lambda_r^{(2)}$ obey equation (4.16) the total reaction flux $s_{tot} = s^{(1)} + s^{(2)}$ is then positive outside the droplet, while it is negative inside. A concrete implementation of such a system is discussed in the Supporting Information of Ref. [73].

We showed that droplet material can be produced in one phase while it is destroyed in the other when the basal fluxes Γ_{in} and Γ_{out} have opposite sign. Do similar conditions apply to the elasticity coefficients k_{in} and k_{out} ? We showed in section 4.2 that negative $s'(c)$ has a stabilising effect and we would thus expect that droplets can persist if $k > 0$. Conversely, since positive $s'(c)$ can destabilise homogeneous phases, the active droplets we discuss here might be unstable if $k < 0$. However, there is a smallest length scale q_{max}^{-1} below which the instability cannot develop. This length scale can be determined from equation (4.11) and the condition $\omega(q_{max}) = 0$, yielding

$$q_{max}^{-1} \approx \left[\frac{\zeta(c_{in}^{(0)})}{s'(c_{in}^{(0)})} \right]^{\frac{1}{2}}, \quad (4.17)$$

for weak reactions, $s'(c_{in}^{(0)}) \ll \zeta(c_{in}^{(0)})$. In the case where q_{max}^{-1} is large compared to the droplet radius, the instability is effectively suppressed and the droplet could be stable even if $k_{in} < 0$. Conversely, the dilute phase will typically be large compared to q_{max}^{-1} , such that an instability would develop there if $k_{out} < 0$. In the following, we thus consider all values of k_{in} , but restrict our discussion to $k_{out} > 0$.

We distinguish different classes of active droplets based on where droplet material is produced. If the reaction fluxes Γ_{in} and Γ_{out} have the same sign, droplet material is produced or destroyed in the entire system and the only stable stationary state are homogeneous. Consequently, stable droplets can only exist if Γ_{in} and Γ_{out} have opposite sign: We denote the case where droplet material is produced outside the droplets ($\Gamma_{out} > 0$, $\Gamma_{in} < 0$) as *externally maintained droplets*, while the opposite case where droplets produce their own material ($\Gamma_{in} > 0$, $\Gamma_{out} < 0$) is called *internally maintained droplets*.

4.2.2. Droplet growth equation. We begin by studying a single, isolated active droplet surrounded by a large dilute phase. The droplet grows if there is a net flux of droplet material toward its surface, see equation (2.47).

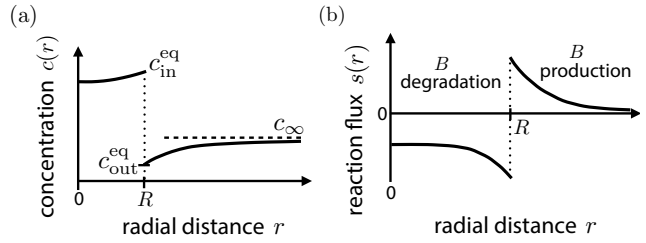


Figure 4.3. Schematic picture of an externally maintained active droplet, where droplet material is produced in the solvent phase. (a) Concentration c of droplet material as a function of the radial distance r . The chemical reactions modify the profiles compared to the passive droplet shown in Figure 2.2(a). (b) Reaction flux s as a function of r . Droplet material is produced outside the droplet while it is degraded inside. The droplet dynamics can strongly deviate from the passive case. In particular, Ostwald ripening can be suppressed and droplets even divide spontaneously (see section 4.3 and 4.4).

In the simple case of a spherical droplet of given radius R and volume $V_d = \frac{4\pi}{3}R^3$, the growth rate reads

$$\frac{dV_d}{dt} \approx \frac{J_{in} - J_{out}}{c_{in}^{(0)} - c_{out}^{(0)}}, \quad (4.18)$$

where we neglected surface tension effects in the denominator and defined the integrated surface fluxes $J_{in/out} = 4\pi R^2 \mathbf{n} \cdot \mathbf{j}_{in/out}$. These fluxes can be determined from the stationary solutions $c_*(r)$ that follow from solving equation (4.13) with the boundary conditions at the interface given in equation (2.45), see figure 4.3(a).

The flux J_{in} inside the droplet interface can be obtained in the quasi-static limit, where it equals the reaction flux $S_{in} = \int d^3r s(c_*(\mathbf{r}))$ inside the droplet volume. In the typical case where the radius R is small compared to the length $\ell_{in} = (D/|k_{in}|)^{\frac{1}{2}}$ generated by the reaction-diffusion system, the concentration inside the droplet is $c_*(\mathbf{r}) \approx c_{in}^{(0)}$, implying

$$J_{in} \approx \Gamma_{in} V_d. \quad (4.19)$$

Droplet material is thus transported toward the interface ($J_{in} > 0$) only in internally maintained droplets ($\Gamma_{in} > 0$).

The integrated flux J_{out} outside the droplet interface can also be obtained in a quasi-static approximation. In contrast to the passive case discussed in section 2.5.2, the supersaturation $\varepsilon = (c_{\infty} - c_{out}^{(0)})/c_{out}^{(0)}$ far away from droplets is now created by chemical reactions. In the typical case where the dilute phase is large compared to the length scale $\ell_{out} = (D/|k_{out}|)^{\frac{1}{2}}$, the chemical reactions equilibrate far away from droplets and the composition thus reaches the value $c_{\infty} = c_{out}^{(0)} + \Gamma_{out}/k_{out}$ where $s(c_{\infty}) = 0$, see figure 4.3(b). Consequently, the supersaturation can be expressed as $\varepsilon =$

$\Gamma_{\text{out}}/(k_{\text{out}}c_{\text{out}}^{(0)})$ and is thus positive if $\Gamma_{\text{out}} > 0$ since the reaction is auto-inhibitory at this point ($k_{\text{out}} > 0$). The resulting transport of droplet material can be quantified by the flux outside the droplet interface, which reads

$$J_{\text{out}} \approx 4\pi DRc_{\text{out}}^{(0)} \left(\frac{\ell_{\gamma}}{R} - \varepsilon \right) \quad (4.20)$$

in the typical case $R \ll \ell_{\gamma}$. The first term in the bracket captures the effect of surface tension, which is typically small. Neglecting this term, we find that droplet material is transported toward the interface ($J_{\text{out}} < 0$) if the dilute phase is supersaturated ($\varepsilon > 0$), which is the case only in externally maintained droplets ($\Gamma_{\text{out}} > 0$).

The droplet growth rate following from combining equations (4.18)–(4.20) reads

$$\frac{dR}{dt} \approx \frac{Dc_{\text{out}}^{(0)}}{R(c_{\text{in}}^{(0)} - c_{\text{out}}^{(0)})} \left(\varepsilon - \frac{\ell_{\gamma}}{R} + \frac{R^2\Gamma_{\text{in}}}{3Dc_{\text{out}}^{(0)}} \right). \quad (4.21)$$

The first term in the bracket describes droplet growth due to a supersaturated environment ($\varepsilon > 0$) or shrinkage in undersaturated environments ($\varepsilon < 0$). The second term, which is only relevant for small droplets, captures the reduction of growth due to surface tension γ . The last term describes the growth of the droplet due to production of droplet material inside if $\Gamma_{\text{in}} > 0$ or its shrinking when $\Gamma_{\text{in}} < 0$. Note that equation (4.21) reduces to equation (2.53) if chemical reactions are absent ($\Gamma_{\text{in}} = 0$) and the supersaturation ε is imposed.

4.2.3. Single droplet in an infinite system. We begin by discussing the growth of a single droplet in an environment with constant supersaturation ε . This corresponds for instance to an infinite system where the supersaturation reaches its equilibrium value $\varepsilon_{\text{eq}} = \Gamma_{\text{out}}/(k_{\text{out}}c_{\text{out}}^{(0)})$ far away from an isolated droplet. The stationary states of this system can be determined from equation (4.21) and correspond to radii R for which the bracket vanishes. The associated cubic equation in R has at most three solutions, which we now classify. If the chemical reactions are too strong, there are no physical solutions. In particular, if $|\Gamma_{\text{in}}| > \Gamma_{\text{in}}^{\text{max}}$ with

$$\Gamma_{\text{in}}^{\text{max}} = \frac{4c_{\text{out}}^{(0)}D|\varepsilon|^3}{9\ell_{\gamma}^2}, \quad (4.22)$$

two solutions are complex while the third one is either negative (if $\Gamma_{\text{in}} < 0$) or smaller than the interface width (if $\Gamma_{\text{in}} > 0$), which is both unphysical. Consequently, stable droplets can only exist for moderate chemical reactions, $|\Gamma_{\text{in}}| < \Gamma_{\text{in}}^{\text{max}}$. In this case, the polynomial equation has three real solutions. One of the solutions

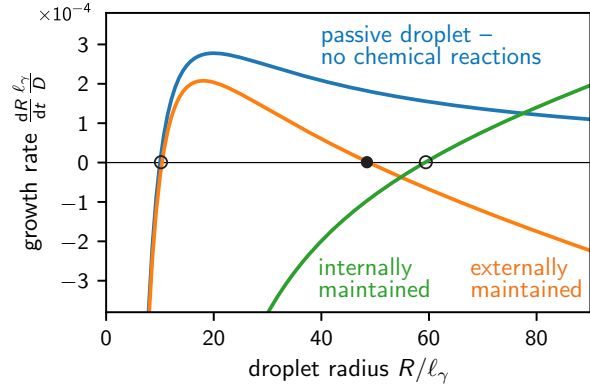


Figure 4.4. Growth rate dR/dt of a single droplet in an infinite system as a function of the droplet radius R . Shown are the values given by equation (4.21) for passive droplets (blue line; $\Gamma_{\text{in}} = 0$, $\varepsilon = 0.1$), externally maintained droplets (orange line; $\Gamma_{\text{in}}/c_{\text{out}}^{(0)} = -10^{-4}D/\ell_{\gamma}$, $\varepsilon = 0.1$), and internally maintained droplets (green line; $\Gamma_{\text{in}}/c_{\text{out}}^{(0)} = 10^{-4}D/\ell_{\gamma}$, $\varepsilon = -0.1$) for $c_{\text{in}}^{(0)}/c_{\text{out}}^{(0)} = 10$. Unstable stationary states are marked with open circles, while the only stable one is marked with a black disk.

is always negative and thus unphysical, while the other two read

$$R^{(1)} \approx \frac{\ell_{\gamma}}{\varepsilon}, \quad (4.23a)$$

$$R^{(2)} \approx \left(\frac{3D\varepsilon c_{\text{out}}^{(0)}}{-\Gamma_{\text{in}}} \right)^{\frac{1}{2}} - \frac{\ell_{\gamma}}{2\varepsilon}, \quad (4.23b)$$

which is correct up to linear order in ℓ_{γ} . The dynamics in the vicinity of these states follow from a linear stability analysis of equation (4.21), where the droplet radius is perturbed away from the stationary state and we determine whether the dynamics will bring the droplet back to its stationary state or not [72]. This gives us enough information to discuss the growth behavior of active droplets qualitatively.

In the case of externally maintained droplets ($\Gamma_{\text{in}} < 0$, $\varepsilon > 0$), we have $0 < R^{(1)} < R^{(2)}$, since $|\Gamma_{\text{in}}| < \Gamma_{\text{in}}^{\text{max}}$. Here, the radius $R^{(1)}$ corresponds to an unstable state, while $R^{(2)}$ is stable, see figure 4.4. Droplets smaller than $R^{(1)}$ dissolve and disappear, so $R^{(1)}$ is a critical radius similar to the one discussed in section 2.5.2. Externally maintained droplets that are larger than the critical radius $R^{(1)}$ grow until they reach the stable stationary state with radius $R^{(2)}$. This state is not present for passive droplets in an infinite system and must thus be a consequence of the chemical reactions. This can be seen by analyzing the two fluxes J_{in} and J_{out} , which must be equal in the stationary state. However, J_{in} scales with the droplet volume, while J_{out} scales with its radius, see equation (4.20). Consequently, if the droplet radius exceeds $R^{(2)}$, the loss due to J_{in} dominates and the droplet shrinks back to the stationary state. The chemical turnover inside

the droplet thus stabilizes the stationary state. Note that the two stationary states given in equation (4.23) only exist if the chemical reactions are not too strong ($|\Gamma_{\text{in}}| < \Gamma_{\text{in}}^{\text{max}}$). In the limiting case $\Gamma_{\text{in}} = -\Gamma_{\text{in}}^{\text{max}}$ the situation is degenerated and the two stationary states are identical. The corresponding radius $R_{\text{min}}^{\text{ext}} = (3\ell_{\gamma})/(2\varepsilon)$ can be determined from equation (4.21) and corresponds to the smallest externally maintained droplet that can be stable.

In the case of internally maintained droplets ($\Gamma_{\text{in}} > 0, \varepsilon < 0$), the first solution given in equation (4.23) is negative and thus unphysical. The second solution is always positive, but unstable to perturbations. Consequently, $R^{(2)}$ is the critical droplets size of internally maintained droplets, which can be significantly larger than critical sizes in externally maintained droplets. Nucleation is thus typically suppressed efficiently, but it can be promoted by catalytically active particles, which catalyze the production of droplet material at their surface [71, 72]. Internally maintained droplets larger than the critical size grow up to the system size and there is no characteristic stable size. This is because such droplets grow quicker if they become larger and this autocatalytic growth only stops when the dilute phase is depleted of material A , which can only happen in a finite system [72].

4.2.4. Single droplet in a finite system. So far, we only considered systems that are large compared to the droplet size, so the supersaturation ε is effectively constant. In contrast, in small systems a growing droplet can deplete the surrounding dilute phase significantly. In particular, the average concentration c of droplet material in the dilute phase evolves as

$$\frac{dc}{dt} = s(c) + \frac{J_{\text{out}}}{V - V_d}, \quad (4.24)$$

where the first term on the right hand side originates from the chemical reactions in the dilute phase and the last term accounts for the diffusive flux at the interface of the droplet of volume V_d . In large systems ($V \gg V_d$), the last term is negligible and c relaxes to c_{∞} , where chemical equilibrium is obeyed, $s(c_{\infty}) = 0$. At this point, the supersaturation $\varepsilon = (c - c_{\text{out}}^{(0)})/c_{\text{out}}^{(0)}$ attains its equilibrium value $\varepsilon_{\text{eq}} = \Gamma_{\text{out}}/(k_{\text{out}}c_{\text{out}}^{(0)})$ and is thus independent of the droplet size, consistent with our assumptions in the previous subsection. In small systems, however, the last term in equation (4.24) is not negligible and ε depends on the droplet volume V_d . For instance, in the case of externally maintained droplets, we have $J_{\text{out}} < 0$ and the concentration c outside the droplet is thus lower than c_{∞} . Consequently, the supersaturation is smaller for smaller systems and we would expect a reduced

stationary droplet radius $R^{(2)}$, see equation (4.23b). Indeed, when we solve for the stationary states of equations (4.21) and (4.24), we find in the simple case of large diffusion and small surface tension that there is a stationary state with volume

$$V_* \approx \frac{\Gamma_{\text{out}} V}{\Gamma_{\text{out}} - \Gamma_{\text{in}}}, \quad (4.25)$$

which is stable for externally maintained droplets and unstable for internally maintained ones. This stationary state thus corresponds to the one with radius $R^{(2)}$ in large systems. Consequently, the size of stable stationary droplets that are externally maintained depends on system size in small systems, while it is independent of the system size in large systems, see equation (4.23).

Similar to passive droplets, we find that active droplets also have a critical radius, below which they shrink and disappear. Consequently, droplets can only be nucleated spontaneously if a concentration fluctuation creates a large enough initial droplet. In externally maintained droplets, this mechanism is similar to passive droplets, where the nucleation barrier is higher for larger surface tension and smaller supersaturation. Conversely, the critical radius is generally larger for internally maintained droplets, but it becomes smaller for larger surface tension and smaller supersaturation. This is because only a large enough droplet can produce enough droplet material to balance the efflux into the dilute phase. This efflux is smaller for larger surface tension, so surface tension actually helps to nucleate internally maintained droplets.

Once droplets exceed their critical radius they grow spontaneously by absorbing droplet material from the surrounding (passive and externally maintained droplets) or by producing more droplet material (internally maintained droplets). In the first case, the droplet growth rate is larger for smaller droplets and higher supersaturation. However, the growth of externally maintained droplets comes to a stop at a finite size, at which the loss of droplet material due to the chemical reactions inside is balanced by its influx over the surface. Conversely, internally maintained droplets grow indefinitely in an infinite system, similar to passive droplets. However, in contrast to passive droplets, this growth accelerates because of its autocatalytic nature. Consequently, in the simple case of a binary fluid in an infinite system, only externally maintained droplets reach a finite droplet size, while both passive and internally maintained droplets grow to occupy the whole system.

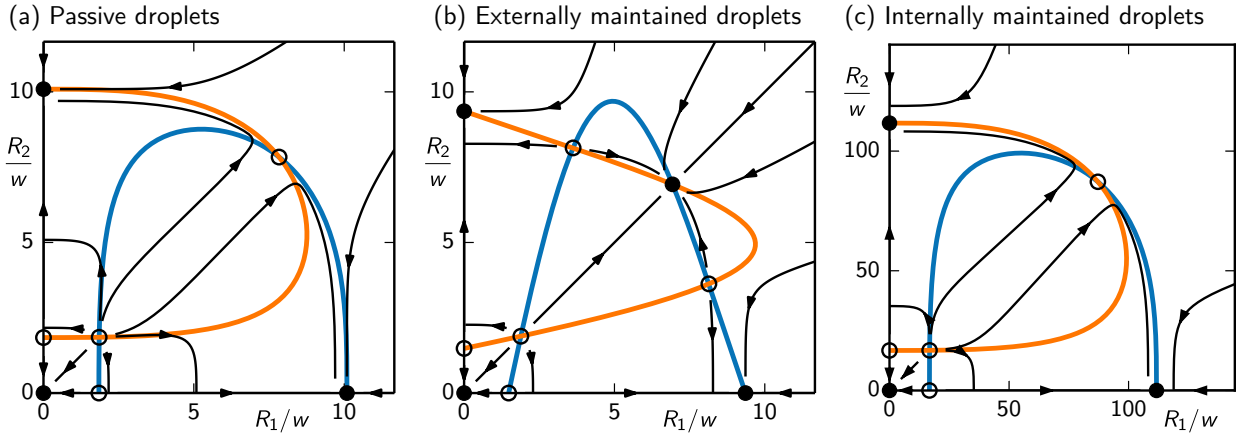


Figure 4.5. Behavior of two droplets as a function of their radii R_1 and R_2 , normalized with the interface width w . The black arrows indicate the temporal evolution of the state variables R_1 and R_2 following from equation (4.21), with ε given by equation (4.27). The blue and orange lines are the nullclines, which indicate where the growth rate of droplets 1 and 2 vanish, respectively. Their intersections are stable (disks) or unstable fixed points (open circles). (a) Passive droplets ($\Gamma_{\text{in}} = \Gamma_{\text{out}} = 0$) (b) Externally maintained droplets ($\Gamma_{\text{in}} < 0, \Gamma_{\text{out}} > 0$) (c) Internally maintained droplets ($\Gamma_{\text{in}} > 0, \Gamma_{\text{out}} < 0$).

4.3. Arrest of droplet coarsening: Suppression of Ostwald ripening

If many active droplets are present in the same system, their dynamics will be coupled because they share the material in the dilute phase. Intuitively, this coupling will be stronger if the droplets are closer together. For instance, for externally maintained droplets, the length scale over which they deplete the surrounding dilute phase is given by ℓ_{out} and we thus expect that such droplets do not interact significantly when they are further apart. In particular, their stationary state radius $R^{(2)}$ given in equation (4.23b) should not be affected much. Conversely, if externally maintained droplets are close, they compete strongly for the material produced in the solvent and might thus only reach a smaller size. This is in strong contrast to passive and internally maintained droplets that grow unbounded and will thus interact eventually, independent of the initial separation.

We study the interaction of multiple droplets in the simple case of sparse systems, where droplets are far apart from each other. In this case, the growth dynamics of the droplets are coupled because they all exchange material with the same dilute phase, but direct interactions between droplets can be neglected. Considering N droplets in a finite system of volume V , the supersaturation ε in the dilute phase evolves as

$$\frac{d\varepsilon}{dt} \approx \Gamma_{\text{out}} - k_{\text{out}} c_{\text{out}}^{(0)} \varepsilon + \frac{1}{V} \sum_{i=1}^N J_{\text{out},i}, \quad (4.26)$$

which follows by generalizing equation (4.24) to many droplets in the limit that V is large compared to the total volume of all droplets, $V \gg \sum_i V_i$. Here, R_i and $V_i = \frac{4\pi}{3} R_i^3$ are the respective radii and volumes

of the droplets for $i = 1, \dots, N$ and $J_{\text{out},i}$ is the flux of droplet material right outside the interface of the i -th droplet integrated over its surface, which follows from equation (4.20). For simplicity, we here consider the quasi-static case, where the concentration profile between droplets relaxes quickly compared to the growth of the droplets themselves, which is the typical situation [72]. In this case, ε will attain its stationary state value

$$\varepsilon_* = \frac{4\pi N \ell_{\gamma} D + \Gamma_{\text{out}} V \frac{1}{c_{\text{out}}^{(0)}}}{k_{\text{out}} V + 4\pi D \sum_i R_i}. \quad (4.27)$$

Note that in the limit of a dilute system, $V/N \gg \ell_{\text{out}}^3$, we recover the supersaturation at chemical equilibrium, $\varepsilon_{\text{eq}} = \Gamma_{\text{out}}/k_{\text{out}}$. Conversely, in passive or dense systems, the supersaturation is set by the equilibrium condition at the droplet surfaces, $\varepsilon_* = \ell_{\gamma}/R_*$, when all droplets have the same radius R_* .

The growth rate of each individual droplet is still described by equation (4.21), but with the supersaturation now given by equation (4.27). For simplicity, we consider the case where all droplets have the same stationary radius R_* , which can be determined from the stationary state of equation (4.21). Similar to the discussion of isolated droplets above, we can then use a linear stability analysis to discuss the qualitative dynamics in the vicinity of this state. The detailed analysis given in Ref. [72] shows that there are two independent perturbation modes with qualitatively different dynamics: The fast mode associated with the total droplet volume describes the fact that all droplets quickly take up excess material from the dilute phase until the stationary state of the total droplet volume is reached. All other perturbation modes are associated with a slower exchange of material between droplets.

These modes all have the same perturbation growth rate ω given by

$$\omega = \frac{1}{c_{\text{in}}^{(0)} - c_{\text{out}}^{(0)}} \left(\frac{\ell_\gamma D c_{\text{out}}^{(0)}}{R_*^3} + \frac{2\Gamma_{\text{in}}}{3} \right). \quad (4.28)$$

If ω is positive, the associated mode is unstable and material will flow from smaller to larger droplets, e.g., during Ostwald ripening. Conversely, negative ω indicates stable states, where this coarsening is suppressed.

Passive systems ($\Gamma_{\text{in}} = 0$) are always unstable ($\omega > 0$) and the droplets thus exhibit Ostwald ripening as discussed in section 2.5.3. The redistribution of material between droplets is driven by surface tension, which causes a larger concentration of droplet material right outside of smaller droplets, see equation (2.45). Moreover, the associated perturbation rate ω is smaller for larger mean droplet size, such that exchange of material will be slower between larger droplets. This implies that the coarsening of droplets slows down and only stops when a single droplet remains.

Internally maintained droplets ($\Gamma_{\text{in}} > 0$) are also unstable and the associated growth rate is larger than that of passive droplets. This is because the autocatalytic growth allows larger droplets to outcompete smaller ones, independent of surface tension effects. Internally maintained droplets are thus more unstable than passive ones, but they can be stabilised by particles that catalyse the production of droplet material within the droplets [71, 72].

Multiple externally maintained droplets ($\Gamma_{\text{in}} < 0$) can coexist when $\omega < 0$. This is the case if their radius R_* exceeds the critical value

$$R_{\text{stab}} = \left(\frac{3D\ell_\gamma c_{\text{out}}^{(0)}}{-2\Gamma_{\text{in}}} \right)^{\frac{1}{3}}, \quad (4.29)$$

see equation (4.28). This expression reveals that the stability originates from a competition of the destabilising effect of surface tension, which tends to increase R_{stab} , and the stabilising effects induced by the diffusive fluxes driven by the chemical reactions. This is similar to the isolated droplets that we discussed in the previous section: the influx toward a droplet scales at most with the droplet radius, see equation (4.20), while the material loss scales with the volume. Consequently, multiple externally maintained droplets can stably coexist when the supersaturation in the dilute phase sustains the influx.

We showed that multiple active droplets interact because they compete for the same material from the dilute phase. The associated diffusive fluxes between droplets are caused by surface tension effects and chemical reactions. The flux due to surface tension is generally destabilising and causes the classical

Ostwald ripening. Conversely, the flux due to chemical reactions can be either destabilising (for internally maintained droplets) or stabilising (for externally maintained droplets). If the stabilising contribution of the chemical reactions is stronger than the destabilising one due to surface tension, multiple active droplets can coexist in a stable state.

4.4. Spontaneous division of active droplets

So far, we analyzed the growth rate of active droplets assuming they maintain a spherical shape. We found that the droplet growth dynamics are often determined by a competition between surface tension effects and diffusive fluxes toward the droplet interface. Both effects depend on the droplet radius, or, more precisely, on the mean curvature of the droplet interface, which is given by R^{-1} for spherical droplets. In contrast, the mean curvature varies in non-spherical droplets, which suggests that the competition between the two effects plays a role in the shape dynamics of active droplets.

The dynamics of a non-spherical droplet are described by the same physical principles that we discussed so far. In particular, the interface velocity in its normal direction, given by equation (2.47), depends on the local net flux of droplet material, which follows from the reaction-diffusion equations in the bulk phases. Solving these equations numerically reveals that active droplets can show behaviours that are not present in passive droplets [73]. Figure 4.6a shows that externally maintained droplets can divide spontaneously, which can also happen multiple times [73]. A linear stability analysis with respect to the droplet shape reveals that the shape becomes unstable when the mean droplet radius R exceeds the critical value [73]

$$R_{\text{div}} \approx \frac{11\ell_\gamma}{\varepsilon}, \quad (4.30)$$

which is an approximation in the limit of large diffusive length scales ($\ell_{\text{in}}, \ell_{\text{out}} \gg R$). Figure 4.6b shows that there are typically three different regimes of externally maintained droplets for a given turnover Γ_{in} of droplet material inside the droplet. If the supersaturation ε that is set by the chemical reactions in the dilute phase is too low, droplets cannot exist at all. For intermediate values of ε , droplets larger than the critical radius grow to their stationary size as discussed in section 4.2.2. For even larger ε , droplets at the stationary size become unstable ($R_* > R_{\text{div}}$) and growing droplets start dividing before they reach a stationary size. After division, these droplets can grow further and divide again. This proliferation continues until the system is depleted of droplet material and the supersaturation ε decreases to a point where the stationary state is stable with respect to shape changes.

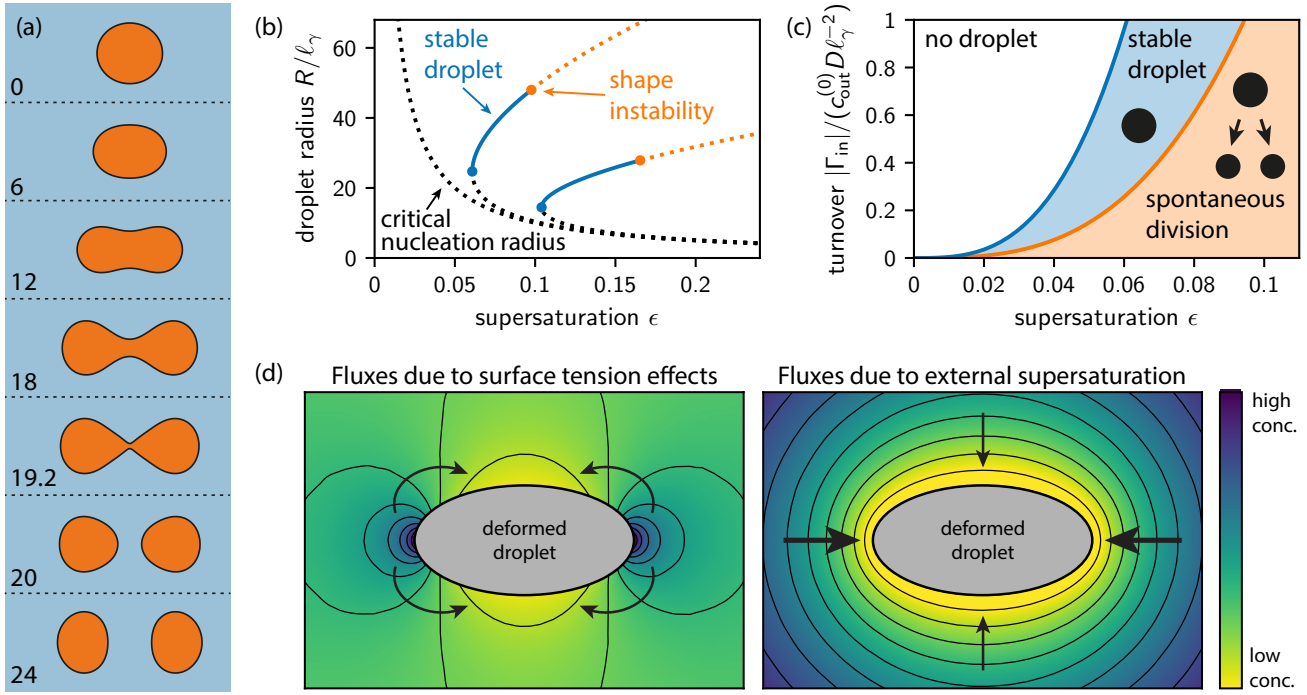


Figure 4.6. Spontaneous division of externally maintained droplets. (a) Sequence of shapes of a dividing droplet at different times as indicated (reproduced from [73]). (b) Stationary droplet radii R as a function of the supersaturation ϵ for three different turnovers ($\Gamma_{in}/\Gamma_0 = 0, 1, 5$; from left to right, with $\Gamma_0 = -10^{-5} c_{in}^{(0)} D \ell_\gamma^{-2}$ and $c_{in}^{(0)}/c_{out}^{(0)} = 10$). Solid lines indicate stable stationary states, while dotted lines indicate states that are unstable with respect to size (black) or shape (orange). The radii R were determined from equation (4.21), assuming that droplets become unstable when $R > R_{div}$ given by equation (4.30). (c) Stability diagram of externally maintained droplets as a function of the supersaturation ϵ and the turnover Γ_{in} . Droplets dissolve and disappear (white region), are stable and attain a spherical shape (blue region), or undergo cycles of growth and division (orange region). The lines were determined analogously to (b) using the same parameters. (d) Schematics of deformed droplets and the surrounding concentration fields created by surface tension effects (left) and an external supersaturation (right). Material is transported from dark to light regions by diffusive fluxes (black arrows) perpendicular to the isocontours (black lines). Fluxes due to surface tension transport material from regions of high to low curvature, thus making droplets more circular (left). Conversely, the influx driven by an external supersaturation amplifies non-spherical shapes (right). The concentration fields have been obtained by solving the stationary diffusion equation (2.40). The boundary condition (2.45) at the surface of the deformed droplet accounts for surface tension effects (left) and a constant concentration c_∞ far away from the droplet represents the external supersaturation (right).

Whether externally maintained droplets divide or not depends on the balance between the availability of droplet material (supersaturation ϵ) and the turnover inside the droplet (reaction flux Γ_{in}), see figure 4.6c.

The instability of the shape of externally maintained droplets can be qualitatively explained by a competition of surface tension effects with diffusive fluxes [146], similar to the multiple droplets discussed in the previous section. Because of surface tension, interface regions of larger mean curvature exhibit a larger concentration of droplet material right outside the interface, see equation (2.45). This reduces the influx of droplet material and thus attenuates growth at regions of high curvature, stabilising the spherical shape, see figure 4.6d. Conversely, an externally driven material influx enhances the growth at regions of high curvature where the influx is larger, which is evident from the closer isocontour lines in figure 4.6d. This effect generally destabilises the spherical shape and has been described for phase separating systems by Mullins and

Sekerka [147, 148]. If the total volume of the droplet is limited, i.e., by the internal turnover Γ_{in} of active droplets, this surface instability leads to a division of the droplet. However, whether the instability can dominate the stabilising surface tension effects depends on the parameters, as shown in figure 4.6c.

In internally maintained droplets the diffusive fluxes are reversed. Consequently, both the surface tension effect and the closer isocontour lines enhance the efflux of material at regions of higher curvature, which thus stabilizes the spherical shape of internally maintained droplets. We thus expect that internally maintained droplets are more stable with respect to shape perturbations than passive droplets.

5. Active emulsions: relevance to biology with versatile applications

In this review we have discussed the physics of phase separation and the dynamics of droplets under condi-

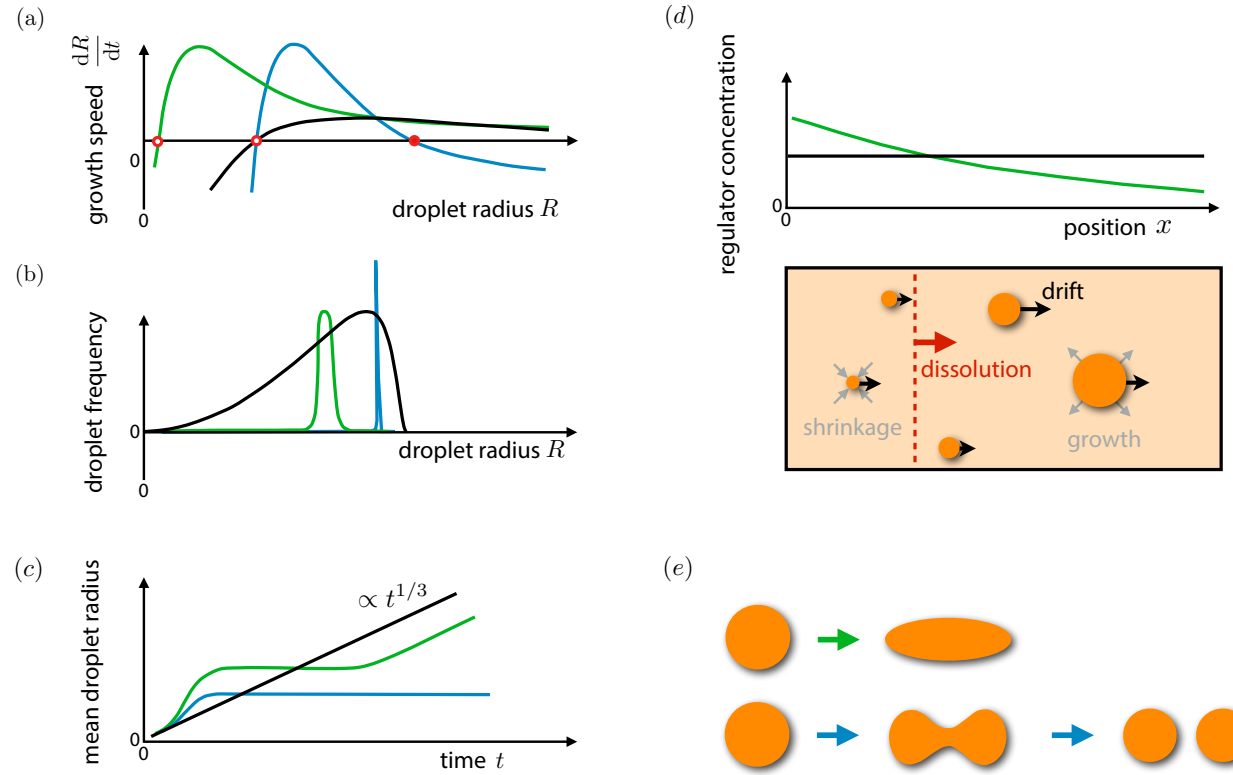


Figure 5.1. Overview of the novel behaviour and phenomena that occur in active emulsions. Curves in green correspond to droplets in a gradient of molecules which affect phase separation while blue curves indicate droplets in the presence of non-equilibrium chemical reactions. Results for passive systems are depicted as black lines. (a) Droplet growth speed and (b) droplet frequency as a function of droplet radius R . The (unstable) critical radius is indicated by an open red circle, while there can be a stable stationary radius in the case of non-equilibrium chemical reactions (shown as bold and red circle). (c) Mean droplet radius as a function of time t . The radius of passive droplets grows $\propto t^{1/3}$, while active emulsion break this scaling law. (d) Positioning of droplets to one boundary of the system (bottom) in the presence of a regulator gradient (top) by droplet drift and position-dependent dissolution and growth. (e) In the presence of a regulator gradient droplet can deform (top), while in the presence of non-equilibrium chemical reactions droplets can even undergo a shape instability and divide (bottom).

tions that deviate from passive systems. In particular, we discussed demixing systems in the presence of a concentration gradient of a component that affects phase separation and droplets in the presence of chemical reactions that are driven away from thermal equilibrium, see figure 5.1. In both systems the dynamics of phase separation is significantly affected. The systems favour non-equilibrium stationary states and exhibit novel phenomena that are not present in phase separating systems at thermal equilibrium. We therefore refer to this novel class of physical systems as *active emulsions*.

The difference to passive systems becomes apparent already at the level of a single droplet, which can exhibit a qualitatively different growth speed in case of active droplets, see figure 5.1(a). For passive systems, the growth speed as a function of the radius of the droplet has an unstable fixed point. The associated critical radius increases over time and drives the coarsening in emulsions. Actively spending energy to create

and maintain a regulator gradient that affects phase separation can reduce the critical radius in a position-dependent manner. Droplets at one end of the regulator gradient grow faster than droplets at the other end. Eventually, the larger droplets outcompete the smaller ones, much like in Ostwald ripening, but the positional bias by the gradient effectively positions the surviving droplets toward one end. Concomitantly, these larger droplets all grow to a similar size, i.e., the droplet size distribution narrows during the positing dynamics (figure 5.1(b)). This narrowing is in stark contrast to the universal size distribution of passive droplets undergoing Ostwald ripening. As most droplets are positioned to one end, the ripening arrests for a certain time period, thus breaking the universal growth law in passive systems where droplet size increases proportional to $t^{1/3}$ (figure 5.1(c)). Besides this position-dependent dissolution and growth process, droplets also drift along the gradient (figure 5.1(d)). During this drift, droplets deform (figure 5.1(e)). In contrast,

in passive systems, droplets maintain their spherical shape and do not drift. However, when all droplets are at one end of the gradient, the environment becomes locally homogeneous and the dynamics slowly returns to classical Ostwald ripening.

If the regulator concentration gradient is created by an inhomogeneous external potential, a phase separated system can favour novel equilibrium states. The condensed phase either sits at the minimum or the maximum of the external potential, i.e., the concentration profile describing the condensed phase is either correlated or anti-correlated with the regulator profile. The system can also undergo a discontinuous phase transition between these two states when the interactions between the molecules are changed. In the absence of an external potential there is no positional bias and each position of the condensed phase corresponds to the same free energy.

Droplet dynamics can also be affected by spending energy to drive chemical reactions that involve the droplet material away from equilibrium. In this case, single droplets can exhibit a stable stationary state at a finite size, see figure 5.1(a). Consequently, all droplets larger than the critical size tend toward this stationary radius, leading to a suppression of the Ostwald ripening that would occur in passive systems. These dynamics leads to an infinitely sharp distribution in the absence of fluctuations (figure 5.1(b)) with a mean droplet size that saturates at this stable radius (figure 5.1(c)). Chemical reactions can thus modify the dynamics of phase separation such that the universal broadening is replaced by an evolution to a non-equilibrium stationary state of a monodisperse, active emulsion. Moreover, in the presence of non-equilibrium chemical reactions, droplets can also undergo shape instabilities triggering the division of droplets, see figure 5.1(e). In contrast, passive droplets only exhibit the reverse process of droplet fusion, which is driven by surface tension effects. In active droplets, this stabilizing tendency of surface tension can be overcome by the influx of droplet material sustained by the non-equilibrium chemical reactions.

Demixing systems in the presence of external forces, like a maintained regulator gradient or non-equilibrium chemical reactions, share some inherent similarities. Both systems break the universal coarsening dynamics of Ostwald ripening and modify the stationary state of the system. While a regulator gradient causes a bias in the position of the single stationary droplet, the non-equilibrium chemical reactions can select a state composed of multiple droplets of equal size. The breaking of the universal dynamics occurs via additional fluxes that are absent in classical phase separation. These fluxes are generated by the dissipation of energy, either to

assemble and maintain a concentration gradient that in turn interacts with the demixing components or to drive chemical reactions of the demixing components away from their equilibrium.

Active fluxes are ubiquitous in living systems to keep them away from thermal equilibrium. In fact, if such systems were to reach equilibrium, they would be non-living, passive matter. At the same time, it has been shown that liquid phase separated compartments are important for the spatial organisation inside a large variety of cells (see reference [81] and references therein). Such compartments can organise biomolecules in space and time to control chemical reactions, which is an essential building block for biological function. Studying the physics of phase separation in non-equilibrium environments is thus highly relevant for cell biology [82].

Although several novel phenomena arising from active fluxes have been discovered in phase separating systems, many aspects have not been addressed, yet. For example, in order to realise an experimental system in which non-equilibrium reactions suppress Ostwald ripening or drive the division of droplets, a better understanding of the couplings of the chemical pathways to phase separation is necessary. To this end, one major challenge is to find a proper choice of chemicals [149]. Specifically, what is the minimal system that can be realised experimentally? If such experimental conditions were found, such systems could be used to set the droplet size in microfluidic devices in the context of chemical engineering [150].

Droplets can also carry information encoded in their chemical composition, i.e., a specific set of molecules dissolved inside. Controlling such droplets with non-equilibrium chemical reactions not only allows the change of the droplet size but also the information content. Such a system offers the opportunity to perform aqueous computing at larger-than-molecular scales [151, 152]. In addition, concentration gradients can be used to position these droplets. As droplets have reached their target position this chemical information can be released by droplet dissolution, which can be induced by modifying the interactions between the droplet material and the solvent. Such a liquid system could represent a first building block for aqueous computing, which allows to process chemical information in space.

Controlled active emulsions could also be used to physically seal or open junctions in microfluidic devices. The control over the droplet position also enables to modify the physical properties of target surfaces inside devices by wetting. All these tasks require a solid theoretical understanding of how the formation, position and composition of droplets can be controlled and how physical parameters should be

chosen.

In summary, we have discussed a new class of physical systems which we refer to as *active emulsions*. These emulsions are relevant to cell biology and may allow to develop novel applications in the field of chemical engineering or aqueous computing. However, these systems also challenge our theoretical understanding and can be used to refine theoretical concepts. In particular, *active emulsions* are characterised by non-equilibrium fluxes that maintain these system away from thermal equilibrium. The physics of phase separation in the presence of non-equilibrium chemical reactions pose several theoretical challenges and questions, such as the role of fluctuations, the couplings of diffusive and chemical fluxes, and what are the minimally required ingredients necessary for the phenomena discussed in this review.

Acknowledgments

We would like to thank Omar Adame Arana, Giacomo Bartolucci, Siheng Chen, Erwin Frey, Elisabeth Fischer-Friedrich, David Fronk, Jacqueline Janssen, Jan Kirschbaum, Samuel Krüger, Matthias Merkel, Nirbhay Patil, Payam Payamyar, Orit Peleg, Wolfram Pönisch, Rabea Seyboldt, and Jean David Wurtz, for helpful comments and discussions on our review. We thank Samuel Krüger for proving the data for Fig. 3.1 and Fig. 3.2. Finally, we would like to acknowledge Simon Alberti, Martin Z. Bazant, Edgar Boczek, Clifford P. Brangwynne, Andres Diaz, Titus Franzmann, Anatol Fritsch, Alf Honigmann, Anthony A. Hyman, Louise Jawerth, Jose Alberto Morin Lantero, Mark Leaver, Avinash Patel, Shambaditya Saha, Jeffrey B. Woodruff, and Oliver Wuescke for stimulating scientific discussions about active emulsions and droplet-like compartment inside cells. C.A.W. and D.Z. also thank the German Research Foundation (DFG) for financial support.

Appendix A. Stability of the interfacial profile

The stability of the inhomogeneous solution $c_I(x)$ given in equation (2.28) can be assessed by considering the change in free energy $\Delta F[c_I, \epsilon]$ due to an infinitesimal perturbation $\epsilon(x)$. Using equation (2.30), we have

$$\Delta F[c_I, \epsilon] = \int d^3r \left[\frac{b\epsilon^2}{2} \left(3 \tanh^2 \left(\frac{x}{w} \right) - 1 \right) + \frac{\kappa}{2} (\partial_x \epsilon)^2 \right]. \quad (\text{A.1})$$

The reference state $c_I(x)$ is stable if all perturbations increase the free energy, i.e., if $\Delta F[c_I, \epsilon] > 0$ for all permissible functions $\epsilon(x)$. Note that without chemical reactions the mass of the individual components is

conserved, which implies that only those $\epsilon(x)$ are permissible that obey the constraint $\int \epsilon dx = 0$.

To see whether all perturbations lead to positive ΔF , we determine the perturbation $\epsilon_*(x)$ with the minimal ΔF . If this value is positive, all other perturbations also increase the free energy and the base state $c_I(x)$ is stable. A necessary condition for $\epsilon_*(x)$ is that it satisfies the Euler-Lagrange equations corresponding to equation (A.1). Defining the linear operator $\mathcal{A}(\epsilon) = \delta \Delta F / \delta \epsilon$,

$$\mathcal{A}(\epsilon) = b\epsilon \left[3 \tanh^2 \left(\frac{x}{w} \right) - 1 \right] - \kappa \partial_x^2 \epsilon, \quad (\text{A.2})$$

the Euler-Lagrange equations can be expressed as

$$\mathcal{A}(\epsilon_*) = \tilde{\lambda}. \quad (\text{A.3})$$

Here, $\tilde{\lambda}$ is a Lagrange multiplier that ensures mass conservation in the case without chemical reactions, while $\tilde{\lambda} = 0$ in the case with chemical reactions. Using partial integration on equation (A.1), we also have

$$\Delta F[c_I, \epsilon] = \frac{1}{2} \int d^3r \epsilon \mathcal{A}(\epsilon), \quad (\text{A.4})$$

where we neglected the boundary terms assuming that the perturbation vanishes at the boundary or the system exhibits periodic boundary conditions. To evaluate ΔF , it is convenient to express $\epsilon_*(x)$ in terms of the eigenfunctions $\epsilon_n(x)$ of the operator \mathcal{A} . The associated eigenvalue problem $\zeta_n \epsilon_n = \mathcal{A}(\epsilon_n)$ has already been considered in the context of Schrödinger's equation with a potential similar to the first term in equation (A.2) [153]. In particular, it has been shown that the discrete part of the spectrum consists of only two eigenvalues, $\zeta_0 = 0$ and $\zeta_1 = \frac{3}{2}b$, while the continuous spectrum obeys $\zeta \geq 2b$. In the following, the sum symbol will denote both summation over the discrete and integration over the continuous part of the spectrum. The solution $\epsilon_*(x)$ can then be expressed as

$$\epsilon_*(x) = \sum_{n=0}^{\infty} a_n \epsilon_n(x), \quad (\text{A.5})$$

where a_n are the corresponding series coefficients, which have to obey $\sum_{n=0}^{\infty} a_n \zeta_n = \tilde{\lambda}$. Using this in equation (A.4), we find

$$\Delta F[c_I, \epsilon_*] = \frac{A}{2} \sum_{n=1}^{\infty} \zeta_n \int dx a_n^2 \{ \epsilon_n(x) \}^2 \geq 0, \quad (\text{A.6})$$

where A is the cross-sectional area $A = \int dy dz$. Equation (A.6) implies $\Delta F > 0$ if any $a_n \neq 0$ for $n \geq 1$, so the base state is stable with respect to these perturbations. In particular, the state c_I would only be unstable if there are perturbations with $a_0 \neq 0$

and $a_n = 0$ for $n \geq 1$. Note that the term for $n = 0$ does not appear in equation (A.6) since the eigenvalue ζ_0 vanishes. The associated eigenfunction is $\epsilon_0(x) = \partial_x c_I(x)$, which does not conserve the mass of the individual components since $\int \epsilon_0(x) dx = 2(b/a)^{1/2}$. Consequently, this mode is forbidden if chemical reactions are absent, so that all perturbations increase the free energy in this case. Conversely, with chemical reactions, $a_0 \neq 0$ is allowed and this mode is marginal since it does not change the free energy, $\Delta F(c_I, \epsilon_0) = 0$.

Taken together, we showed that the interfacial profile $c_I(x)$ given in equation (2.28) is stable in the case without chemical reactions. Chemical reactions introduce a marginal mode, which corresponds to a translation of the interface. However, for finite systems, the boundary conditions (2.27), and thus the interface profile $c_I(x)$, are only approximate and all inhomogeneous states might be unstable in very small systems [40].

Appendix B. Entropy production of a system with phase separation and chemical reactions

To derive dynamical equations for a binary fluid exhibiting phase separation and chemical reactions, we here consider the associated entropy production. For a closed, isothermal system of constant volume, the entropy production is related to the change of free energy, $dS/dt = -T^{-1}dF/dt$. For simplicity, we here consider a free energy $F = \int d^3r f(c_A, c_B)$ without the contributions proportional to the gradients of the concentration fields. Hence,

$$\begin{aligned} \frac{dF}{dt} &= \int d^3r (\mu_A \partial_t c_A + \mu_B \partial_t c_B) \\ &= - \int d^3r [\mu_A (\nabla \cdot \mathbf{j}_A + s) + \mu_B (\nabla \cdot \mathbf{j}_B - s)] \\ &= \int d^3r [\nabla \mu_A \cdot \mathbf{j}_A + \nabla \mu_B \cdot \mathbf{j}_B - s(\mu_A - \mu_B)] \\ &\quad + \text{boundary terms}, \end{aligned} \quad (\text{B.1})$$

where we have used $\mu_A = \partial f / \partial c_A$, $\mu_B = \partial f / \partial c_B$, and the conservation laws $\partial_t c_A = -\nabla \cdot \mathbf{j}_A - s$ and $\partial_t c_B = -\nabla \cdot \mathbf{j}_B + s$. Note that the boundary terms originating from partial integration can be neglected when appropriate boundary conditions are applied or an infinite system is considered.

For each component i , the flux \mathbf{j}_i can be split into a convective part with velocity \mathbf{v} and an exchange current \mathbf{j} . As discussed in section 2.4, incompressibility and equal molecular volumes then imply $\mathbf{j}_A = \mathbf{v} c_A + \mathbf{j}$ and $\mathbf{j}_B = \mathbf{v} c_B - \mathbf{j}$. Moreover, changes of the intensive thermodynamic quantities are coupled, implying the Gibbs-Duhem relationship $c_A d\mu_A + c_B d\mu_B = dp$,

where p is the pressure. Hence,

$$\frac{dF}{dt} = \int d^3r (\mathbf{j} \cdot \nabla \bar{\mu} + p \nabla \cdot \mathbf{v} - s \bar{\mu}) , \quad (\text{B.2})$$

where $\bar{\mu} = \mu_A - \mu_B$ is the exchange chemical potential. In the case of equal molecular volumes of A and B , incompressibility implies $\nabla \cdot \mathbf{v} = 0$ [126], leading to

$$\frac{dS}{dt} = \frac{1}{T} \int d^3r (-\mathbf{j} \cdot \nabla \bar{\mu} + s \bar{\mu}) . \quad (\text{B.3})$$

This expression reveals that the thermodynamic fluxes \mathbf{j} and s are coupled to the thermodynamic forces $\nabla \bar{\mu}$ and $\bar{\mu}$, respectively. Expressing the fluxes as linear functions of their forces, we obtain $\mathbf{j} = -\Lambda \nabla \bar{\mu}$ and $s = \Lambda_r \bar{\mu}$, where the Onsager coefficients Λ and Λ_r must be positive to obey the second law of thermodynamics ($dS/dt \geq 0$). The entropy production only vanishes at equilibrium, where the equilibrium conditions $\nabla \bar{\mu} = 0$ and $\bar{\mu} = 0$ are obeyed and the fluxes vanish.

Appendix C. Thermodynamic constraints on chemical reaction rates

We consider a simple conversion reaction $A \rightleftharpoons B$ in a binary system with local equilibrium. The system is described by the concentrations of the B and the A -particles. Both concentrations are connected via the relationship $c_B = \nu^{-1} - c_A$, where ν is the molecular volume of both species. The concentration of B particles changes in time as

$$\partial_t c_B = s_{\rightarrow} - s_{\leftarrow} , \quad (\text{C.1})$$

where s_{\rightarrow} and s_{\leftarrow} denote the respective forward and backward reaction flux. To derive the condition on the ratio of these fluxes given in equation (4.1), we here analyze the associated lattice model introduced in section 2.1.

We consider a system of M lattice sites and focus on the reactions occurring at the arbitrary lattice site n . The probabilities to find an A or B particle at this site are given by $P(\sigma_n, t)$ or $P(\bar{\sigma}_n, t)$, respectively. Here, the configuration of all particles on the lattice where lattice site n is occupied by an A particle ($\sigma_n = 1$) is denoted as $\sigma_n = \sigma_1, \dots, \sigma_n = 1, \dots, \sigma_M$. Conversely, $\bar{\sigma}_n = \sigma_1, \dots, \sigma_n = 0, \dots, \sigma_M$, is a configuration where the n -th site is occupied by B . These probability functions are related to the considered volume fraction and concentration fields by

$$\phi = c_A \nu = \sum_{\Omega_n} P(\sigma_n, t) , \quad (\text{C.2a})$$

$$1 - \phi = c_B \nu = \sum_{\bar{\Omega}_n} P(\bar{\sigma}_n, t) , \quad (\text{C.2b})$$

where Ω_n or $\bar{\Omega}_n$ denote the set of all possible configurations with an A or B particle at lattice site n , respectively. The time evolution of the probabilities is captured by the master equation

$$\begin{aligned}\partial_t P(\bar{\sigma}_n, t) &= -\partial_t P(\sigma_n, t) \\ &= k_{\rightarrow}^n(\sigma_n)P(\sigma_n, t) - k_{\leftarrow}^n(\bar{\sigma}_n)P(\bar{\sigma}_n, t),\end{aligned}\quad (\text{C.3})$$

where $k_{\rightarrow}^n(\sigma_n)$ and $k_{\leftarrow}^n(\bar{\sigma}_n)$ denote the forward and backward rates, which generally depend on the configuration. The equations discussed so far also hold when the reaction is not in equilibrium.

When the chemical reactions are equilibrated, the probability distribution is time independent, leading to the condition of detailed balance:

$$k_{\rightarrow}^n(\sigma_n)P^{\text{eq}}(\sigma_n) = k_{\leftarrow}^n(\bar{\sigma}_n)P^{\text{eq}}(\bar{\sigma}_n). \quad (\text{C.4})$$

Here, the equilibrium distribution to find a specific configuration, $\sigma_1, \dots, \sigma_M$, is given as

$$P^{\text{eq}}(\sigma_1, \dots, \sigma_M) = \frac{1}{Z} \exp\left(-\frac{H(\sigma_1, \dots, \sigma_M)}{k_{\text{B}}T}\right), \quad (\text{C.5})$$

with the Hamiltonian $H(\sigma_1, \dots, \sigma_M)$ defined in equation (2.2) and the partition function Z given by equation (2.1). Using equation (C.4), we have

$$\begin{aligned}\frac{k_{\rightarrow}^n(\sigma_n)}{k_{\leftarrow}^n(\bar{\sigma}_n)} &= \frac{P^{\text{eq}}(\bar{\sigma}_n)}{P^{\text{eq}}(\sigma_n)} \\ &= \exp\left[-\frac{H(\bar{\sigma}_n) - H(\sigma_n)}{k_{\text{B}}T}\right].\end{aligned}\quad (\text{C.6})$$

For the considered case of a single reaction step and for short ranged interactions, the forward and backward rates do not depend on the full configuration $\{\sigma\}$. Instead, the rates solely depend on the particle configurations in the vicinity of site n , which is determined by the characteristic length scale of the interaction. In particular, using a mean field approximation, the rates solely depend on the local volume fraction ϕ . In this case, the energy difference appearing in equation (C.6) simplifies to

$$H(\bar{\sigma}_n) - H(\sigma_n) = \frac{1}{M} \frac{dE(\phi)}{d\phi}, \quad (\text{C.7})$$

where $E(\phi)$ is the mean field energy given by equation (2.6), such that

$$\frac{dE(\phi)}{d\phi} = zM [e_{AA}\phi + e_{AB}(1 - 2\phi) - e_{BB}(1 - \phi)]. \quad (\text{C.8})$$

Combining equations (C.6) and (C.7), we find that the rates solely depend on the local volume fraction ϕ , i.e., $k_{\rightarrow}^n(\sigma_n) = k_{\rightarrow}(\phi)$ and $k_{\leftarrow}^n(\bar{\sigma}_n) = k_{\leftarrow}(\phi)$.

We now return to the case where chemical reactions are not equilibrated. Taking the time

derivative of equation (C.2b) and using equation (C.3), we write the time evolution of the composition as

$$\begin{aligned}\partial_t c_B &= \frac{1}{\nu} \sum_{\bar{\Omega}_n} \left[k_{\rightarrow}^n P(\sigma_n, t) - k_{\leftarrow}^n P(\bar{\sigma}_n, t) \right] \\ &= k_{\rightarrow}(\phi) (\nu^{-1} - c_B) - k_{\leftarrow}(\phi) c_B,\end{aligned}\quad (\text{C.9})$$

where we have used that the forward and backward rate solely depend on ϕ within the mean field approximation. Comparing with equation (C.1), we can identify the forward and backward reaction flux as $s_{\rightarrow} = k_{\rightarrow}(\phi) (\nu^{-1} - c_B)$ and $s_{\leftarrow} = k_{\leftarrow}(\phi) c_B$. Hence, using $\phi = 1 - \nu c_B$, the fraction of the reaction fluxes read

$$\frac{s_{\rightarrow}}{s_{\leftarrow}} = \frac{k_{\rightarrow}(\phi)}{k_{\leftarrow}(\phi)} \frac{\phi}{(1 - \phi)} = \exp\left(\frac{\bar{\mu}}{k_{\text{B}}T}\right). \quad (\text{C.10})$$

where we defined

$$\begin{aligned}\bar{\mu} &= z [e_{AA}\phi + e_{AB}(1 - 2\phi) - e_{BB}(1 - \phi)] \\ &+ k_{\text{B}}T \ln\left(\frac{\phi}{1 - \phi}\right),\end{aligned}\quad (\text{C.11})$$

which can be identified with the exchange chemical potential $\bar{\mu} = \mu_A - \mu_B = \nu \frac{\partial f}{\partial \phi}$ associated with the free energy density $f(\phi)$ given in equation (2.8). Note that equation (C.11) does not contain any gradient term since we here focused on the simple case of homogeneous mean field. However, equation (C.10) also holds for more general situations and is referred to as detailed balance of the rates [133].

References

- [1] Syrbe A, Bauer W, Klostermeyer H. Polymer science concepts in dairy systems: an overview of milk protein and food hydrocolloid interaction. *International Dairy Journal*. 1998;8(3):179–193.
- [2] Clerk-Maxwell J. On the dynamical evidence of the molecular constitution of bodies. *Nature*. 1875;11(279):357–359.
- [3] Flory PJ. Thermodynamics of high polymer solutions. *The Journal of chemical physics*. 1942;10(1):51–61.
- [4] Huggins ML. Some Properties of Solutions of Long-chain Compounds. *The Journal of Physical Chemistry*. 1942;46(1):151–158.
- [5] Ostwald W. Studien über die Bildung und Umwandlung fester Körper. *Zeitschrift für physikalische Chemie*. 1897;22(1):289–330.
- [6] Lifshitz IM, Slyozov VV. The kinetics of precipitation from supersaturated solid solutions. *Journal of Physics and Chemistry of Solids*. 1961;19(1?2):35–50.
- [7] Wagner C. Theorie der Alterung von Niederschlägen durch Umlösen (Ostwald-Reifung). *Berichte der Bunsengesellschaft für physikalische Chemie*. 1961;65(7):581–591.
- [8] Bray AJ. Theory of phase-ordering kinetics. *Advances in Physics*. 1994;43(3):357–459.
- [9] Cahn JW. Critical point wetting. *The Journal of Chemical Physics*. 1977;66(8):3667–3672.

[10] Moldover M, Cahn JW. An interface phase transition: Complete to partial wetting. *Science*. 1980;207(4435):1073–1075.

[11] Pohl D, Goldburg W. Wetting transition in lutidine-water mixtures. *Physical Review Letters*. 1982;48(16):1111.

[12] Style RW, Sai T, Fanelli N, Ijavi M, Smith-Mannschott K, Xu Q, et al. Liquid-Liquid Phase Separation in an Elastic Network. *Physical Review X*. 2018;8(1):011028.

[13] Herminghaus S, Maass CC, Krüger C, Thutupalli S, Goehring L, Bahr C. Interfacial mechanisms in active emulsions. *Soft Matter*. 2014 jun;10(36):7008–7022. Available from: <http://pubs.rsc.org/en/content/articlehtml/2014/sm/c4sm00550c&http://xlink.rsc.org/?DOI=C4SM00550C>.

[14] Izri Z, van der Linden MN, Michelin S, Dauchot O. Self-Propulsion of Pure Water Droplets by Spontaneous Marangoni-Stress-Driven Motion. *Phys Rev Lett*. 2014 dec;113(24):248302. Available from: <http://link.aps.org/doi/10.1103/PhysRevLett.113.248302>.

[15] Maass CC, Krüger C, Herminghaus S, Bahr C. Swimming droplets. *Annual Review of Condensed Matter Physics*. 2016;7:171–193.

[16] Seemann R, Fleury JB, Maass CC. Self-propelled droplets. *Eur Phys J Spec Top*. 2016;225(11-12):2227–2240. Available from: <http://link.springer.com/10.1140/epjst/e2016-60061-7>.

[17] Jin C, Krüger C, Maass CC. Chemotaxis and autochemotaxis of self-propelling droplet swimmers. *Proc Natl Acad Sci*. 2017;114(20):5089–5094. Available from: <http://www.ncbi.nlm.nih.gov/pubmed/28465433>.

[18] Caschera F, Rasmussen S, Hanczyc MM. An Oil Droplet Division-Fusion Cycle. *Chempluschem*. 2013 jan;78(1):52–54. Available from: <http://doi.wiley.com/10.1002/cplu.201200275>.

[19] Sellier M, Nock V, Verdier C. Self-propelling, coalescing droplets. *International Journal of Multiphase Flow*. 2011;37(5):462–468.

[20] Jehannin M, Charton S, Karpitschka S, Zemb T, Möhwald H, Riegler H. Periodic precipitation patterns during coalescence of reacting sessile droplets. *Langmuir*. 2015;31(42):11484–11490.

[21] Cira NJ, Benusiglio A, Prakash M. Vapour-mediated sensing and motility in two-component droplets. *Nature*. 2015 Mar;519(7544):446–50.

[22] Tan H, Diddens C, Lv P, Kuerten JGM, Zhang X, Lohse D. Evaporation-triggered microdroplet nucleation and the four life phases of an evaporating Ouzo drop. *Proc Natl Acad Sci U S A*. 2016 08;113(31):8642–7.

[23] Löwen H. Colloidal soft matter under external control. *Journal of Physics: Condensed Matter*. 2001;13(24):R415. Available from: <http://stacks.iop.org/0953-8984/13/i=24/a=201>.

[24] Lee KWD, Chan PK, Feng X. Morphology development and characterization of the phase-separated structure resulting from the thermal-induced phase separation phenomenon in polymer solutions under a temperature gradient. *Chemical Engineering Science*. 2004;59(7):1491 – 1504.

[25] Kokal SL, et al. Crude oil emulsions: A state-of-the-art review. *SPE Production & facilities*. 2005;20(01):5–13.

[26] Matsuyama H, Berghmans S, Lloyd DR. Formation of anisotropic membranes via thermally induced phase separation. *Polymer*. 1999;40(9):2289–2301.

[27] Matsuyama H, Yuasa M, Kitamura Y, Teramoto M, Lloyd DR. Structure control of anisotropic and asymmetric polypropylene membrane prepared by thermally induced phase separation. *Journal of Membrane Science*. 2000;179(1):91–100.

[28] Caneba GT, Soong DS. Polymer membrane formation through the thermal-inversion process. 1. Experimental study of membrane structure formation. *Macromolecules*. 1985;18(12):2538–2545.

[29] Caneba GT, Soong DS. Polymer membrane formation through the thermal-inversion process. 2. Mathematical modeling of membrane structure formation. *Macromolecules*. 1985;18(12):2545–2555.

[30] Lee CF, Brangwynne CP, Gharakhani J, Hyman AA, Jülicher F. Spatial Organization of the Cell Cytoplasm by Position-Dependent Phase Separation. *Phys Rev Lett*. 2013 Aug;111:088101.

[31] Weber CA, Lee CF, Jülicher F. Droplet ripening in concentration gradients. *New Journal of Physics*. 2017;19(5):053021. Available from: <http://stacks.iop.org/1367-2630/19/i=5/a=053021>.

[32] Song H, Chen DL, Ismagilov RF. Reactions in droplets in microfluidic channels. *Angewandte chemie international edition*. 2006;45(44):7336–7356.

[33] Fallah-Araghi A, Meguellati K, Baret JC, Harrak AE, Mangeat T, Karplus M, et al. Enhanced Chemical Synthesis at Soft Interfaces: A Universal Reaction-Adsorption Mechanism in Microcompartments. *Physical Review Letters*. 2014 jan;112(2):28301. Available from: <http://link.aps.org/doi/10.1103/PhysRevLett.112.028301>.

[34] John K, Bär M, Thiele U. Self-propelled running droplets on solid substrates driven by chemical reactions. *The European Physical Journal E: Soft Matter and Biological Physics*. 2005;18(2):183–199.

[35] Yabunaka S, Ohta T, Yoshinaga N. Self-propelled motion of a fluid droplet under chemical reaction. *The Journal of chemical physics*. 2012;136(7):074904.

[36] Seemann R, Fleury JB, Maass CC. Self-propelled droplets. *The European Physical Journal Special Topics*. 2016;225(11-12):2227–2240.

[37] Kuksenok O, Jasnow D, Yeomans J, Balazs AC. Periodic Droplet Formation in Chemically Patterned Microchannels. *Phys Rev Lett*. 2003 Sep;91:108303. Available from: <https://link.aps.org/doi/10.1103/PhysRevLett.91.108303>.

[38] Delgado J, Li N, Leda M, González-Ochoa HO, Fraden S, Epstein IR. Coupled oscillations in a 1D emulsion of Belousov-Zhabotinsky droplets. *Soft Matter*. 2011;7(7):3155–3167.

[39] Vanag VK, Epstein IR. Excitatory and inhibitory coupling in a one-dimensional array of Belousov-Zhabotinsky micro-oscillators: Theory. *Physical Review E*. 2011;84(6):066209.

[40] Krapivsky PL, Redner S, Ben-Naim E. *A Kinetic View of Statistical Physics*. Cambridge University Press; 2010. Available from: <http://books.google.co.uk/books?id=cc3pApnX3kYC>.

[41] Puri S, Frisch H. Segregation dynamics of binary mixtures with simple chemical reactions. *J Phys A*. 1994 00;27:6027–6038. Available from: <http://iopscience.iop.org/0305-4470/27/18/013>.

[42] Glotzer SC, Stauffer D, Jan N. Monte Carlo simulations of phase separation in chemically reactive binary mixtures. *Phys Rev Lett*. 1994 00;72(26):4109–4112. Available from: http://prl.aps.org/abstract/PRL/v72/i26/p4109_1.

[43] Glotzer SC, Coniglio A. Self-consistent solution of phase separation with competing interactions. *Phys Rev E*. 1994 00;50(5):4241–4244. Available from: http://pre.aps.org/abstract/PRE/v50/i5/p4241_1.

[44] Glotzer SC, Di Marzio EA, Muthukumar M. Reaction-controlled morphology of phase-separating mixtures. *Phys Rev Lett*. 1995 00;74(11):2034–2037. Available from: http://prl.aps.org/abstract/PRL/v74/i11/p2034_1.

[45] Glotzer SC, Stauffer D, Jan N. Glotzer, Stauffer, and Jan Reply. *Phys Rev Lett.* 1995 00;75(8):1675. Available from: http://prl.aps.org/abstract/PRL/v75/i8/p1675_1.

[46] Verdasca J, Borckmans P, Dewel G. Chemically frozen phase separation in an adsorbed layer. *Phys Rev E.* 1995 00;52(5):R4616–R4619.

[47] Christensen JJ, Elder K, Fogedby HC. Phase segregation dynamics of a chemically reactive binary mixture. *Phys Rev E.* 1996 00;54(3):R2212–R2215. Available from: http://pre.aps.org/abstract/PRE/v54/i3/pR2212_1.

[48] Toxvaerd S. Molecular dynamics simulations of phase separation in chemically reactive binary mixtures. *Phys Rev E.* 1996 00;53(4):3710–3716. Available from: http://pre.aps.org/abstract/PRE/v53/i4/p3710_1.

[49] Motoyama M. Morphology of Binary Mixtures Which Undergo Phase Separation during Chemical Reactions. *J Phys Soc Jpn.* 1996 00;65(7):1894–1897. Available from: <http://www.scopus.com/inward/record.url?partnerID=yv4JPVwI&eid=2-s2.0-0030508032&md5=a77bd1fc1518a4204eeefedbdb27b6a>.

[50] Motoyama M, Ohta T. Morphology of Phase-Separating Binary Mixtures with Chemical Reaction. *J Phys Soc Jpn.* 1997 00;66(9):2715–2725. Available from: <http://www.scopus.com/inward/record.url?partnerID=yv4JPVwI&eid=2-s2.0-0031480095&md5=05df460f4fb86d8024dfb60c2de2b9ca>.

[51] Huo Y, Zhang H, Yang Y. Effects of reversible chemical reaction on morphology and domain growth of phase separating binary mixtures with viscosity difference. *Macromolecular theory and simulations.* 2004;13(3):280–289.

[52] Travasso RD, Kuksenok O, Balazs AC. Harnessing light to create defect-free, hierarchically structured polymeric materials. *Langmuir.* 2005;21(24):10912–10915.

[53] Kuksenok O, Travasso RDM, Balazs AC. Dynamics of ternary mixtures with photosensitive chemical reactions: creating three-dimensionally ordered blends. *Phys Rev E.* 2006 Jul;74(1 Pt 1):011502.

[54] Li H, Liu H, Lu ZY, Wang Q, Sun CC. The effect of viscosity on the phase separation dynamics of binary immiscible mixture coupled with reversible reaction. *International Journal of Modern Physics C.* 2010 00;21(12):1479–1488. Available from: <http://www.scopus.com/inward/record.url?partnerID=yv4JPVwI&eid=2-s2.0-78650720041&md5=2a9c3be451cf13e8a1fb7e993ec9e82c>.

[55] Harada A, Tran-Cong Q. Experimental verification of a scaling law for phase separation kinetics of reacting polymer mixtures. *Macromolecules.* 1996;29(13):4801–4803.

[56] Tran-Cong Q, Harada A. Reaction-induced ordering phenomena in binary polymer mixtures. *Phys Rev Lett.* 1996 00;76:1162–1165. Available from: <http://link.aps.org/doi/10.1103/PhysRevLett.76.1162>.

[57] Tran-Cong Q, Ohta T, Urakawa O. Soft-mode suppression in the phase separation of binary polymer mixtures driven by a reversible chemical reaction. *Physical Review E.* 1997;56(1):R59.

[58] Ohta T, Urakawa O, Tran-Cong Q. Phase separation of binary polymer blends driven by photoisomerization: An example for a wavelength-selection process in polymers. *Macromolecules.* 1998;31(20):6845–6854.

[59] Tran-Cong Q, Kawai J, Endoh K. Modes selection in polymer mixtures undergoing phase separation by photochemical reactions. *Chaos.* 1999 00;9(2):298–307. Available from: http://chaos.aip.org/resource/1/chaoeh/v9/i2/p298_s1.

[60] Tran-Cong Q, Kawai J, Nishikawa Y, Jinnai H. Phase separation with multiple length scales in polymer mixtures induced by autocatalytic reactions. *Phys Rev E.* 1999 00;60(2 Pt A):R1150–3. Available from: http://pre.aps.org/abstract/PRE/v60/i2/pR1150_1.

[61] Sutton D, Stanford J, Ryan A. Reaction-Induced Phase-Separation in Polyoxyethylene/Polystyrene Blends. II. Structure Development. *Journal of Macromolecular Science, Part B.* 2004;43(1):233–251.

[62] Tran-Cong-Miyata Q, Nakanishi H. Phase separation of polymer mixtures driven by photochemical reactions: current status and perspectives. *Polymer International.* 2017;66(2):213–222.

[63] Tanaka H, Suzuki T, Hayashi T, Nishi T. New type of pattern formation in polymer mixtures caused by competition between phase separation and chemical reaction. *Macromolecules.* 1992;25(17):4453–4456.

[64] Inoue T. Reaction-induced phase decomposition in polymer blends. *Progress in Polymer Science.* 1995;20(1):119–153.

[65] Williams RJJ, Rozenberg BA, Pascault JP. In: *Reaction-induced phase separation in modified thermosetting polymers.* Berlin, Heidelberg: Springer Berlin Heidelberg; 1997. p. 95–156. Available from: https://doi.org/10.1007/3-540-61218-1_7.

[66] Chan PK, Rey AD. Polymerization-induced phase separation. 1. Droplet size selection mechanism. *Macromolecules.* 1996;29(27):8934–8941.

[67] Chan PK, Rey AD. Polymerization-induced phase separation. 2. Morphological analysis. *Macromolecules.* 1997;30(7):2135–2143.

[68] Girard-Reydet E, Sautereau H, Pascault JP, Keates P, Navard P, Thollet G, et al. Reaction-induced phase separation mechanisms in modified thermosets. *Polymer.* 1998;39(11):2269–2279.

[69] Kataoka K, Urakawa O, Nishioka H, Tran-Cong Q. Directional phase separation of binary polymer blends driven by photo-cross-linking with linearly polarized light. *Macromolecules.* 1998;31(25):8809–8816.

[70] Locatelli A, Mentes TO, Aballe L, Mikhailov A, Kiskinova M. Formation of regular surface-supported mesostructures with periodicity controlled by chemical reaction rate. *J Phys Chem B.* 2006 Oct;110(39):19108–11.

[71] Zwicker D, Decker M, Jaensch S, Hyman AA, Jülicher F. Centrosomes are autocatalytic droplets of pericentriolar material organized by centrioles. *Proc Natl Acad Sci USA.* 2014;111(26):E2636–45.

[72] Zwicker D, Hyman AA, Jülicher F. Suppression of Ostwald ripening in Active Emulsions. *Phys Rev E.* 2015;92:012317.

[73] Zwicker D, Seyboldt R, Weber CA, Hyman AA, Jülicher F. Growth and division of active droplets provides a model for protocells. *Nat Phys.* 2017;13:408–413.

[74] Tena-Solsona M, Rieß B, Grötsch RK, Löhrer FC, Wanzke C, Käsdorf B, et al. Non-equilibrium dissipative supramolecular materials with a tunable lifetime. *Nature communications.* 2017;8:15895.

[75] Tena-Solsona M, Wanzke B Caren Rieß, Bausch AR, Boekhoven J. Self-selection of dissipative assemblies driven by primitive chemical reaction networks. *Nature communications.* 2018;9:2044.

[76] Ernster L, Schatz G. Mitochondria: a historical review. *J Cell Biol.* 1981;91(3):227s–255s.

[77] Brangwynne CP. Soft active aggregates: mechanics, dynamics and self-assembly of liquid-like intracellular protein bodies. *Soft Matter.* 2011;7(7):3052–3059.

[78] Hyman AA, Brangwynne C. Beyond Stereospecificity: Liquids and Mesoscale Organization of Cytoplasm. *Dev Cell.* 2011 00;21(1):14–16. Available from: <http://eutils.ncbi.nlm.nih.gov/entrez/eutils/elink.fcgi?dbfrom=pubmed&id=21763600&retmode=>

ref&cmd=prlinks.

[79] Hyman AA, Weber CA, Jülicher F. Liquid-liquid phase separation in biology. *Annual review of cell and developmental biology*. 2014;30:39–58.

[80] Brangwynne CP, Tompa P, Pappu RV. Polymer physics of intracellular phase transitions. *Nature Physics*. 2015;11(11):899–904.

[81] Banani SF, Lee HO, Hyman AA, Rosen MK. Biomolecular condensates: organizers of cellular biochemistry. *Nature Reviews Molecular Cell Biology*. 2017;18(5):285–298.

[82] Berry J, Brangwynne CP, Haataja M. Physical principles of intracellular organization via active and passive phase transitions. *Reports on Progress in Physics*. 2018;81(4):046601. Available from: <http://stacks.iop.org/0034-4885/81/i=4/a=046601>.

[83] Sear RP. Dishevelled: a protein that functions in living cells by phase separating. *Soft Matter*. 2007;3(6):680–684. Available from: <http://dx.doi.org/10.1039/B618126K>.

[84] Brangwynne CP, Eckmann CR, Courson DS, Rybarska A, Hoege C, Gharakhani J, et al. Germline P Granules Are Liquid Droplets That Localize by Controlled Dissolution/Condensation. *Science*. 2009;324(5935):1729–1732.

[85] Saha S, Weber CA, Nousch M, Adame-Arana O, Hoege C, Hein MY, et al. Polar Positioning of Phase-Separated Liquid Compartments in Cells Regulated by an mRNA Competition Mechanism. *Cell*. 2016;166(6):1572–1584.

[86] Woodruff JB, Gomes BF, Widlund PO, Mahamid J, Honigmann A, Hyman AA. The centrosome is a selective condensate that nucleates microtubules by concentrating tubulin. *Cell*. 2017;169(6):1066–1077.

[87] Brangwynne CP, Mitchison TJ, Hyman AA. Active liquid-like behavior of nucleoli determines their size and shape in *Xenopus laevis* oocytes. *Proceedings of the National Academy of Sciences*. 2011;108(11):4334–4339.

[88] Feric M, Vaidya N, Harmon TS, Mitrea DM, Zhu L, Richardson TM, et al. Coexisting liquid phases underlie nucleolar subcompartments. *Cell*. 2016;165(7):1686–1697.

[89] Sear RP, Cuesta JA. Instabilities in Complex Mixtures with a Large Number of Components. *Physical Review Letters*. 2003 dec;91(24):245701. Available from: <https://link.aps.org/doi/10.1103/PhysRevLett.91.245701>.

[90] Jacobs WM, Frenkel D. Phase Transitions in Biological Systems with Many Components. *Biophysical Journal*. 2017 feb;112(4):683–691. Available from: <http://www.cell.com/article/S0006349516343363/fulltext>.

[91] Cates ME, Tjhung E. Theories of binary fluid mixtures: from phase-separation kinetics to active emulsions. *Journal of Fluid Mechanics*. 2018;836.

[92] Balian R. From microphysics to macrophysics: methods and applications of statistical physics. vol. 1. Springer Science & Business Media; 2007.

[93] Frenkel D. Why colloidal systems can be described by statistical mechanics: some not very original comments on the Gibbs paradox. *Molecular Physics*. 2014;112(17):2325–2329.

[94] Safran SA. Statistical Thermodynamics of Surface, Interfaces and Membranes. Addison-Wesley Publishing Company; 1994.

[95] Israelachvili JN. Intermolecular and surface forces. Academic press; 2011.

[96] Rubinstein M, Colby RH. Polymer physics. Oxford: OUP Oxford; 2003.

[97] Yeomans JM. Statistical mechanics of phase transitions. Clarendon Press; 1992.

[98] Balian R. From microphysics to macrophysics: methods and applications of statistical physics. vol. 2. Springer Science & Business Media; 2007.

[99] Callen HB. Thermodynamics and an Introduction to Thermostatistics. Wiley; 1985.

[100] De Groot SR, Mazur P. Non-equilibrium thermodynamics. Courier Corporation; 2013.

[101] Onuki A. Phase transition dynamics. Cambridge University Press. 2002.

[102] Chaikin PM, Lubensky TC. Principles of Condensed Matter Physics. Cambridge University Press; 2000. Available from: <http://www.amazon.ca/exec/obidos/redirect?tag=citeulike09-20&path=ASIN/0521794501>.

[103] Cahn JW. On spinodal decomposition. *Acta Metallurgica*. 1961;9(9):795 – 801. Available from: <http://www.sciencedirect.com/science/article/pii/0001616061901821>.

[104] Siggia ED. Late stages of spinodal decomposition in binary mixtures. *Phys Rev A*. 1979 Aug;20:595–605. Available from: <http://link.aps.org/doi/10.1103/PhysRevA.20.595>.

[105] Tanaka H. A new coarsening mechanism of droplet spinodal decomposition. *The Journal of Chemical Physics*. 1995;103(6):2361–2364. Available from: <http://scitation.aip.org/content/aip/journal/jcp/103/6/10.1063/1.469658>.

[106] Mecke KR, Sofonea V. Morphology of spinodal decomposition. *Physical Review E*. 1997;56(4):R3761.

[107] Hayward S, Heermann DW, Binder K. Dynamic percolation transition induced by phase separation: A Monte Carlo analysis. *Journal of statistical physics*. 1987;49(5-6):1053–1081.

[108] Wagner AJ, Yeomans JM. Spinodal decomposition in two-dimensional binary fluids. *International Journal of Modern Physics C*. 1998;9(08):1373–1382.

[109] Sappelt D, Jäckle J. Percolation inversion in spinodal decomposition of mixtures with strong kinetic asymmetry. *Polymer*. 1998;39(21):5253 – 5256. Available from: <http://www.sciencedirect.com/science/article/pii/S0032386197100829>.

[110] Ip SW, Toguri JM. The Equivalency of Surface-Tension, Surface-Energy and Surface Free-Energy. *J Mater Sci*. 1994 00;29(3):688–692.

[111] Landau LD, Lifshitz EM. Course of theoretical physics 6, Hydrodynamics. Elsevier; 2013.

[112] Hohenberg P, Halperin B. Theory of dynamic critical phenomena. *Rev Mod Phys*. 1977 00;49:435–479. Available from: http://rmp.aps.org/abstract/RMP/v49/i3/p435_1.

[113] Cates M. Complex fluids: the physics of emulsions. *Soft Interfaces: Lecture Notes of the Les Houches Summer School*: Volume 98, July 2012. 2017;98:317.

[114] Tolman RC. The effect of droplet size on surface tension. *J Chem Phys*. 1949;17(3):333–337.

[115] Blokhuis EM, Kuipers J. Thermodynamic expressions for the Tolman length. *J Chem Phys*. 2006 Feb;124(7):74701.

[116] Lifshitz EM, Pitaevskii LP. Physical Kinetics: Volume 10 (Course of Theoretical Physics). Butterworth-Heinemann; 1981.

[117] Binder K, Stauffer D. Statistical theory of nucleation, condensation and coagulation. *Advances in Physics*. 1976;25(4):343–396. Available from: <http://www.tandfonline.com/doi/abs/10.1080/00018737600101402>.

[118] Binder K. Nucleation barriers, spinodals, and the Ginzburg criterion. *Physical Review A*. 1984;29(1):341.

[119] Yao JH, Elder K, Guo H, Grant M. Ostwald ripening in two and three dimensions. *Physical Review B*. 1992;45(14):8173.

[120] Yao JH, Elder K, Guo H, Grant M. Theory and simulation of Ostwald ripening. *Physical review B*. 1993;47(21):14110.

[121] Siggia E. Late stages of spinodal decomposition in binary mixtures. *Physical Review A*. 1979;20(2):595–605. Available from: <http://dx.doi.org/10.1103/PhysRevA.20.595>.

[122] Tanaka H. Viscoelastic phase separation. *Journal of Physics: Condensed Matter*. 2000;12(15):R207. Available from: <http://stacks.iop.org/0953-8984/12/i=15/a=201>.

[123] Araki T, Tanaka H. Three-Dimensional Numerical Simulations of Viscoelastic Phase Separation: Morphological Characteristics. *Macromolecules*. 2001;34(6):1953–1963. Available from: <http://pubs.acs.org/doi/abs/10.1021/ma001569n>.

[124] Tanaka H, Araki T. Viscoelastic phase separation in soft matter: Numerical-simulation study on its physical mechanism. *Chemical Engineering Science*. 2006;61(7):2108 – 2141. Available from: <http://www.sciencedirect.com/science/article/pii/S0009250905004069>.

[125] Weiss M, Elsner M, Kartberg F, Nilsson T. Anomalous subdiffusion is a measure for cytoplasmic crowding in living cells. *Biophysical journal*. 2004 nov;87(5):3518–24.

[126] Jülicher F, Prost J. Generic theory of colloidal transport. *The European Physical Journal E: Soft Matter and Biological Physics*. 2009;29(1):27–36.

[127] Tenlen J, Molk J, London N, Page B, Priess J. MEX-5 asymmetry in one-cell *C. elegans* embryos requires PAR-4- and PAR-1-dependent phosphorylation. *Development*. 2008;135(22):3665–3675.

[128] Griffin E, Odde D, Seydoux G. Regulation of the MEX-5 Gradient by a Spatially Segregated Kinase/Phosphatase Cycle. *Cell*. 2011;146(6):955–968.

[129] Lajzerowicz J, Sivardière J. Spin-1 lattice-gas model. I. Condensation and solidification of a simple fluid. *Physical Review A*. 1975;11(6):2079.

[130] Sivardière J, Lajzerowicz J. Spin-1 lattice-gas model. II. Condensation and phase separation in a binary fluid. *Physical Review A*. 1975;11(6):2090.

[131] Krüger S, Weber CA, Sommer JU, Jülicher F. Switching Droplet Positions by Concentration Gradients. *arXiv preprint arXiv:170407276*. 2017;.

[132] Krüger S, Weber CA, Sommer JU, Jülicher F. in preparation;.

[133] Jülicher F, Ajdari A, Prost J. Modeling molecular motors. *Rev Mod Phys*. 1997 00;69(4):1269–1282. Available from: <http://link.aps.org/doi/10.1103/RevModPhys.69.1269>.

[134] Allen SM, Cahn JW. A microscopic theory for antiphase boundary motion and its application to antiphase domain coarsening. *Acta Metallurgica*. 1979;27(6):1085–1095.

[135] Gitterman M, Steinberg V. Thermodynamic stability and phase transitions in systems with a chemical reaction. *The Journal of Chemical Physics*. 1978;69(6):2763–2770.

[136] Lamorgese A, Mauri R. Spinodal decomposition of chemically reactive binary mixtures. *Phys Rev E*. 2016 Aug;94(2-1):022605.

[137] Gunton J. The dynamics of first-order phase transitions. *Phase transitions and critical phenomena*. 1983;8:267.

[138] Lefever R, Carati D, Hassani N. Comment on "Monte Carlo Simulations of Phase Separation in Chemically Reactive Binary Mixtures". *Phys Rev Lett*. 1995 00;75(8):1674. Available from: http://prl.aps.org/abstract/PRL/v75/i8/p1674_1.

[139] Liu F, Goldenfeld N. Dynamics of phase separation in block copolymer melts. *Phys Rev A*. 1989 00;39(9):4805–4810. Available from: http://pra.aps.org/abstract/PRA/v39/i9/p4805_1.

[140] Muratov CB. Theory of domain patterns in systems with long-range interactions of Coulomb type. *Phys Rev E*. 2002 00;66(6 Pt 2):066108. Available from: <http://pre.aps.org/abstract/PRE/v66/i6/e066108>.

[141] Sagui C, Desai RC. Ostwald ripening in systems with competing interactions. *Phys Rev Lett*. 1995;74(7):1119.

[142] Sagui C, Desai RC. Effects of long-range repulsive interactions on Ostwald ripening. *Phys Rev E*. 1995;52(3):2822.

[143] Carati D, Lefever R. Chemical freezing of phase separation in immiscible binary mixtures. *Phys Rev E*. 1997 00;56(3 B):3127–3136. Available from: <http://www.scopus.com/inward/record.url?partnerID=yv4JPVwI&eid=2-s2.0-0031222291&md5=e3425af640abdbd6bf5a50f6f36fb76a>.

[144] Bazant MZ. Thermodynamic stability of driven open systems and control of phase separation by electro-autocatalysis. *Faraday discussions*. 2017;199:423–463.

[145] Kacser H, Burns JA, Fell DA. The control of flux. *Biochem Soc Trans*. 1995;23(2):341–366.

[146] Golestanian R. Origin of life: Division for multiplication. *Nature Physics*. 2017;13(4):323–324.

[147] Mullins WW, Sekerka RF. Morphological stability of a particle growing by diffusion or heat flow. *J Appl Phys*. 1963;34(2):323–329.

[148] Mullins WW, Sekerka RF. Stability of a Planar Interface During Solidification of a Dilute Binary Alloy. *J Appl Phys*. 1964 00;35(2):444–451. Available from: <http://scitation.aip.org/content/aip/journal/jap/35/2/10.1063/1.1713333>.

[149] Boekhoven J, Hendriksen WE, Koper GJ, Eelkema R, van Esch JH. Transient assembly of active materials fueled by a chemical reaction. *Science*. 2015;349(6252):1075–1079.

[150] Morel F, Morgan J. Numerical method for computing equilibria in aqueous chemical systems. *Environmental Science & Technology*. 1972;6(1):58–67.

[151] Head T, Yamamura M, Gal S. Aqueous computing: writing on molecules. In: *Evolutionary Computation*, 1999. CEC 99. Proceedings of the 1999 Congress on. vol. 2. IEEE; 1999. p. 1006–1010.

[152] Head T, Chen X, Yamamura M, Gal S. Aqueous computing: a survey with an invitation to participate. *Journal of Computer Science and Technology*. 2002;17(6):672–681.

[153] Landau LD, Lifshitz EM. *Quantum Mechanics: Non-Relativistic Theory*. Course of Theoretical Physics. Elsevier Science; 1981. Available from: <https://books.google.co.uk/books?id=SvdoN3k8EysC>.